Unterschrift BetreuerIn

TECHNISCHE
UNIVERSITÄT
WIEN
Vienna University of Technology

DIPLOMARBEIT

# Diagrammatic representation and evaluation of multi-boson contributions to optical conductivity

ausgeführt am Institut für Festkörperphysik
der Technischen Universität Wien

unter der Anleitung von
**Univ.Prof. Dipl.-Phys. Dr rer.nat. Karsten Held und Dr. Anna Kauch**

durch

**Julius M. Schnee**

Nymphengasse 1/13, 1120 Wien

December 17, 2024

Unterschrift StudentIn

## Abstract

Conductivity is a quantity that is often used in applied physics today. Especially in the optical regime, there is a wide range of applications where the conductivity is of great interest. In order to develop new technologies, a better understanding and knowledge is always an advantage. Therefore, in this work, higher order contributions are analysed and calculated according to quantum field theory for many-body systems, so that the optical conductivity is better known. In detail, we use a mixed approach which originates from the DΓA and uses parts of the parquet, Hedin, single (SBE) and multi-boson exchange (MBE) method. Within our method the full vertex function plays an important role for the higher order vertex corrections. In this work the first higher order terms of the full vertex function, multi-boson contributions, are identified and calculated numerically. The multi-boson contributions are derived from theory of the optical conductivity in the form of mathematical expressions and the corresponding Feynman diagrams. The expressions are numerically calculated and analysed in full.

## Zusammenfassung

Die Leitfähigkeit ist eine Größe, die häufig in der angewandten Physik vorkommt. Gerade im optischen Bereich gibt es eine Fülle von Anwendungen, in der die Leitfähigkeit von großem Interesse ist. Um neue Technologien zu entwickeln, ist ein besseres Verständnis und Wissen immer von Vorteil. Daher werden in dieser Arbeit höhere Ordnungsbeiträge analysiert und ausgerechnet im Rahmen der Quantenfeldtheorie für Vielteilchensysteme, sodass die optische Leitfähigkeit besser verstanden wird. Im Detail benutzen wir einen gemischten Ansatz mit Teilen aus der Dynamischen Vertex Approximation, der Parkett-, der Hedin- sowie der Ein- und Mehr-Bosonen-Austausch-Methode. Innerhalb unserer Methode spielt die volle Vertexfunktion eine wichtige Rolle für die Vertexkorrekturen höherer Ordnung. In dieser Arbeit werden die ersten Terme höherer Ordnung der vollen Vertexfunktion, die Multi-Boson-Beiträge, identifiziert und numerisch ausgerechnet. Die Multi-Boson-Beiträge werden aus der Theorie der optischen Leitfähigkeit hergeleitet in Form von mathematischen Ausdrücken und den dazugehörigen Feynman Diagrammen. Diese Ausdrücke werden numerisch berechnet und in vollem Umfang analysiert.

# Contents

# 1. Introduction

Calculating the properties of many-body condensed matter systems is challenging. Nevertheless, we take the challenge and apply quantum mechanical and quantum field theoretical methods and try to address at least simple models representing the physics. In general, we can very rarely solve problems exactly in the strongly correlated regime. Despite this, we can come to solutions and results, under certain conditions, that are useful and educational. In this work, we try to answer the question of how a solid responds to electromagnetic radiation in the wavelength range of visible light. The radiation will create electron-hole pairs via the photoelectric effect, and we would like to know how they interact and propagate through the solid. A property that tells us something about the movement of charged particles is the optical conductivity. Our study of this property is motivated by parquet equations calculation of optical conductivity ([1]) and a recent multi-boson exchange (MBE) single-boson exchange (SBE) reformulation [2], which allows for a new approach and savings regarding the computational effort. In is shown that there are large SBE contributions and much smaller MBE contributions [3]. Several physical questions arise, which are yet not answered: Are the MBE contributions coming predominantly from the lowest order in the screened interaction $W$? Do terms from different scattering channels (particle-hole (ph), particle-particle (pp), and vertical particle-hole ($\overline{\text{ph}}$)) cancel? Which channel dominates? Another question is how low order MBE contributions compare to the full MBE vertex contributions from full parquet calculations? To this aim we took one particle self energies, screened interactions $W$ and three-point vertices $\gamma$ from a full scale parquet calculation [2] and built low-order MBE diagrams (second order in $W$). The results are then analysed in terms of channels (ph, pp, $\overline{\text{ph}}$) and spin components (magnetic, density, singlet) and compared to the full parquet results.
These are the purposes of the thesis, which is structured as follows: First, in chapter 2 the background of Green's functions and the diagrammatic method in quantum field theory for many body systems is explained. Subsequently, in chapter 3 the Hamiltonian and the Matsubara formalism are inducted. After that we cover in subchapter 3.1 and 3.2 the concepts of one and two particle reducibility, the classification of spin and particle channels, the screened interaction and the Hedin vertices 3.3. With those concepts, the expressions for the current-current correlation function and the optical conductivity are formulated. The theoretical core follows in chapter 4 where we derive the lowest multi-boson order, after we introduced the formulas to calculate the full vertex function and decompose it into the scattering channels. The subchapters 4.3, 4.4 and 4.5 contain the expressions for the lowest multi-boson order and their respective Feynman diagrams. This concludes the first part of the thesis. The second part begins with chapter 5 where the solution with numerical methods is described. In chapter 6 we analyse the obtained results, concerning structure, magnitude, and behaviour. Furthermore, we compare the results with the total multi-boson order for different values of the bare interaction (subchapter 6.2). We also analyse the asymptotic approximation (subchapter 6.3), where the Hedin vertices and the screened interaction take constant values. At the end, we present

in chapter 7 a conclusion. In appendix A derivations can be found which describes the connection between different multi-boson contributions. Apart from that, two Appendices (B, C) can be found which prove the realness of the Matsubara current-current correlation function in the case of the bubble part and the SBE $\overline{\text{ph}}$ contributions. At last, in appendix D additional plots can be found of the lowest multi-boson order for $U = 3, 4$ and the asymptotic approximation with $U = 2, 3, 4$.

## 2. Green's function and diagrammatic method in quantum field theory

The mathematical definition of a Green's function is: $\hat{\mathcal{L}}(x)G(x) = \delta(x)$. Many of the Green's function which are used in the domain of many-body systems will not fulfil such an equation, strictly speaking, they are not mathematical Green's functions. Although in some cases it is possible. However, let us start with the free Schrödinger equation. we can rewrite it in a Green's equation, and we can find a Green's function for this. Often the Fourier transformation is used to solve it or to change the representation. As a next step, we use the occupation number formalism (second quantisation) [4], which is handy for systems with many particles. We define the creation $\hat{c}_k^\dagger$ and the annihilation operator $\hat{c}_k$, which creates or destroys a particle with a set of quantum numbers $k$ (mostly we will use $k$ just for the four-momenta). The one-particle noninteracting Hamiltonian would then look like this:

$$\hat{H}_0 = \sum_k \epsilon_k \hat{c}_k^\dagger \hat{c}_k.$$

One can rewrite the free Schrödinger equation by using the Hamilton operator and get also the Green's function in this formalism. When we do this, the expectation value shows automatically up in the Green's function expression, since the creation and annihilation operator have to act on a state, thus we get the expectation value over the creation and annihilation of a particle. Keep in mind that we have no limit for particle number, it is for an arbitrary particle number $N$. We can now generalise our approach by using an interacting and time dependent Hamilton operator, which can be spilt into an interacting and noninteracting part. To continue further, we use the Heisenberg picture for operators, for example the creation operator, which was time independent before[1]: $\hat{c}_k^\dagger(t) = \exp(\frac{i\hat{H}t}{\hbar})\hat{c}_k^\dagger \exp(\frac{-i\hat{H}t}{\hbar}) = \hat{U}^\dagger(t)\hat{c}_k^\dagger\hat{U}(t)$. We have also defined the time evolution operator as $\hat{U(t)} = \exp(\frac{-i\hat{H}t}{\hbar})$. This operator produces the time evolved state $\psi(t)$ when applied on $\psi(t_0)$: $\psi(t) = \hat{U}(t - t_0)\psi(t_0)$. The creation and annihilation operators create or annihilate a particle with a certain set of quantum numbers $k$ at a certain time $t$. To order the operators correctly, the so-called time ordered product is used, with the time ordering operator $\hat{T}$. The time ordered product of several time dependent operators has several valid combinations (if we no longer consider the simple free one particle Green's function). To calculate these effectively, we use Wicks theorem. The

[1] In this work indices have an additional meaning, they also correspond to arguments of the quantity

one-particle propagator (many-body Green's function) is defined as[2]:

$$G(k_2, k_2, t_2 - t_1) = -i \langle \psi_0 | \hat{T}(\hat{c}_{k_2}(t_2)\hat{c}^{\dagger}_{k_1}(t_1)) | \psi_0 \rangle . \tag{1}$$

But first, let us go a step back.
With the help of Wick's theorem, every Green's function, no matter how complicated, can formally be written as a perturbation series respectively perturbation expansion. Let us go back to the Schrödinger equation with an interacting Hamiltonian. We define a formal solution via the time evolution operator. This operator is rewritten in the interaction picture, where the Hamiltonian is written as follows: $\hat{H} = \hat{H}_0 + \hat{H}_1$, where the first part is noninteracting and the second part includes two (or more) particle interaction. For the time evolution operator in the interaction picture, we obtain a differential equation, which has to be solved iteratively. As a result, one gets a perturbation like expansion where the ordering is important, because among other things Hamiltonians do not commute with different time arguments. One can consolidate the solution with the time ordering operator and the definition of a time ordered exponential function:

$$\tilde{U}(t, t_0) = \sum_{n=0}^{\infty} \frac{(-i)^n}{n!} \int_{t_0}^{t} dt_1 ... \int_{t_0}^{t_n - 1} dt_n \hat{T}[\hat{H}_1(t_1)...\hat{H}_1(t_n)] \equiv \hat{T} \exp(-i \int_{t_0}^{t} dt_1 \hat{H}(t_1)). \tag{2}$$

Now we consider the Green's function again, with its creator an annihilator representation. Using our interaction Hamiltonian, we obtain a similar equation like (1). Here the creation and annihilation operators are in the interaction picture, also we used $\phi_0$ as none interacting ground state, and we normalised the expression [4].

$$G(k_2, k_1, t_2 - t_1) = \lim_{\substack{T_1 \to -\infty(1-i\eta) \\ T_2 \to +\infty(1-i\eta)}} -i \frac{\langle \phi_0 | \hat{T}(\tilde{U}(T_2, T_1)\hat{c}_{k_2}(t_2)\hat{c}^{\dagger}_{k_2}(t_1)) | \phi_0 \rangle}{\langle \phi_0 | \tilde{U}(T_2, T_1) | \phi_0 \rangle}. \tag{3}$$

Next we use the definition of $\tilde{U}$ and we insert the unit operator through a sum over the exact eigenstates of the Hamiltonian. At last, we insert the expansion series expression for $\tilde{U}$. As mentioned, the time ordered products can be evaluated with Wick's theorem. The resulting expression is now the perturbation series for the Green's function.
However, there is another, more intuitive way to handle our problem. Remember, we wanted to describe a particle propagation in an interactive regime. We can think about all processes this particle can undergo, every possible interaction. For example, free propagation, scattering one time, scattering four times, scattering with radiation which then propagates as electron-hole pair until it recombines and so on. All these processes can be written as Feynman diagrams and calculated as probability, respectively probability amplitude. If we then sum up all diagrams and expressions, we get the particle propagation as a whole, because we considered all possible interactions. One may question if this method is exact and legit. Thanks to our preparatory work, we can come to a conclusion regarding this question. Every term in the perturbation series for the

[2]From now on $\hbar$ is set to 1

Green's function is in one to one correspondence to a Feynman diagram. Both ways and methods are equivalent. There are advantages and disadvantages, depending on the problem, we can choose how we want to solve it. At first, it may not seem so, but the diagrammatic technique is very powerful. With additional approaches and further developed techniques, one can define simple diagrams for complicated processes, whose strict mathematical derivation would be very tedious. The diagrammatic method often helps to present complicated things simply and can help by calculating certain parts more effectively.

We also notice that we have matrix elements (terms in our series) that are unlinked, not connected to the internal Green's function line. In the total expression of the Green's function, all of these terms can be factorised in the denominator. In the numerator arises (linked) Feynman diagrams that are violating the Pauli principle, which is a problem at first. These terms can also be factorised in a distinct manner, so that these diagram terms cancel with the unlinked ones in the denominator [4]. Therefore, unlinked diagrams are not to be considered in calculations as well as the 'unphysical' Feynman diagrams. This result is called linked-cluster theory. We cannot exclude these diagrams for the mathematical derivation, because then we would not receive the diagram theory respectively the linked cluster theory in the same rigorous manner. However, one can say the Pauli principle is quasi conserved since the violating diagrams do not contribute to a physical observable.

What we have done was on the basis of a single particle Green's function and without temperature dependence. We can easily extend the Green's function to more particles, this works similar. To imply a finite temperature, we use a modified time evolution operator respectively Hamiltonian[3] according to a thermal ensemble (grand canonical ensemble). The expectation values are thus over a thermal (and particle) ensemble, often it is convenient to express this with the trace and the density operator[4].

## 3. Model and methods

For the optical conductivity, we use a two particle interacting Green's function. Considering the periodicity, integrals, and calculations are always for the first Brillouin zone, which is sufficient. The underlying Hamiltonian is the Hubbard Hamiltonian [5], including the chemical potential:

$$\hat{H} = -t \sum_{\langle ij \rangle, \sigma} \hat{c}^{\dagger}_{i\sigma} \hat{c}_{j\sigma} + U \sum_{i} \hat{n}_{i\uparrow} \hat{n}_{i\downarrow} - \mu \sum_{i} (\hat{n}_{i\uparrow} + \hat{n}_{i\downarrow}), \tag{4}$$

with $i, j$ denoting site indices (the sum is over pairs of nearest neighbours), $\sigma = \uparrow, \downarrow$ denoting spin index, $U$ being the local Coulomb interaction and $\hat{n}_i$ the particle number

[3] $H \to H - \mu N$
[4] $\langle \hat{A} \rangle = \mathrm{Tr}(\hat{A}\hat{\rho})$

operator.
Usually, the time coordinate is transformed by the so-called Wick rotation, $t \to -i\tau$; $\tau = it$. By shifting the time on the imaginary axis, one gets often simpler expressions, for example $\hat{U} = \exp(-\hat{H}\tau)$, also it can be more convenient for calculations. For the sake of completeness, it should be mentioned that the Born-Oppenheimer approximation is applied. We did not include a relativistic treatment as well as spin-orbit interactions. The Hubbard model is restricted to one orbital and a local interaction only, and in equation (4) we only consider nearest neighbour hoppings.
Important properties of the Hamiltonian above are the time and space translation symmetry. Both are time independent, so the corresponding Green's functions depend on time differences instead of all individual times. The lattice symmetry further means that one can perform shifts by the lattice vector and nothing will change. Each symmetry is reducing the number of the degrees of freedom by one, that means in the Fourier representation reducing the dimension of the frequency (time symmetry) respectively the momentum space (space symmetry).
Another important property is the SU(2) symmetry $[\hat{H}, \hat{S}_i] = 0$, the total spin is conserved. that means the dependency of spin arguments for the Green's function is reduced. As an example, the one-particle Green's function would be dependent on two spin variables, but due to the symmetry it only depends on one. These properties reduce the number of free variables, therefore they are useful.

A general condition for the Green's function is the Kubo-Martin-Schwinger condition (see e.g. [6]):

$$G_{n,i_1,i_2,\ldots,i_{2n}}(\tau_1,\ldots,\tau_{2n}) = -G_{n,i_1,i_2,\ldots,i_{2n}}(\tau_1-\beta,\ldots,\tau_{2n}) = -G_{n,i_1,i_2,\ldots,i_{2n}}(\tau_1,\ldots,\tau_{2n}+\beta). \tag{5}$$

Where $\beta = \frac{1}{k_B T}$ is the thermodynamic beta. Equation (5) implies antiperiodicity (for bosons it would be periodicity) and therefore discrete Fourier-components. These discrete frequencies are called Matsubara frequencies:

$$\nu_n = \frac{(2n+1)\pi}{\beta},\ n \in \mathbb{Z}, \tag{6a}$$

$$\omega_n = \frac{2n\pi}{\beta},\ n \in \mathbb{Z}. \tag{6b}$$

In consequence, all Fourier frequency integrals become sums over the Matsubara frequencies. For the fermionic Matsubara frequency, the following relation holds[5]:

$$\nu_n = -\nu_{-n-1}. \tag{7}$$

## 3.1. One-particle reducibility of diagrams

Our formulation of the Green's function as infinite series can be put into another form. One can renormalise it and rewrite it with the Dyson equation (8). We obtain the full

[5] See $-\nu_{-n-1} = -(2(-n-1)+1)\frac{\pi}{\beta} = -(-2n-1)\frac{\pi}{\beta} = (2n+1)\frac{\pi}{\beta} = \nu_n$

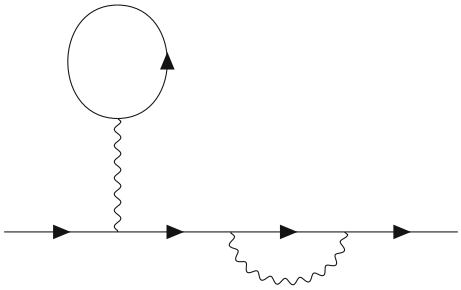

Figure 1: Reducible diagram. One can cut the fermionic line at the bottom after the second arrow and one receive two (irreducible) diagrams.

interacting Green's function defined over the so-called self energy $\Sigma$. The self energy contains all one particle irreducible diagrams

$$G(k) = \frac{1}{i\nu_n - \epsilon_{\boldsymbol{k}} + \mu - \Sigma(k)}, \tag{8}$$

where we introduce a combined momentum-frequency notation $k = (\nu_n, \boldsymbol{k})$, omit the spin index, and introduce $\epsilon_{\boldsymbol{k}}$ as the noninteracting dispersion relation.
Reducible diagrams are diagrams that can be separated by cutting a Green's function line. As a result, we obtain lower order diagrams. In the case of the Dyson equation, we would already have them in our series (if they are not further reducible). Thus, we need to reduce the number of diagrams we really have to cope with. Think about reducible diagrams as of a piece of Lego, we can dissemble it into the base bricks, if this is not possible and the Lego is just the brick itself, the diagram is irreducible. See for example figure 1. To describe the interacting Green's function with diagrams effectively, topologically equivalent diagrams have to be unified. When we work with the diagram method, we do not want to calculate the terms of the Green's function series. Therefore, in general, we do not know how a priori the Feynman diagrams, which will be in total equivalent to the series, are looking like. However, if we construct Feynman diagrams, we are facing the reality of having possible diagrams that are topological equivalent. If we only consider topologically inequivalent diagrams, we can reduce the number of diagrams and cancel a prefactor.

Another helpful concept are the skeleton diagrams. In general, we draw double lines in Feynman diagrams for interacting particles. For example, if we draw a double fermionic line for a one-particle Green's function, all interactions, and processes are included, loops, bubbles ..., all higher orders. In this way, we can draw diagrams more compactly or display complicated diagrams more clearly. A skeleton diagram is thus an irreducible diagram, where additionally the Green's function lines contain all possible self-energy insertions.

## 3.2. Two-particle reducibility and optical conductivity

No matter what technique is used, in the end one always has to calculate the explicit expressions, which are in general not analytically solvable. Attempts are often made with approximations, auxiliary constructions and self-consistent methods in which the solution is calculated in an iteration process. However, there are advanced approaches to reduce the effort and to make life easier. In the following we will use building blocks obtained by the self-consistent solution of parquet equations [2, 3] to calculate contributions to optical conductivity. We will decompose the full vertex function that is needed in the calculation of the optical conductivity into screened interaction $W$ and three-point Hedin vertices $\gamma$. We are describing the fundamental (dominant) interacting process with the exchange of a (quasi) boson. For the Hamiltonian, we use the Hubbard model. The following unit system is used:

$$\begin{aligned} \hbar &= 1, \\ e &= 1, \\ k_{\mathrm{B}} &= 1, \\ a &= 1, \\ t &= 1. \end{aligned}$$

Where $a$ is the lattice constant of our system and $t$ is the hopping parameter from the Hubbard model. Further, we are classifying the Feynman diagrams in so-called channels, the particle-hole channel ph, the vertical particle-hole channel ($\overline{\mathrm{ph}}$), the particle-particle channel pp and a complete irreducible part ($\Lambda$). This classification is typical for the parquet method [3].

The two particle reducibility is defined as follows: A diagram is fully irreducible, or it is reducible in exactly one channel, by cutting two Greens' function lines in the corresponding channel specific way. Because there are more possibilities to cut the two lines than for one particle, there are three specific cut-channels. Reducible in the ph channel corresponds to cut two opposing horizontal fermionic lines vertical, $\overline{\mathrm{ph}}$ reducible is a diagram when cutting two opposing vertical fermionic lines horizontally and pp reducible is a diagram where one can cut two (horizontal or vertical) fermionic lines, that go in the same direction. There is one more kind of reducibility, the U-reducibility, $U$ the bare interaction (4). It is defined as follows: U-reducible is a diagram when it can be cut into two parts by removing a bare interaction line $U^{\alpha}$. There are four cases: $\mathrm{U}^{\mathrm{irr}}$, U-pp, U-ph, U-$\overline{\mathrm{ph}}$. Each case implies the corresponding two particle reducibility (e.g. if the diagram is $U - pp$ reducible it is two particle pp reducible, also called gg-pp reducible). This does not hold vice versa.

Now we include the spin. Our Hamiltonian has a spin dependency, we have to perform

a sum over all possible spin configurations of the particles. The spin notation is:

$$\uparrow\uparrow\uparrow\uparrow \equiv \uparrow\uparrow,$$
$$\uparrow\uparrow\downarrow\downarrow \equiv \uparrow\downarrow,$$
$$\uparrow\downarrow\downarrow\uparrow \equiv \overline{\uparrow\downarrow}.$$

Out of symmetry reasons (SU(2)), it is sufficient to describe four-spin objects with two spins[6]. The equations are adjusted for a global spin flip with a factor of 2, therefore we consider only half of the spin combinations. There are spin channels defined, density d, magnetic m[7], singlet s and triplet t. The definition, using the example of the full vertex function F, is:

$$F^{\mathrm{d}} \equiv F_{\uparrow\uparrow} + F_{\uparrow\downarrow},$$
$$F^{\mathrm{m}} \equiv F_{\uparrow\uparrow} - F_{\uparrow\downarrow},$$
$$F^{\mathrm{s}} \equiv F_{\uparrow\uparrow} - F_{\overline{\uparrow\downarrow}},$$
$$F^{\mathrm{t}} \equiv F_{\uparrow\uparrow}.$$

The full vertex function $F$ is the main object of our interest. It is the main part of the current-current correlation function, which is needed to calculate the optical conductivity. Within the linear response theory and the Sokhotski-Plemelj's formula, we can derive the following equation for the optical conductivity[1]:

$$\Re(\sigma_q) = -\pi\delta(\omega)\left[\Re(\chi_{jj,q}) - \frac{q^2 n_q}{m}\right] + \mathcal{P}\left(\frac{\Im(\chi_{jj,q})}{\omega}\right). \tag{11}$$

The imaginary part can be obtained by using the Kramers-Kronig relations.
The current-current correlation function can be expressed in the quantum field theory formalism (without proof) as follows (see also [1]):

$$\begin{aligned}\chi_{jj,\rho}(q) = &\frac{-2}{(2\pi)^3\beta}\int d\boldsymbol{k}\sum_{\nu}\left(y_\rho^{\boldsymbol{k}\frac{\boldsymbol{q}}{2}}\right)^2 G_k G_{k+q} \\ &- \frac{2}{((2\pi)^6\beta)^2}\int d\boldsymbol{k}\sum_{\nu}\int d\boldsymbol{k'}\sum_{\nu'} y_\rho^{\boldsymbol{k}\frac{\boldsymbol{q}}{2}} y_\rho^{\boldsymbol{k'}\frac{\boldsymbol{q}}{2}} G_k G_{k+q} F^{\mathrm{d}}_{k,k',q} G_{k'+q} G_{k'} \\ &= \chi^{\mathrm{bub}}_{jj,\rho}(q) + \chi^{\mathrm{ver}}_{jj,\rho}(q).\end{aligned} \tag{12}$$

To obtain this result the Peierls approximation [1] is used, the applied field is along a lattice vector, $\rho = x, y, z$, the variation in space of the electric field $\boldsymbol{E}$ is neglected, and the result is for the limit $\boldsymbol{q} \to 0$. The light vertex $y$ is given with the knowledge of the derivative of the dispersion relation, $y_\rho^{\boldsymbol{kq}} = \partial_\rho \epsilon_{\boldsymbol{k}+\boldsymbol{q}}$. Whereby the derivative is

[6] It is to note that for the two particle Green's function it is adequate to only calculate $G_{2\uparrow\downarrow}$ and $G_{2\uparrow\uparrow}$. All other nonvanishing Green's functions can be calculated with them

[7] In some publications the naming is different, the density channel is called charge ch and the magnetic channel is called spin sp

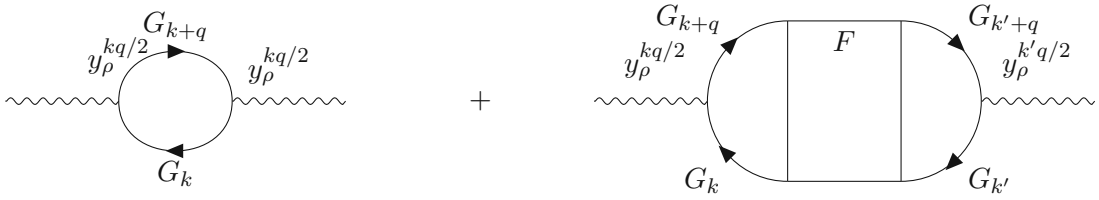


Figure 2: Current-current correlation function needed for optical conductivity in diagrammatic representation.

in $\rho = x, y$ or $z$ direction. The integrals are usually replaced with discrete sums. The current-current correlation function in terms of diagrams can be seen in figure 2. The first term in 12 proportional to two Green's functions describes a self interacting particle and hole independently propagating. This term is known as the bubble term. The second term proportional to four single particle Green's functions and the full vertex function is the description for the interacting two particle Green's function. Remember, the single particle Green's functions are interacting ones (self interaction), expressed with the Dyson equation and the self-energy. The interacting two particle vertex function $F$ is here dependent on three four-momenta. The spin is within our description fixed in one channel (density), but as we see later during decomposing, the finer structured quantities form the individual specific spin combinations. The next step is to evaluate and further describe the full vertex function $F$. Therefore, two quantities have to be established first, the boson propagator or screened interaction $W$ and the Hedin vertex $\gamma$.

The screened interaction describes the energy and momentum exchange for the interaction processes the particle undergoes by travelling through the solid. we can look upon it as a dressed interaction where the exchange particle is not the bare exchange particle (just a photon for the bar Coulomb interaction), it is surrounded by a cloud of other particles. The effective interaction our particles feel is a mix of all emitted potentials in the system. Therefore, the Coulomb interaction which applies to the electron is screened or modified in a certain way and thus "dressed" in comparison to the bare Coulomb interaction. The definition of the screened interaction is:

$$W_q^{\mathrm{d/m}} = \frac{U^{\mathrm{d/m}}}{1 - U^{\mathrm{d/m}}\Pi_q^{\mathrm{d/m}}}, \tag{13a}$$

$$W_q^{\mathrm{s}} = \frac{U^{\mathrm{s}}}{1 - \frac{1}{2}U^{\mathrm{s}}\Pi_q^{\mathrm{s}}}, \tag{13b}$$

$$W_q^{\mathrm{t}} = 0. \tag{13c}$$

As seen, the bare interaction is different for each spin channel $U^{\mathrm{d}} = U$, $U^{\mathrm{m}} = -U$, $U^{\mathrm{s}} = 2U$, $U^{\mathrm{t}} = 0$. The other variable on which the screened interaction depends is the polarisation $\Pi_q$. This in turn depends on the Green's function and a Hedin vertex. This brings us to the next chapter.

## 3.3. Definition of the Hedin vertices

The Hedin vertex originates from the Hedin formalism [7]. This vertex, written as $\gamma$ with two input arguments, whether as subscripts or in brackets, is a three point vertex. It connects two fermionic propagators and a bosonic one. The first input is fermionic, the second of bosonic nature, it carries a spin channel dependence. This vertex represents all possible fermion-boson interactions for the constituents. One can think of it as a box, which contains all Feynman diagrams for this case. This construction helps us further to effectively describe our problems. More information of the mathematical background can be found in [8] and related articles. One can define for example the vertex for the s channel as:

$$\gamma^{\mathrm{s}}_{kq} = -1 + \frac{1}{2}\sum_{k'} \left(F^{\mathrm{s}}_{kk'q} - \Delta^{\mathrm{s}}_{kk'q}\right) G_{k'} G_{q-k'}.$$

As we can see the four point vertex $F$ and $\Delta$, which is defined in (17). They cannot be calculated independently, the equations for our problem are linked and coupled with each other, which makes it difficult to solve. As mentioned, often iterative solutions with starting values are used to obtain a solution. In the next subchapters, we look at the representation of $\gamma_{\nu,\omega}$ as Feynman diagram, which fermionic argument is taken, how the propagator directions are, this does matter. We use here $\nu, \omega$ to represent the general fermionic and bosonic argument, respectively, based on the style in [9].
If we choose a spin channel, including frequency and momenta in a four-index, we restrict automatically the possible particle channels. This applies for our case, especially using a one orbital model. We know if we have the density or the magnetic spin channel for the Hedin vertex, it will be a ph or $\overline{\text{ph}}$ vertex. If we choose the singlet channel, we have a pp vertex. Thus, in the following subchapters, $\gamma$ does not carry the spin channel index. Figures 3,4,5 and 6 are showing the same physical Feynman diagram, they are just rotated. The reason they are depicted, is to show the arrangement of the propagator arguments and directions of the lines to have a clear definition of our $\gamma$. It is a question of parametrisation. Also, figure 7 shows identical physical Feynman diagrams with different parametrisations.

### 3.3.1. Particle-hole vertex

The particle-hole vertex connects two horizontal fermionic lines, one incoming, one outgoing and a vertical bosonic line. It describes the scattering of a particle or a hole. In figure 3 we have $\gamma_{\nu,\omega}$. Changing the direction of the boson line changes the sign of $\omega$. The fermionic argument is always that of the line that enters the vertex. The vertex in figure 4 is defined as: $\gamma_{\nu',-\omega}$. The fermionic argument is always the one from the incoming line in the vertex, so for example if the propagator directions flip we would get $\gamma_{\nu,-\omega}$.

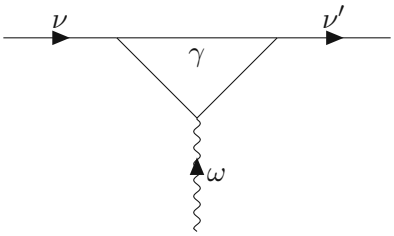


Figure 3: Particle-hole Hedin vertex $\gamma_{\nu,\omega}$.

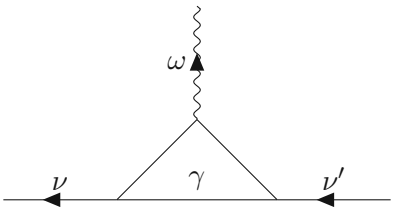


Figure 4: Alternative representation of the particle-hole Hedin vertex with negative sign in the bosonic argument$\gamma_{\nu',-\omega}$.

### 3.3.2. Vertical particle-hole vertex

The vertical particle-hole vertex connects two horizontal fermionic lines, again one ingoing, one outgoing. The bosonic line is now horizontal too. It describes the scattering of a particle with and a hole. For the left sided vertex, the definition is: $\gamma_{\nu,\omega}$. A sign

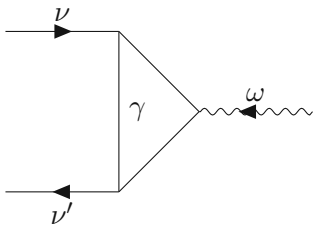


Figure 5: Vertical particle-hole Hedin vertex $\gamma_{\nu,\omega}$.

change appears when the bosonic line direction is flipped. The fermionic argument is always the incoming one. For the right sided vertex, the definition is: $\gamma_{\nu',\omega}$. Again, with a bosonic line direction flip, one gets a sign change. The fermionic argument is always the outgoing one. The reason we draw them here, even tho they are the same physical Feynman diagrams like in 3.3.1 is the sign difference if we just rotate them. For example, if we rotate the diagram in figure 6 by 90 degree clockwise and bend the fermionic lines horizontal, we see in comparison to the diagram in figure 4 a sign change in the bosonic argument. The fermionic argument is in this case not the same just because the incoming fermionic line is labelled differently, but the sign change in the bosonic argument is not a labelling issue, both propagators are outgoing. This behaviour is the

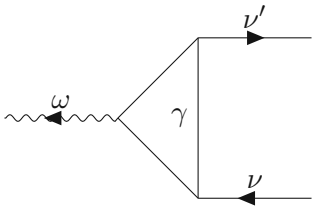


Figure 6: Alternative representation of the vertical particle-hole Hedin vertex $\gamma_{\nu',\omega}$.

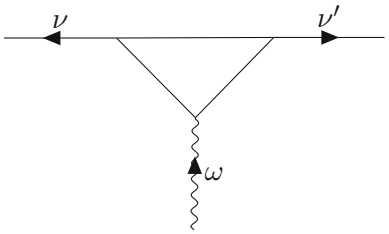


(a) Creation pp Hedin vertex

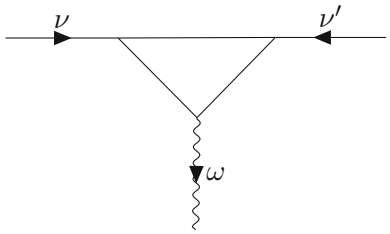


(b) Annihilation pp Hedin vertex

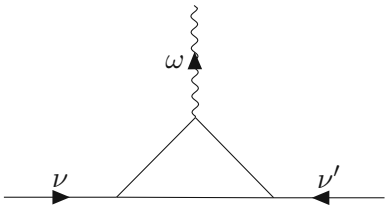


(c) Alternative annihilation pp Hedin vertex

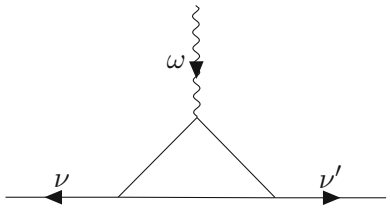


(d) Alternative creation pp Hedin vertex

Figure 7: Different representations of the particle-particle Hedin vertex, but with the same argument structure $\gamma_{\nu',\omega}$.

reason one have to pay attention when drawing those diagrams and the legitimation of this subchapter.

### 3.3.3. Particle-particle vertex

The particle-particle vertex connects two ingoing or two outgoing fermionic lines. With this, it describes the creation or annihilation of a particle-particle pair. In figure 7 all diagrams have the same Hedin vertex structure: $\gamma_{\nu',\omega}$. Pay attention to the direction of the boson line, if it is in the opposite direction we get a minus sign and therefore $\gamma_{\nu',-\omega}$.

## 4. Derivation of the lowest order multi-boson contributions in the full vertex function

To calculate the conductivity, we need to know the current-current correlation function. The bubble part of the current-current correlation function is not difficult to determine,

unlike the vertex part with the full vertex function $F$. However, we do not attempt to calculate $F$ in total. An important result of the parquet formalism is that $F$ can be decomposed (parquet equations) into the reducible vertices $\Phi^\alpha$ and a fully irreducible vertex $\Lambda^{\text{irr}}$. Reducibility refers here to the two particle reducibility and the different channels.

The first order of $F$ with respect to the screened interaction $W$, which is second order in Hedin vertices, is known exactly in diagrammatic form (see for example [2]). Our goal is now to identify the exact diagrammatic contribution for the second order of $F$ in $W$ (which is unknown) and to calculate it as good as possible. In this chapter, we will express these second order contributions in terms of the one-particle Green's function $G$, the screened interaction $W$ and the Hedin vertices $\gamma$. These contributions are of fourth order in the Hedin vertices, and second order in the screened interaction $W$ as well as the bare interaction $U$. In the next chapter we will omit the bare interaction to get contributions, which are the true multi-boson diagrams we are interested in.

## 4.1. Bethe-Salpeter equations within the mutli-boson approach

In the multi-boson exchange approach [9], the full vertex $F$ is decomposed into single- and multi-boson contributions. We denote the multi-boson vertices with $M$. They can be obtained from the following Bethe-Salpeter equations (BSEs):

$$M^{\text{d/m}}_{kk'q} = \sum_{k''} S^{\text{d/m}}_{kk'q} G_{k''} G_{k''+q} T^{\text{d/m}}_{k''k'q}, \tag{14a}$$

$$M^{\text{s/t}}_{kk'q} = \mp \sum_{k''} S^{\text{s/t}}_{kk''q} G_{k''} G_{q-k''} T^{\text{s/t}}_{k''k'q}. \tag{14b}$$

$$M^{\alpha}_{kk'q} = T^{\alpha}_{kk'q} - S^{\alpha}_{kk'q}. \tag{15}$$

The kernels $S$ of the above BSEs are given by the parquet equations that include both the mulit-boson vertices $M$ and single-boson contributions $\Delta$:

$$S^{\text{d}}_{kk'q} = \Lambda^{\text{Uirr,d}} - M^{\text{d}}_{kk'q} - \frac{1}{2}\Delta^{\text{d}}_{k,k+q,k'-k} - \frac{3}{2}\Delta^{\text{m}}_{k,k+q,k'-k} + \frac{1}{2}\Delta^{\text{s}}_{k,k',k+k'+q} - 2U^{\text{d}}, \tag{16a}$$

$$S^{\text{m}}_{kk'q} = \Lambda^{\text{Uirr,m}} - M^{\text{m}}_{kk'q} - \frac{1}{2}\Delta^{\text{d}}_{k,k+q,k'-k} + \frac{1}{2}\Delta^{\text{m}}_{k,k+q,k'-k} - \frac{1}{2}\Delta^{\text{s}}_{k,k',k+k'+q} - 2U^{\text{m}}, \tag{16b}$$

$$\begin{aligned} S^{\text{s}}_{kk'q} =& \Lambda^{\text{Uirr,s}} - M^{\text{s}}_{kk'q} + \frac{1}{2}\Delta^{\text{d}}_{k,k',q-k'-k} - \frac{3}{2}\Delta^{\text{m}}_{k,k',q-k'-k} + \frac{1}{2}\Delta^{\text{d}}_{k,q-k',k'-k} \\ & - \frac{3}{2}\Delta^{\text{m}}_{k,q-k',k'-k} - U^{\text{d}} + 3U^{\text{m}}, \end{aligned} \tag{16c}$$

$$S^{\text{t}}_{kk'q} = \Lambda^{\text{Uirr,t}} - M^{\text{t}}_{kk'q} + \frac{1}{2}\Delta^{\text{d}}_{k,k',q-k'-k} + \frac{1}{2}\Delta^{\text{m}}_{k,k',q-k'-k} - \frac{1}{2}\Delta^{\text{d}}_{k,q-k',k'-} - \frac{1}{2}\Delta^{\text{m}}_{k,q-k',k'-k}. \tag{16d}$$

The single-boson exchange contribution is simply given by:

$$\Delta^{\alpha}_{k,k',q} = \gamma^{\alpha}_{k,q} W^{\alpha}_{q} \gamma^{\alpha}_{k',q}. \tag{17}$$

The formulas (14)-(17) can be found in [8] and here they are used with a slightly different notation. Equations (14) are the Bethe-Salpeter equations for the MBE approach. The multi-boson vertices $M$ correspond to the higher orders of $F$ and since we want the lowest multi-boson order of $F$ we have to calculate $M$, which will follow in chapter 4.2. With the bare interaction $U$ known, we can close the BSE with equation (15) and the parquet equation (16).
For completeness we also write the realtion between the reducible vertex $\Phi$ and the single- and multi-boson vertices:

$$\Phi^{\alpha}_{k,k',q} = \Delta^{\alpha}_{k,k',q} + M^{\alpha}_{k,k',q} - U^{\alpha}. \tag{18}$$

Equation (18) is used to rewrite the parquet form of $F$ into the MBE formalism of (21). The equation for $F$ in parquet formalism can be found in [8].
The building blocks that we will use for constructing second order diagrams in $W$ obey certain identities that are related to symmetries:

$$\gamma^{\alpha}_{k,q} = \gamma^{\alpha}_{k+q,-q,} \tag{19a}$$
$$\gamma^{\mathrm{s}}_{k+q,q} = \gamma^{\mathrm{s}}_{-k,q}, \tag{19b}$$
$$\gamma^{\alpha^*}_{k,q} = \gamma^{\alpha}_{-k,-q}, \tag{19c}$$
$$\gamma^{\alpha^*}_{-\nu,\boldsymbol{k},-\omega,\boldsymbol{q}} = \gamma^{\alpha}_{\nu,\boldsymbol{k},\omega,\boldsymbol{q}}, \tag{19d}$$
$$W^{\alpha}(w,\boldsymbol{q}) = W^{\alpha^*}(-w,\boldsymbol{q}). \tag{19e}$$

The identities (19d) and (19e) are only valid if the system has inversion symmetry. All Identities in (19) are useful and applied, for example, to rewrite the argument combinations of Hedin vertices to connect the "$B$" expressions to graphical representation through diagrams. We obtain these $B$-terms as a result of applying the BSE[8]. The identities are based on definition, time-reversal symmetry and SU(2) symmetry. There are given here without proof. Also, there are more, but we just need these.

The following identities, among others, apply to the Green's function:

$$G(\nu,\boldsymbol{k}) = G(\nu,-\boldsymbol{k}), \tag{20a}$$
$$G(\nu,\boldsymbol{k}) = G^*(-\nu,\boldsymbol{k}). \tag{20b}$$

Equation (20a) always applies if the lattice posses the inversion symmetry.

## 4.2. Decomposition of the full vertex function

To obtain the optical conductivity, it is sufficient to calculate $F$ in the density channel, because it contains the relevant spin combination for the optical conductivity (this is not the general case). We reduce the general parquet expression from the decomposition of the full vertex function to the density spin channel case. After that, we write out $\Lambda^{\mathrm{Uirr},\alpha}_{k,k',q}$.[9]:

[8] See the equations (24), (25 and (26), where we get the mentioned $B$ terms proportional to four Hedin vertices.
[9] $\Lambda^{\mathrm{Uirr},\alpha}_{k,k',q}$ is related to the parquet $\Lambda$ with: $\tilde{\Lambda}^{\alpha} = \Lambda^{\alpha} - U^{\alpha}$ where $\tilde{\Lambda}^{\alpha}$ is a part of $\Lambda^{\mathrm{Uirr},\alpha}$

$$
\begin{aligned}
F^{\mathrm{d}}_{kk'q} &= \Delta^{\mathrm{d},ph}_{kk'q} - \frac{1}{2}\Delta^{\mathrm{d},\overline{ph}}_{k,k+q,k'-k} - \frac{3}{2}\Delta^{\mathrm{m},\overline{ph}}_{k,k+q,k'-k} + \frac{1}{2}\Delta^{\mathrm{s},pp}_{k,k',k+k'+q} \\
&\quad + \Lambda^{\mathrm{Uirr,d}}_{k,k',q} - 2U^{\mathrm{d}} \\
&= \Delta^{\mathrm{d},ph}_{kk'q} - \frac{1}{2}\Delta^{\mathrm{d},\overline{ph}}_{k,k+q,k'-k} - \frac{3}{2}\Delta^{\mathrm{m},\overline{ph}}_{k,k+q,k'-k} + \frac{1}{2}\Delta^{\mathrm{s},pp}_{k,k',k+k'+q} \\
&\quad + \tilde{\Lambda}^{\mathrm{d}}_{k,k',q} - 2U^{\mathrm{d}} \\
&\quad + M^{\mathrm{d},ph}_{kk'q} - \frac{1}{2}M^{\mathrm{d},\overline{ph}}_{k,k+q,k'-k} - \frac{3}{2}M^{\mathrm{m},\overline{ph}}_{k,k+q,k'-k} + \frac{1}{2}M^{\mathrm{s},pp}_{k,k',k+k'+q} + \frac{3}{2}M^{\mathrm{t},pp}_{k,k',k+k'+q}.
\end{aligned} \tag{21}
$$

In equation (21) the $\Delta$ terms represent the known first order. The terms proportional to $M$ are of higher order, and we are just interested in them. So for the different particle channels the equation (21) splits into these higher order parts:

$$F^{\mathrm{d},ph}_{kk'q} = M^{\mathrm{d}}_{kk'q}, \tag{22a}$$

$$F^{\mathrm{d},\overline{ph}}_{kk'q} = -\frac{1}{2}M^{\mathrm{d}}_{k,k+q,k'-k} - \frac{3}{2}M^{\mathrm{m}}_{k,k+q,k'-k}, \tag{22b}$$

$$F^{\mathrm{d},pp}_{kk'q} = \frac{1}{2}M^{\mathrm{s}}_{k,k',k+k'+q} + \frac{3}{2}M^{\mathrm{t}}_{k,k',k+k'+q}. \tag{22c}$$

The aim is to calculate and identify the multi-boson diagrams of fourth order in the Hedin vertices, these are the true first multi-boson contributions, but $M$ contains all higher orders. To obtain the wanted order, we neglect in equation (16) all terms except the $\Delta$ terms and equation (15) is transformed to $S$ where we neglect $M$, so we approximate $T$ with $S$. Now we use equation (14) to calculate the first order of the multi-boson diagrams for the different channels, given in equation (21). They will be $\propto \Delta^2 \propto \gamma^4$ as intended. To distinguish these contributions from the normal (full) multi-boson part, we named it $L$. Why we neglected the $M$ terms in (16) should be clear, but what about $\Lambda^{\mathrm{Uirr},\alpha}$? This can be written as $\Lambda^{\mathrm{Uirr},\alpha} = \tilde{\Lambda}^{\alpha} + \mathcal{M} = \Lambda^{\alpha} - U^{\alpha} + \mathcal{M}$. Again it is clear that the complete multi-boson part of it can be neglected, on the other hand $\Lambda^{\alpha}$ contains a $U$ term, but $\Lambda^{\mathrm{Uirr},\alpha}$ is completely irreducible when it comes to the bare interaction, therefore $U$ is subtracted as we see it in the formula. In total, there is no $U$ term in $\Lambda^{\mathrm{Uirr},\alpha}$ and $\Lambda^{\alpha}$ is not a part of our multi-boson order. Therefore, $\Lambda^{\mathrm{Uirr},\alpha}$ is neglected as a whole.

*However, what is really important, is that we have to take into account the bare interaction in equation* (16) *after all, which we have neglected in first place*! A single $\Delta$ term is in the lowest order a $U$ term. We have three of them. To avoid overcounting, we have to subtract $U$ again, and cannot neglect them. $M$ does not contain simple $U$ terms, but it does contain terms $\propto U^2$. If one uses equation (14) with the mentioned adjustments, one gets to second order in $U$ terms $\propto \Delta\Delta, \Delta U, U^2$ which contain all $U^2$ parts and therefore are a part of our order.
There is a smart way to adjust our notation to this fact. We do the following transformation:

$$\Delta^{\alpha}_{k,k',q} \to \Delta^{\alpha}_{k,k',q} - U^{\alpha}. \tag{23}$$

In that manner, we can neglect the bare interaction terms at the end of (16), but have them covered automatically with the right prefactors due to the transformation (23). For convenience and concise notation, we do not introduce a new symbol for that. For the rest of this work (unless explicitly stated otherwise), all double $\Delta$ terms $\Delta \cdot \Delta$ are to be understood with this transformation. Also, single $\Delta$ terms are meant like that if they are mentioned in a multi-boson context. In principle this change only affects numerically calculated values and not any derivation, equation forms, or the general physics. we can easily apply this change to constructing Feynman diagrams too, just think of the two Hedin vertices and the screened interaction between, adjusted by the bare interaction. That means, we can draw the same diagrams.
Now, in the following subchapters, the individual lowest order multi-boson part for each channel is calculated. For clarity, the structure, derivation, nomenclature, methods, and approach are first explained for the example of the vertical particle-hole channel (4.3) and then also applied to the horizontal particle-hole and particle-particle channels.

### 4.3. Vertical particle-hole channel contribution

By evaluating the BSE equation (14a) and taking only the single-boson terms in (16a), we obtain

$$
\begin{aligned}
L^{\overline{ph}}_{k,k',q} &= \frac{1}{(2\pi)^3\beta}\int dk''\left[-\frac{1}{2}S^{\mathrm{d}}_{k,k'',k'-k}G_{k''}G_{k''+k'-k}S^{\mathrm{d}}_{k'',k+q,k'-k}\right.\\
&\left.-\frac{3}{2}S^{\mathrm{m}}_{k,k\prime\prime,k'-k}G_{k''}G_{k''+k'-k}S^{\mathrm{m}}_{k'',k+q,k'-k}\right]\\
&= \int dk''\left[-\frac{1}{2}(-\frac{1}{2}\Delta^{\mathrm{d}}_{k,k\prime,k''-k}-\frac{3}{2}\Delta^{\mathrm{m}}_{k,k\prime,k''-k}+\frac{1}{2}\Delta^{\mathrm{s}}_{k,k'',k''+k\prime})\right.\\
&(-\frac{1}{2}\Delta^{\mathrm{d}}_{k'',k''+k\prime-k,k+q-k''}-\frac{3}{2}\Delta^{\mathrm{m}}_{k',k''+k'-k,k+q-k''}+\frac{1}{2}\Delta^{\mathrm{s}}_{k'',k+q,k''+q+k'})\\
&\left.G_{k''}G_{k''+k'-k}-\frac{3}{2}\ldots\right]\\
&= \frac{1}{N_{k''}\beta}\sum_{k''}\left[-\frac{1}{2}\right.\\
&(+\frac{1}{4}\Delta^{\mathrm{d}}_{k,k',k''-k}\Delta^{\mathrm{d}}_{k'',k''+k'-k,k+q-k''} && \leftarrow B_1\\
&+\frac{3}{4}\Delta^{\mathrm{d}}_{k,k',k''-k}\Delta^{\mathrm{m}}_{k'',k''+k'-k,k+q-k''} && \leftarrow B_2\\
&-\frac{1}{4}\Delta^{\mathrm{d}}_{k,k',k''-k}\Delta^{\mathrm{s}}_{k'',k+q,k''+q+k'} && \leftarrow B_3\\
&+\frac{3}{4}\Delta^{\mathrm{m}}_{k,k',k''-k}\Delta^{\mathrm{d}}_{k'',k''+k'-k,k+q-k''} && \leftarrow B_4\\
&+\frac{9}{4}\Delta^{\mathrm{m}}_{k,k',k''-k}\Delta^{\mathrm{m}}_{k'',k''+k'-k,k+q-k''} && \leftarrow B_5\\
&-\frac{3}{4}\Delta^{\mathrm{m}}_{k,k',k''-k}\Delta^{\mathrm{s}}_{k'',k+q,k''+q+k'} && \leftarrow B_6\\
&-\frac{1}{4}\Delta^{\mathrm{s}}_{k,k'',k''+k'}\Delta^{\mathrm{d}}_{k'',k''+k'-k,k+q-k''} && \leftarrow B_7\\
&-\frac{3}{4}\Delta^{\mathrm{s}}_{k,k'',k''+k'}\Delta^{\mathrm{m}}_{k'',k''+k'-k,k+q-k''} && \leftarrow B_8\\
&+\frac{1}{4}\Delta^{\mathrm{s}}_{k,k'',k''+k'}\Delta^{\mathrm{s}}_{k'',k+q,k''+q+k'}) && \leftarrow B_9\\
&\left.-\frac{3}{2}(\ldots)\right]G_{k''}G_{k''+k'-k}\\
&= \frac{1}{N_{k''}\beta}\sum_{k''}(-\frac{1}{2})\sum_{i=1}^{9}B_i-\frac{3}{2}(B_1-\frac{1}{3}B_2-B_3-\frac{1}{3}B_4+\frac{1}{9}B_5+\frac{1}{3}B_6-B_7+\frac{1}{3}B_8+B_9)\\
&= \frac{1}{N_{k''}\beta}\sum_{k''}-2B_1+B_3-\frac{2}{3}B_5-B_6+B_7-B_8-2B_9.
\end{aligned}
\tag{24}
$$

Because $S^{\mathrm{d}}$ and $S^{\mathrm{s}}$ have the same argument structure, we get the same terms with different prefactors. We label the double $\Delta$ terms simply with $B_1$ and so on[10]. If we sum up all terms, some of them cancel. This means some spin combinations for certain diagrams do not contribute to $L$ and therefore to the current-current correlation function and the optical conductivity. Every unique argument structure of the $\Delta$ terms corresponds to a unique multi-boson diagram for this channel. Each diagram has different spin combinations. It is to be noted that even though some spin combinations vanish, no complete diagram vanishes. At least one spin combination of a diagram is always left. This is true for all particle channels. Every particle channel has four unique diagrams. In the case of $\overline{ph}$ each group of terms $B_{1,2,4,5}, B_{3,6}, B_{7,8}, B_9$ represents a diagram.

### 4.3.1. Numerical evaluation

The formal integration over the four-momenta[11] in equation (24) is meant in frequency space as the Matsubara sum, since we use the Matsubara formalism. The integration of $\boldsymbol{k''}$ takes place over the first Brillouin zone $[0, 2\pi]$ and is substituted with a numerical integration, by using the trapezoidal-rule. Therefore, the integration goes over in a finite sum. By dividing the interval in $N$ steps of width $\Delta$, with $\Delta = \frac{2\pi}{N}$, we get rid of the prefactor $\frac{1}{(2\pi)^3}$ and are only left with the grid factors. The general grid factor $N_k$ depends on how many dimensions one calculates as well as the grid size in the specific dimension (it does not need to be equal for every dimension), thus we do not specify the grid factor further and just write in general $N_k$. Since our functions and quantities are $2\pi$ periodic, the $2\pi$ points are not calculated or are part of the numeric arrays[12]. Every k-space integration is handled like this. Note that the sum over the four-momenta is a shorthand notation, where we have a Matsubara sum and a numerical sum over a discrete k-space. It is common in this subject area to right away write a sum instead of an integral, like in (14), but one always have to keep in mind what is a real sum and what would be a formal integral.

### 4.3.2. Diagrammatic representation

The explicit diagrams which represent the algebraic formulas are now given. The equations below the diagrams represent the arguments of the specific quantity.

[10] E.g. $B_1^{ph} = +\frac{1}{4}\Delta^{\mathrm{d}}_{k,k',k''-k}\Delta^{\mathrm{d}}_{k'',k''+k'-k,k+q-k''}$ In this chapter, we do not use the particle channel index for $B$

[11] The prefactor for the four dimensional integration is $\frac{1}{(2\pi)^3\beta}$

[12] In that way the simple numeric integration gets even easier. The first and last points have factors of $0.5\Delta$, since they have equal values, one can rewrite it as just the first point without 0.5. Effectively, this leaves us with a sum over $k_i = 0, 2\pi - \Delta$, for one k dimension. Our integral approximation gets in total quite simple to just a sum over our discrete interval $[0, 2\pi)$ with the prefactor of $\frac{1}{N}$ for each momenta dimension.

**Diagram for** $B^{\overline{ph}}_{1,2,4,5}$

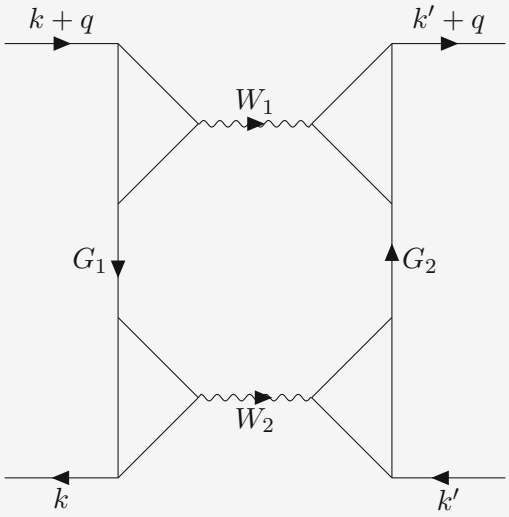


$$G_1 = k''$$
$$G_2 = k'' + k' - k$$
$$W_1 = k + q - k''$$
$$W_2 = k'' - k$$

$$\gamma_1 = k+q, -(k+q-k'') = k'', k+q-k''$$
$$\gamma_2 = k'', -(k''-k) = k, k''-k$$
$$\gamma_3 = k''+k'-k, -(k''-k) = k', k''-k$$
$$\gamma_4 = k'+q, -(k''+k+q) = k''+k'-k, k+q+k''$$

For the Hedin $\gamma$ vertices in every diagram, we used equation (19a) to get the same expressions as in (24), when needed. Keep in mind that for all diagrams there are other possible momentum and frequency parametrisations that fulfil the energy and momentum conservation, these are also valid solutions. We choose our solution in such a way that it matches the expressions calculated via the BSE. we can also find a solution where the free exchange momentum $k''$ has a bosonic character. The arguments of the Green's function or the screened interaction remain fermionic and bosonic, for example $G(k-k'')$ and $W(k''+q)$. This would be invalid if $k''$ is of fermionic character.

**Diagram for $B_{3,6}^{\overline{ph}}$**

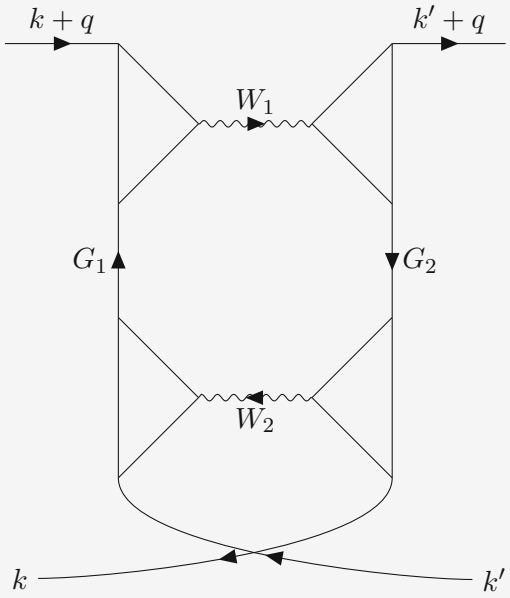


$$G_1 = k'' + k' - k$$
$$G_2 = k''$$
$$W_1 = k'' + q + k'$$
$$W_2 = k'' - k$$

$$\gamma_1 = k + q, k'' + q + k'$$
$$\gamma_2 = k', k'' - k$$
$$\gamma_3 = k, k'' - k$$
$$\gamma_4 = k' + q, k'' + q + k' = -k' - q + k'' + q + k', k'' + q + k' = k'', k'' + q + k'$$

Pay attention to the type of the Hedin vertex. For $\gamma_4$ of the diagram that belongs to $B_{3,6}^{\overline{ph}}$, we used the relation (19b) because gamma belongs to $\Delta^{\mathrm{s}}$ and is a pp vertex. The other Feynman diagrams are given here and in the following subchapters without additional commentary.

**Diagram for** $B_{7,8}^{\overline{ph}}$

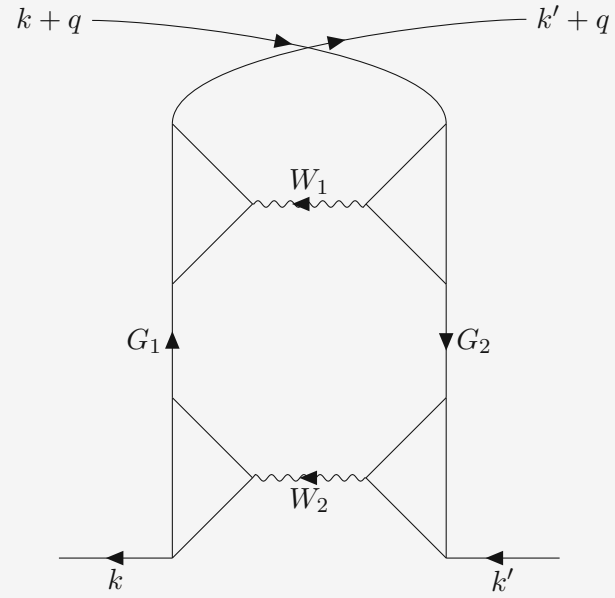


$$G_1 = k'' + k' - k$$
$$G_2 = k''$$
$$W_1 = k + q - k''$$
$$W_2 = k'' + k'$$

$$\gamma_1 = k'' + k' - k, k + q - k''$$
$$\gamma_2 = k'' + k' - k, k'' + k' = k, k'' + k'$$
$$\gamma_3 = k'', k'' + k'$$
$$\gamma_4 = k'', k + q - k''$$

**Diagram for $B_9^{\overline{ph}}$**

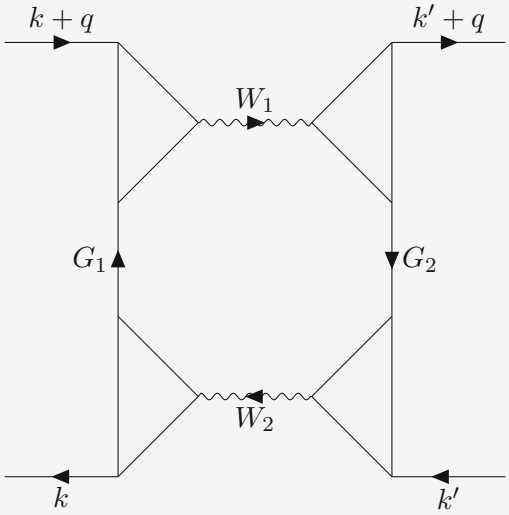


$$G_1 = k'' + k' - k$$
$$G_2 = k''$$
$$W_1 = k'' + q + k'$$
$$W_2 = k'' + k'$$

$$\gamma_1 = k + q, k'' + q + k'$$
$$\gamma_2 = k'' + k' - k, k'' + k' = -k'' - k' + k + k'' + k', k'' + k\prime = k, k'' + k'$$
$$\gamma_3 = k'', k'' + k'$$
$$\gamma_4 = k'' + q, k'' + q + k' = -k' - q + k' + q + k', k'' + q + k' = k'', k'' + q + k'$$

### 4.4. Particle-hole channel contribution

The particle-hole channel gives the following contribution:

$$
\begin{aligned}
L^{ph}_{k,k',q} &= \frac{1}{(2\pi)^3\beta}\int dk''\left[S^{\mathrm{d}}_{k,k'',q}G_{k''}G_{k''+q}S^{\mathrm{d}}_{k'',k',q}\right] \\
&= \int dk''\Bigg[(-\frac{1}{2}\Delta^{\mathrm{d}}_{k,k+q,k''-k} - \frac{3}{2}\Delta^{\mathrm{m}}_{k,k+q,k''-k} + \frac{1}{2}\Delta^{\mathrm{s}}_{k,k'',k+k''+q}) \\
&\quad (-\frac{1}{2}\Delta^{\mathrm{d}}_{k'',k''+q,k'-k''} - \frac{3}{2}\Delta^{\mathrm{m}}_{k'',k''+q,k'-k''} + \frac{1}{2}\Delta^{\mathrm{s}}_{k'',k',k''+k'+q}) \\
&\quad G_{k''}G_{k''+k'-k}] \\
&= \frac{1}{N_{k''}\beta}\sum_{k''}\Bigg[\frac{1}{4}\Delta^{\mathrm{d}}_{k,k+q,k''-k}\Delta^{\mathrm{d}}_{k'',k''+q,k'-k''} && \leftarrow B_1 \\
&\quad + \frac{3}{4}\Delta^{\mathrm{d}}_{k,k+q,k''-k}\Delta^{\mathrm{m}}_{k'',k''+q,k'-k''} && \leftarrow B_2 \\
&\quad - \frac{1}{4}\Delta^{\mathrm{d}}_{k,k+q,k''-k}\Delta^{\mathrm{s}}_{k'',k',k''+k'+q} && \leftarrow B_3 \\
&\quad + \frac{3}{4}\Delta^{\mathrm{m}}_{k,k+q,k''-k}\Delta^{\mathrm{d}}_{k'',k''+q,k'-k''} && \leftarrow B_4 \\
&\quad + \frac{9}{4}\Delta^{\mathrm{m}}_{k,k+q,k''-k}\Delta^{\mathrm{m}}_{k'',k''+q,k'-k''} && \leftarrow B_5 \\
&\quad - \frac{3}{4}\Delta^{\mathrm{m}}_{k,k+q,k''-k}\Delta^{\mathrm{s}}_{k'',k',k''+k'+q} && \leftarrow B_6 \\
&\quad - \frac{1}{4}\Delta^{\mathrm{s}}_{k,k'',k+k''+q}\Delta^{\mathrm{d}}_{k'',k''+q,k'-k''} && \leftarrow B_7 \\
&\quad - \frac{3}{4}\Delta^{\mathrm{s}}_{k,k'',k+k''+q}\Delta^{\mathrm{m}}_{k'',k''+q,k'-k''} && \leftarrow B_8 \\
&\quad + \frac{1}{4}\Delta^{\mathrm{s}}_{k,k'',k+k''+q}\Delta^{\mathrm{s}}_{k'',k',k''+k'+q}\Bigg] && \leftarrow B_9 \\
&\quad G_{k''}G_{k''+q} \\
&= \frac{1}{N_{k''}\beta}\sum_{k''}\sum_{i=1}^{9}B_i.
\end{aligned}
\tag{25}
$$

For the $ph$ channel, the unique argument combinations are $B_{1,2,4,5}, B_{3,6}, B_{7,8}, B_9$. No spin combination vanishes because there is just the density contribution.

**Diagram for** $B^{ph}_{1,2,4,5}$

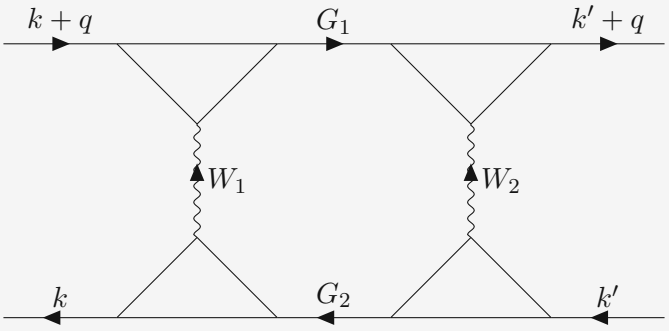


$$G_1 = k'' + q$$
$$G_2 = k''$$
$$W_1 = k'' - k$$
$$W_2 = k' - k''$$

$$\gamma_1 = k + q, k'' - k$$
$$\gamma_2 = k'', -(k'' - k) = k, k'' - k$$
$$\gamma_3 = k', -(k' - k'') = k'', k' - k''$$
$$\gamma_4 = k'' + q, k' - k''$$

**Diagram for** $B^{ph}_{3,6}$

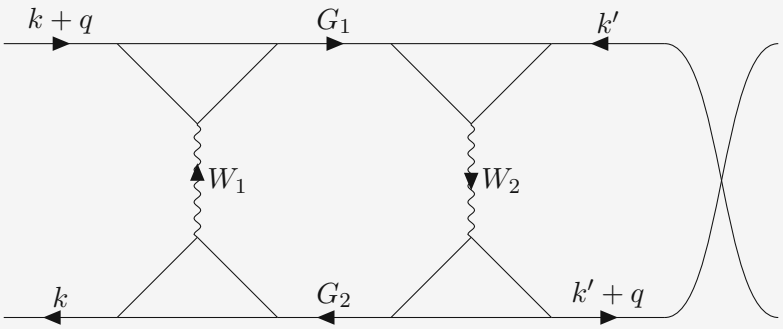


$$G_1 = k'' + q$$
$$G_2 = k''$$
$$W_1 = k'' - k$$
$$W_2 = k'' + k' + q$$

$$\gamma_1 = k + q, k'' - k$$
$$\gamma_2 = k'', -(k'' - k) = k, k'' - k$$
$$\gamma_3 = k' + q, k'' + k' + q = -k' - q + k'' + k' + q, k'' + k' + q = k'', k'' + k' + q$$
$$\gamma_4 = k', k'' + k' + q$$

**Diagram for** $B^{ph}_{7,8}$

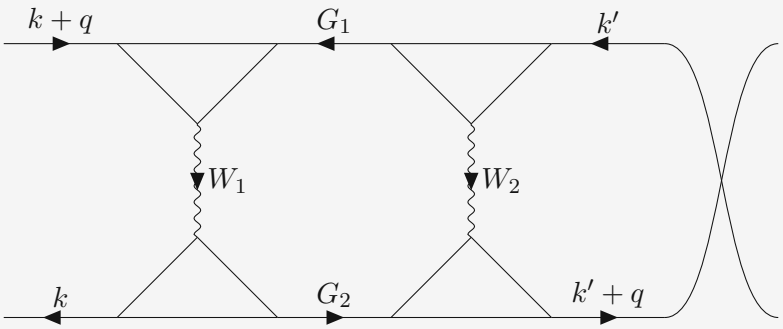


$$G_1 = k''$$
$$G_2 = k'' + q$$
$$W_1 = k + k'' + q$$
$$W_2 = k' - k''$$

$$\gamma_1 = k'', k + q + k''$$
$$\gamma_2 = k'' + q, k + q + k'' = -k'' - q + k + q + k'', k + q + k'' = k, k + q + k''$$
$$\gamma_3 = k'' + q, k' - k''$$
$$\gamma_4 = k', -(k' - k'') = k' - k' + k'', k' - k'' = k'', k' - k''$$

**Diagram for** $B_9^{ph}$

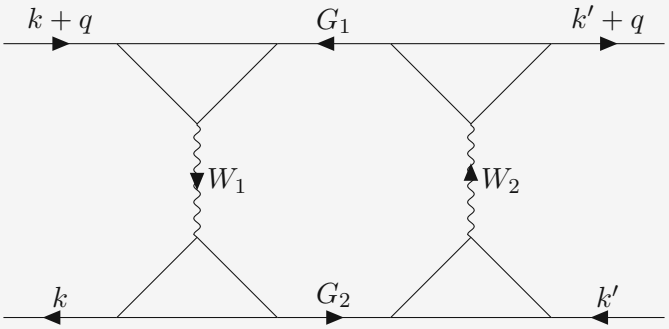


$$G_1 = k''$$
$$G_2 = k'' + q$$
$$W_1 = k + k'' + q$$
$$W_2 = k'' + q + k'$$

$$\gamma_1 = k'', k + q + k''$$
$$\gamma_2 = k'' + q, k + q + k'' = k, k + q + k''$$
$$\gamma_3 = k', k'' + k' + q$$
$$\gamma_4 = k' + q, k'' + k' + q = k'', k'' + k' + q$$

## 4.5. Particle-particle channel contribution

The particle-particle channel gives the following contribution:

$$
\begin{aligned}
L^{pp}_{k,k',q} &= \frac{1}{(2\pi)^3\beta}\int dk''\left[\frac{1}{2}(-1)S^{\mathrm{s}}_{k,k'',k+k'+q}G_{k''}G_{k+k'+q-k''}S^{\mathrm{s}}_{k'',k',k+k'+q}\right.\\
&\left.+\frac{3}{2}S^{\mathrm{t}}_{k,k'',k+k'+q}G_{k''}G_{k+k'+q-k''}S^{\mathrm{t}}_{k'',k',k+k'+q}\right]\\
&=\int dk''\left[-\frac{1}{2}(\frac{1}{2}\Delta^{\mathrm{d}}_{k,k'',k'+q-k''}-\frac{3}{2}\Delta^{\mathrm{m}}_{k,k'',k'+q-k''}\right.\\
&+\frac{1}{2}\Delta^{\mathrm{d}}_{k,k+k'+q-k'',k''-k}-\frac{3}{2}\Delta^{\mathrm{m}}_{k,k+k'+q-k'',k''-k})\\
&(\frac{1}{2}\Delta^{\mathrm{d}}_{k'',k',k+q-k''}-\frac{3}{2}\Delta^{\mathrm{m}}_{k'',k',k+q-k''}+\frac{1}{2}\Delta^{\mathrm{d}}_{k'',k+q,k'-k''}-\frac{3}{2}\Delta^{\mathrm{m}}_{k'',k+q,k'-k''})\\
&\left.+\frac{3}{2}(...)(...)\right]G_{k''}G_{k+k'+q-k''}\\
&=\frac{1}{N_{k''}\beta}\sum_{k''}\left[-\frac{1}{2}(\frac{1}{4}\Delta^{\mathrm{d}}_{k,k'',k'+q-k''}\Delta^{\mathrm{d}}_{k'',k',k+q-k''}\right. && \leftarrow B_1\\
&-\frac{3}{4}\Delta^{\mathrm{d}}_{k,k'',k'+q-k''}\Delta^{\mathrm{m}}_{k'',k',k+q-k''} && \leftarrow B_2\\
&+\frac{1}{4}\Delta^{\mathrm{d}}_{k,k'',k'+q-k''}\Delta^{\mathrm{d}}_{k'',k+q,k'-k''} && \leftarrow B_3\\
&-\frac{3}{4}\Delta^{\mathrm{d}}_{k,k'',k'+q-k''}\Delta^{\mathrm{m}}_{k'',k+q,k'-k''} && \leftarrow B_4\\
&-\frac{3}{4}\Delta^{\mathrm{m}}_{k,k'',k'+q-k''}\Delta^{\mathrm{d}}_{k'',k',k+q-k''} && \leftarrow B_5\\
&+\frac{9}{4}\Delta^{\mathrm{m}}_{k,k'',k'+q-k''}\Delta^{\mathrm{m}}_{k'',k',k+q-k''} && \leftarrow B_6\\
&-\frac{3}{4}\Delta^{\mathrm{m}}_{k,k'',k'+q-k''}\Delta^{\mathrm{d}}_{k'',k+q,k'-k''} && \leftarrow B_7\\
&+\frac{9}{4}\Delta^{\mathrm{m}}_{k,k'',k'+q-k''}\Delta^{\mathrm{m}}_{k'',k+q,k'-k''} && \leftarrow B_8\\
&+\frac{1}{4}\Delta^{\mathrm{d}}_{k,k+k'+q-k'',k''-k}\Delta^{\mathrm{d}}_{k'',k',k+q-k''} && \leftarrow B_9\\
&-\frac{3}{4}\Delta^{\mathrm{d}}_{k,k+k'+q-k'',k''-k}\Delta^{\mathrm{m}}_{k'',k',k+q-k''} && \leftarrow B_{10}\\
&+\frac{1}{4}\Delta^{\mathrm{d}}_{k,k+k'+q-k'',k''-k}\Delta^{\mathrm{d}}_{k'',k+q,k'-k''} && \leftarrow B_{11}\\
&-\frac{3}{4}\Delta^{\mathrm{d}}_{k,k+k'+q-k'',k''-k}\Delta^{\mathrm{m}}_{k'',k+q,k'-k''} && \leftarrow B_{12}\\
&-\frac{3}{4}\Delta^{\mathrm{m}}_{k,k+k'+q-k'',k''-k}\Delta^{\mathrm{d}}_{k'',k',k+q-k''} && \leftarrow B_{13}\\
&+\frac{9}{4}\Delta^{\mathrm{m}}_{k,k+k'+q-k'',k''-k}\Delta^{\mathrm{m}}_{k'',k',k+q-k''} && \leftarrow B_{14}\\
&-\frac{3}{4}\Delta^{\mathrm{m}}_{k,k+k'+q-k'',k''-k}\Delta^{\mathrm{d}}_{k'',k+q,k'-k''} && \leftarrow B_{15}\\
&\left.+\frac{9}{4}\Delta^{\mathrm{m}}_{k,k+k'+q-k'',k''-k}\Delta^{\mathrm{m}}_{k'',k+q,k'-k''}\right) && \leftarrow B_{16}
\end{aligned}
\tag{26}
$$

$$+\frac{3}{2}(...)\Big] G_{k''}G_{k+k'+q-k''}$$
$$= \frac{1}{N_{k''}\beta}\sum_{k''}\frac{-1}{2}\sum_{i=1}^{16}B_i + \frac{3}{2}(B_1 - \frac{1}{3}B_2 - B_3 + \frac{1}{3}B_4 - \frac{1}{3}B_5 + \frac{1}{9}B_6 + \frac{1}{3}B_7 - \frac{1}{9}B_8 - B_9 + \frac{1}{3}B_{10}$$
$$+ B_{11} - \frac{1}{3}B_{12} + \frac{1}{3}B_{13} - \frac{1}{9}B_{14} - \frac{1}{3}B_{15} + \frac{1}{9}B_{16})$$
$$= \frac{1}{N_{k''}\beta}\sum_{k''}B_1 - B_2 - 2B_3 - B_5 - \frac{1}{3}B_6 - \frac{2}{3}B_8 - 2B_9 + B_{11} - B_{12} - \frac{2}{3}B_{14} - B_{15} - \frac{1}{3}B_{16}.$$

In this channel $B_{1,2,5,6}$, $B_{3,4,7,8}$, $B_{9,10,13,14}$ and $B_{11,12,15,16}$ correspond to unique diagrams.

**Diagram for** $B^{pp}_{1,2,5,6}$

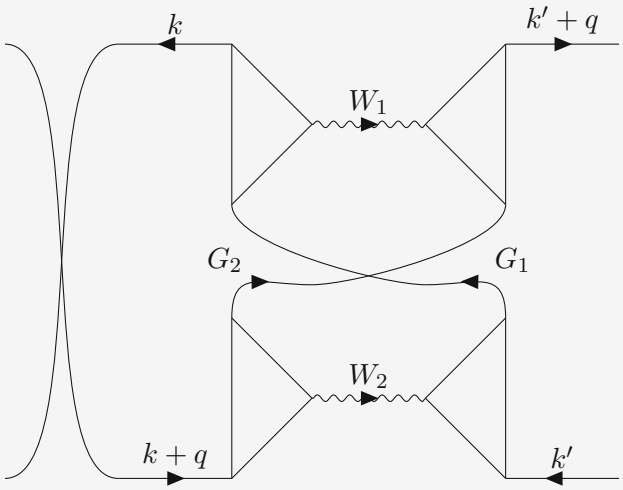


$$G_1 = k + k' + q - k''$$
$$G_2 = k''$$
$$W_1 = k' + q - k''$$
$$W_2 = k + q - k''$$

$$\gamma_1 = k + k' + q - k'', -(k' + q - k'') = k, k' + q - k''$$
$$\gamma_2 = k + q, -(k + q - k'') = k'', k + q - k''$$
$$\gamma_3 = k + k' + q - k'', -(k + q - k'') = k', k + q - k''$$
$$\gamma_4 = k' + q, -(k' + q - k'') = k'', k' + q - k''$$

**Diagram for** $B^{pp}_{3,4,7,8}$

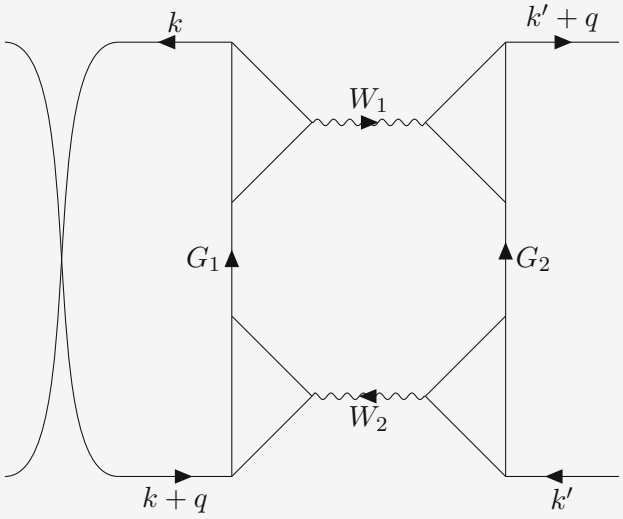


$$G_1 = k + k' + q - k''$$
$$G_2 = k''$$
$$W_1 = k' + q - k''$$
$$W_2 = k' - k''$$

$$\gamma_1 = k + k' + q - k'', -(k' + q - k'') = k, k' + q - k''$$
$$\gamma_2 = k + q, k' - k''$$
$$\gamma_3 = k'', k' - k''$$
$$\gamma_4 = k' + q, -(k' + q - k'') = k'', k' + q - k''$$

**Diagram for** $B^{pp}_{9,10,13,14}$

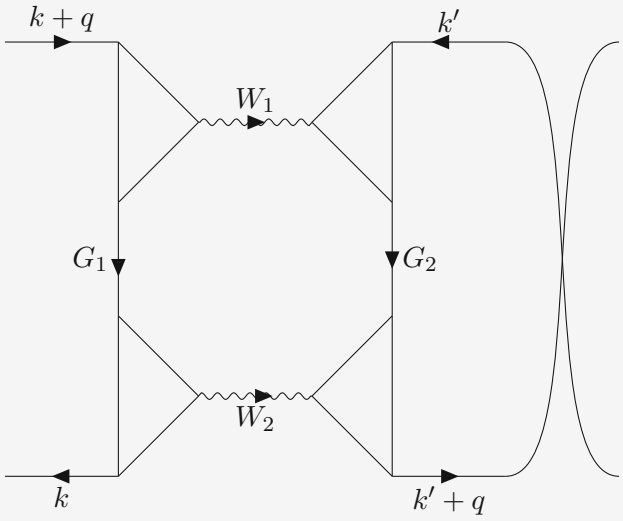


$$G_1 = k''$$
$$G_2 = k + k' + q - k''$$
$$W_1 = k + q - k''$$
$$W_2 = k'' - k$$

$$\gamma_1 = k+q, -(k+q-k'') = k'', k+q-k''$$
$$\gamma_2 = k'', -(k''-k) = k, k''-k$$
$$\gamma_3 = k'+q, -(k''-k) = k+k'+q-k'', k''-k$$
$$\gamma_4 = k+k'+q-k'', -(k+q-k'') = k', k+q-k''$$

**Diagram for** $B^{pp}_{11,12,15,16}$

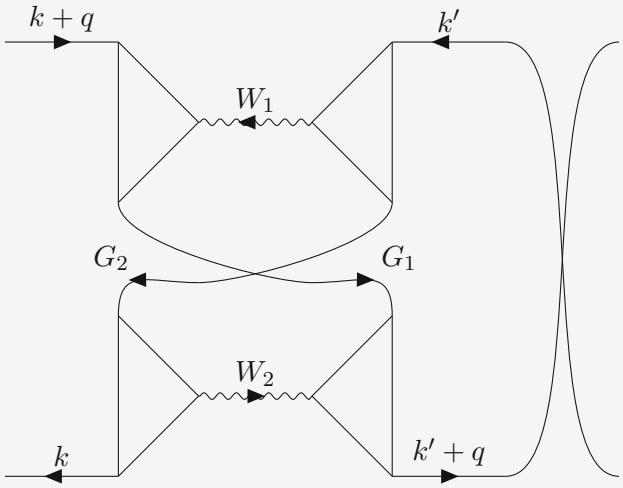


$$G_1 = k + k' + q - k''$$
$$G_2 = k''$$
$$W_1 = k' - k''$$
$$W_2 = k'' - k$$

$$\gamma_1 = k + q, k' - k''$$
$$\gamma_2 = k'', -(k'' - k) = k, k'' - k$$
$$\gamma_3 = k' + q, -(k'' - k) = k' + q - k'' + k, k'' - k$$
$$\gamma_4 = k'', k' - k''$$

# 5. Calculation of the current-current correlation function and its numerical implementation

For the current-current correlation function we include all terms up to the second order in the screened interaction and obtain equation (27):

$$\begin{aligned}\chi_{jj,\rho}(q) \approx & \frac{-2}{N\beta}\sum_{\boldsymbol{k},\nu}\left(y_\rho^{\boldsymbol{k}\frac{q}{2}}\right)^2 G_k G_{k+q} \\ & -\frac{2}{(N\beta)^2}\sum_{\boldsymbol{k},\nu,\boldsymbol{k'},\nu'} y_\rho^{\boldsymbol{k}\frac{q}{2}} y_\rho^{\boldsymbol{k'}\frac{q}{2}} G_k G_{k+q}\left(-\frac{1}{2}\Delta^{\mathrm{d},\overline{ph}}_{k,k+q,k'-k} - \frac{3}{2}\Delta^{\mathrm{m},\overline{ph}}_{k,k+q,k'-k} + \frac{1}{2}\Delta^{\mathrm{s},pp}_{k,k',k+k'+q}\right. \\ & \left. L^{ph}_{k,k',q} + L^{\overline{ph}}_{k,k',q} + L^{pp}_{k,k',q}\right) G_{k'+q} G_{k'}.\end{aligned} \tag{27}$$

We are also including in (27) the single-boson order, because we calculated it for code testing and benchmarking. we notice that for this order the particle-hole contribution is missing, this is because it does not contribute to the current-current correlation function out of symmetry reasons. If calculated, it will yield zero. Nonetheless, we are more interested on how the lowest order multi-boson part contributes to the current-current correlation function (12) relative to the bubble part and the full multi-boson order.
Now we have to evaluate the expressions. To remember, each $L$ has an internal sum over the exchange momentum and the frequency as well as several terms in the sum. They look as follows:

$$\begin{aligned}\frac{1}{N_{k''}\beta}\sum_{k''} B_1^{pp} &= \frac{1}{N_{k''}\beta}\sum_{k''}\frac{1}{4}\Delta^{\mathrm{d}}_{k,k'',k'+q-k''}\Delta^{\mathrm{d}}_{k'',k',k+q-k''} \\ &= \frac{1}{4}\frac{1}{N_{k''}\beta}\sum_{k''}(\gamma^{\mathrm{d}}_{k,k'+q-k''}W^{\mathrm{d}}_{k'+q-k''}\gamma^{\mathrm{d}}_{k'',k'+q-k''} - U^\alpha) \\ &\quad (\gamma^{\mathrm{d}}_{k'',k+q-k''}W^{\mathrm{d}}_{k+q-k''}\gamma^{\mathrm{d}}_{k',k+q-k''} - U^\alpha).\end{aligned}$$

We will solve the task of calculating the different contributions to the current-current correlation function numerically. For this evaluation, we still need the screened interaction and the Hedin vertex. Fortunately, we can fall back on the work [3] here. In this work, the screened interaction and the Hedin vertex, among other quantities, were calculated within a certain parameter regime by the use of parquet formalism with the multi-boson exchange approach. This data will serve as input, especially the screened interaction, the Hedin vertices and the self-energy. All data used for the input was generated with the approximation of $\Lambda^\alpha_{k,k',\omega} = \Lambda^\alpha_{\nu,\nu',\omega} = \Lambda^{\alpha,\mathrm{DMFT}}_{\nu,\nu',\omega}$. Another approximation is the so-called parquet approximation, where we substitute $\Lambda^\alpha_{k,k',\omega}$ simply with $U^\alpha$. The two approximations deliver similar results but only up to $U = 2t$, after this limit (in units of $t$) the differences between both are getting bigger.

## 5.1. Numerical implementation

For our program, we restrict ourselves to two dimensions in momentum space. The momentum grid is equally sized over an interval of $[0, 2\pi)$. All frequencies are implemented as Matsubara frequencies. Since various argument combinations appear within the equations[13] we have to choose the grid big enough and the sums correspondingly smaller, or we need boundary conditions. Periodic boundary conditions are used for the momenta and asymptotic values or formulas are used for the frequencies. Since the multi-boson vertex $L$ depends on nine single variables, storage and memory issues can arise (especially since we work with double precision and imaginary quantities, so the requested memory space doubles). Therefore, this quantity is calculated on the fly, as well as the Green's function. We calculate the Green's function via the Dyson equation, so the self-energy is needed:

$$G_k = \frac{1}{i\nu_n + \mu - \epsilon_{\boldsymbol{k}} - \Sigma_k},$$
$$\epsilon_{\boldsymbol{k}} = -2t(\cos(k_x) + \cos(k_y)),$$

($\epsilon_{\boldsymbol{k}}$ is the dispersion relation). Like the Hedin vertex and the screened interaction, the self-energy is pre-calculated as an array and fed into the program from a HDF5-file at the beginning of the code. For the array indices, boundary checks are implied and also a function to calculate the correct index from the real variable or from the grid index used in the program (because in general the grid differs from the one where these quantities are defined). For the periodicity, a function is used when needed. The derivative of the dispersion relation is calculated as an array, which we need for the light vertex, that is given here together with the thermodynamic beta:

$$y_\rho^{\frac{\boldsymbol{kq}=0}{2}} = \frac{\partial \epsilon_{\boldsymbol{k}}}{\partial k_\rho} = 2t\sin(k_\rho),$$
$$\beta = \frac{1}{T}.$$

[13] It is convenient in the frequency space to use the discrete Matsubara index for describing and noting frequency arguments. However, one has to keep attention in terms with several frequencies. E.g. $\nu_n + \nu_m = \omega_l = (2n+1)\frac{\pi}{\beta} + (2m+1)\frac{\pi}{\beta} = 2l\frac{\pi}{\beta}$, where the new index $l$ is not simply the sum of $n+l$, instead it is $l = n + m + 1$, the index is shifted. So one should always check frequency terms in this regard

As already mentioned, periodic boundaries are used for the three-momentum $\boldsymbol{k}$ , but for the frequency asymptotic values instead. In the case $\nu, \omega \to \pm\infty$ they look like:

$$\begin{aligned}
\gamma^{\mathrm{d}} &\to 1, \\
\gamma^{\mathrm{m}} &\to 1, \\
\gamma^{\mathrm{s}} &\to -1, \\
W^{\mathrm{d}} &\to U, \\
W^{\mathrm{m}} &\to -U, \\
W^{\mathrm{s}} &\to 2U, \\
G_k &\to \frac{1}{i\nu_n + \mu - \epsilon_{\boldsymbol{k}} - \frac{U}{2} n_p},
\end{aligned}$$

where $n_p$ is the average particle density (in the case of data from [2], $n_p = 0.5$).
For the initial photon frequency, $\omega$ we only consider non-negative values, because only this regime contributes to the current-current correlation function and the conductivity. The fermionic Matsubara frequencies are symmetrically distributed around zero, e.g. if the grid dimension is 4 we have $-3, -1, 1, 3$ times the corresponding factor as Matsubara frequencies. Since the Hedin vertex, the screened interaction and the self-energy are calculated for a finite grid, we are applying the asymptotic values when we exceed the boundary of the quantity. Throughout this thesis the grid size in frequency is for the Hedin vertex 32 fermionic and 31 for the bosonic argument, for the screened interaction 16, and for the self-energy 64.

The source code is written in Matlab. The base structure is an extensive function with inputs. The input is the data contained in the HDF5 file (passed by reference) and the name of the contribution one wants to calculate, e.g. "ph1" is the first contribution of the particle-hole channel. Within the function there are nested function out of practical programming reasons. Right at the beginning, dimensions, step widths and similar parameters are set. File names are created, one for the output and one for all information during the runtime. Array quantities are calculated, and then a case differentiation takes place. Basically, it will calculate the requested contribution by using furthermore several general argument dependent functions in loops. For the nine variables there have to be nine loops, they should be optimised. Results were not saved after the program is finished, but rather saved in steps during runtime.
There are 34 different contributions in total. A superordinated program will read in the HDF5 file and call the main function in a parallel loop. It will also pass the inputs to the function. In this manner, all contributions can be effectively calculated parallel. However, this program is not the head of the program order, there is one more short script. This script sets up the cluster parameters for the parallel computing, it also documents the process. The program as such then runs as a batch job in the script. In the end, each individual contribution is then calculated by a core alone and this at the same time (parallel). The computing was done at the Vienna Scientific Cluster (VSC). During the work on this project, the first order parts of the current-current correlation

function were also calculated. The same base script is used, the first order cases are included there. Just the file with the parallel loop (requests only the single-boson contributions to calculate) and the batch job file is different, slightly modified in comparison to the multi-boson scripts. For the bubble part of the current-current correlation function, the same program structure is used, though not needed in this manner. But when doing so we can calculate all the bubble, the first and the second order with the same base script. Therefore, just another case condition and macro function is implied. The bubble part is calculated after the equation (12).

# 6. Results

In this chapter, we will mainly focus on the example of the $U = 2$ data set. We will discuss in this example the relation between different contributions and their structure. Later we quickly discuss what changes with higher $U$ and we talk about an asymptotic approximation.
For the presented results, the calculations were done with various dimensions of the four-momenta space. The input data from the MBE parquet calculation [2] were obtained on the 16x16 momentum grid, 32 frequencies for $\gamma$ and $W$ and up to 128 frequencies for $G$. For the computation of the bubble part, we also used 16x16 grid in momenta and 128 frequencies, but for the multi-boson part, to reduce the computational effort, we took only 8x8 grid in momenta and 16 frequencies. In the case of first order, we took 16x16 in momenta and 16 in frequencies. In this case we have also checked that taking the 8x8 momentum grid does not lead to significant differences in the results for the value of $U$ and $\beta$ used. This was also confirmed in other calculations [3]. The output of the numerical code consists of 34 contributions of the form:

$$C_i^\alpha(q) \equiv -\frac{2}{N_k N_{k'} \beta^2} \frac{1}{N_{k''} \beta} \sum_{\boldsymbol{k},\boldsymbol{k'},\boldsymbol{k''},\nu,\nu',\nu''} y_\rho^{\boldsymbol{k}\frac{\boldsymbol{q}}{2}} y_\rho^{\boldsymbol{k'}\frac{\boldsymbol{q}}{2}} G_k G_{k+q} B_i^\alpha G_{k'+q} G_{k'}. \tag{31}$$

In the upcoming plots these contributions are ordered according to diagrams they are belonging to. In the plots for the total particle channel contributions, they are summed up to the total diagram contribution with their corresponding factor that appears in the last line of the equations (25), (24) and (26). We then also look at the first order contribution and the bubble part, and a comparison of all contributions.

$$
\begin{aligned}
D_1^{ph} &= C_1^{ph} + C_2^{ph} + C_4^{ph} + C_5^{ph}, \\
D_3^{ph} &= C_3^{ph} + C_6^{ph}, \\
D_7^{ph} &= C_7^{ph} + C_8^{ph}, \\
D_9^{ph} &= C_9^{ph}, \\
D_1^{\overline{ph}} &= -2C_1^{\overline{ph}} + 0C_2^{\overline{ph}} + 0C_4^{\overline{ph}} - \frac{2}{3}C_5^{\overline{ph}}, \\
D_3^{\overline{ph}} &= C_3^{\overline{ph}} - C_6^{\overline{ph}}, \\
D_7^{\overline{ph}} &= C_7^{\overline{ph}} - C_8^{\overline{ph}}, \\
D_9^{\overline{ph}} &= -2C_9^{\overline{ph}}, \\
D_1^{pp} &= C_1^{pp} - C_2^{pp} - C_5^{pp} - \frac{1}{3}C_6^{pp}, \\
D_3^{pp} &= -2C_3^{pp} + 0C_4^{pp} + 0C_7^{pp} - \frac{2}{3}C_8^{pp}, \\
D_9^{pp} &= -2C_9^{pp} + 0C_{10}^{pp} + 0C_{13}^{pp} - \frac{2}{3}C_{14}^{pp}, \\
D_{11}^{pp} &= C_{11}^{pp} - C_{12}^{pp} - C_{15}^{pp} - \frac{1}{3}C_{16}^{pp}.
\end{aligned}
\tag{32}
$$

## 6.1. U=2

The results were calculated with these parameters:

$$
\begin{aligned}
U &= 2, \\
t &= 1, \\
\beta &= 5, \\
\mu &= 1, \\
n_p &= 1.
\end{aligned}
\tag{33}
$$

### 6.1.1. Particle-hole channel

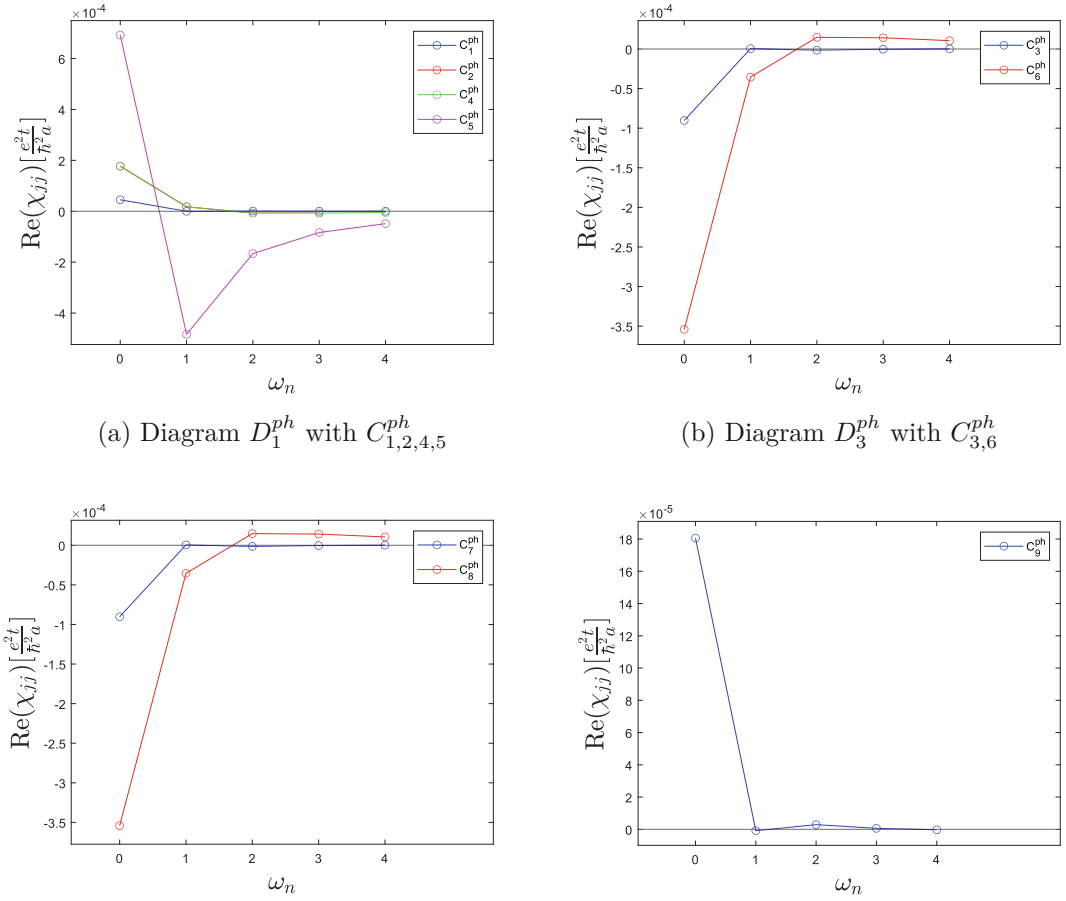


(a) Diagram $D_1^{ph}$ with $C_{1,2,4,5}^{ph}$

(b) Diagram $D_3^{ph}$ with $C_{3,6}^{ph}$

(c) Diagram $D_7^{ph}$ with $C_{7,8}^{ph}$

(d) Diagram $D_9^{ph}$ with $C_9^{ph}$

Figure 8: Particle-hole channel C contributions to the current-current correlation function, organised in their diagrams. See equation (31).

The general behaviour of all contributions is similar: There is a big contribution at the zeroth Matsubara frequency and then all diagrams go asymptotically towards zero. It can be recognised that the magnetic and singlet spin channel combinations yield greater contributions than others. These combinations of $\Delta$ terms are mm, ms, sm, and ss corresponding to $C_5^{ph}, C_6^{ph}, C_8^{ph}, C_9^{ph}$. In figure 8a the result for $C_2^{ph}$ is hidden behind that of $C_4^{ph}$, these contributions are very similar, but not totally equal. The relative difference is 0.19% and below.

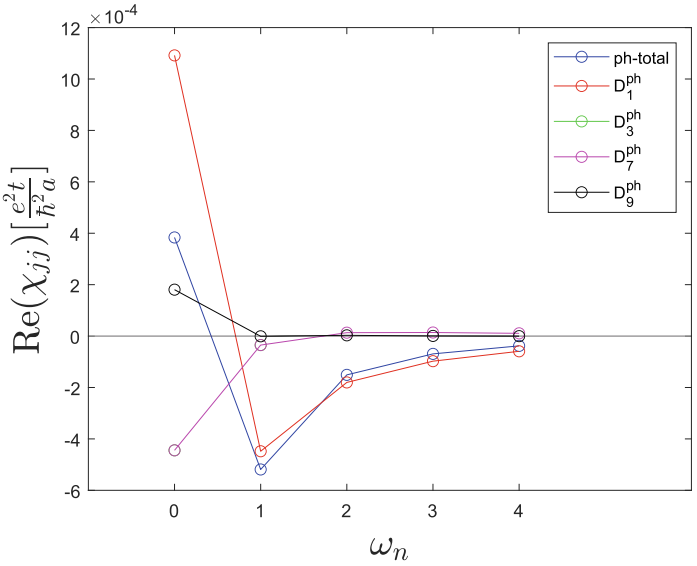


Figure 9: Graph of all contributions from the four diagrams ($D_i^{ph}$) of the particle-hole channel, where ph-total is the sum of the diagrams (see also equation (32)). The graph of $D_3^{ph}$ is hidden under $D_7^{ph}$.

In figure 9 we show that the biggest contribution comes from the $D_1^{ph}$ diagram, what means the process from diagram $B_{1,2,4,5}^{ph}$ is the most important one for the particle-hole channel. Again, one chart is hidden because the values are very similar ($D_3^{ph}, D_7^{ph}$).

### 6.1.2. Vertical particle-hole channel

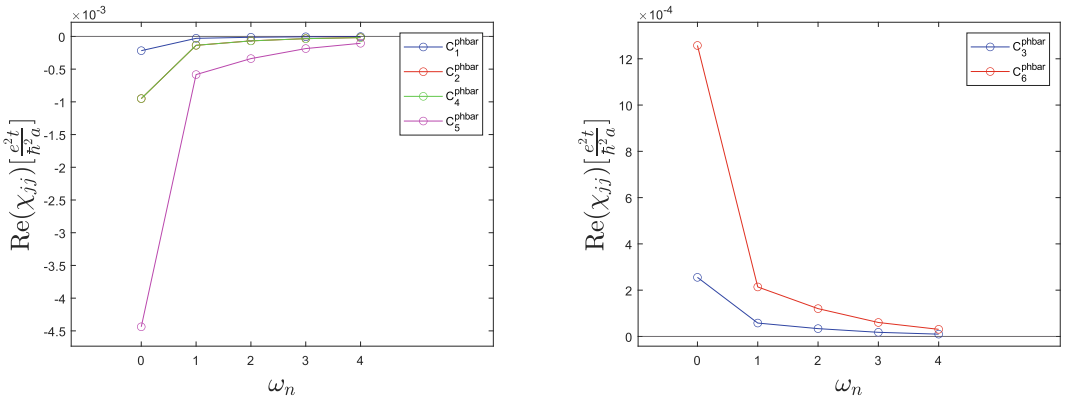


(a) Diagram $D_1^{\overline{ph}}$ with $C_{1,2,4,5}^{\overline{ph}}$




(b) Diagram $D_3^{\overline{ph}}$ with $C_{3,6}^{\overline{ph}}$

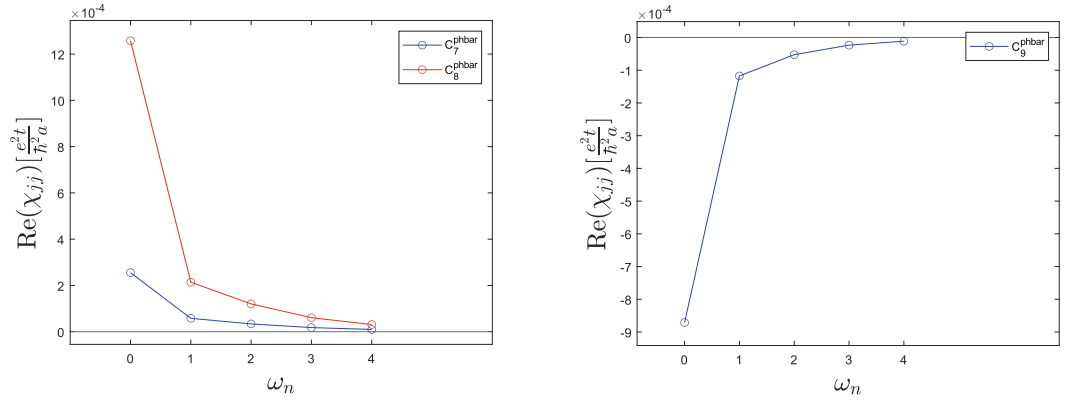


(c) Diagram $D_7^{\overline{ph}}$ with $C_{7,8}^{\overline{ph}}$




(d) Diagram $D_9^{\overline{ph}}$ with $C_9^{\overline{ph}}$

Figure 10: Vertical particle-hole channel C contributions to the current-current correlation function, organised in their diagrams. See equation (31).

The results for the vertical particle-hole channel posses the same general features and behaviour like the particle-hole channel (first point is the most important, then decay to zero, and magnetic and singlet spin combinations are dominant). The exact graphs are of course different, and overall the contributions are roughly one order of magnitude larger. In figure 10a the contribution of $C_2^{\overline{ph}}$ is hidden under the one from $C_4^{\overline{ph}}$
For the total diagram contributions and the total channel result, we have similar behaviour for the diagrams $D_3^{\overline{ph}}$ and $D_7^{\overline{ph}}$. The dominant diagram is $D_1^{\overline{ph}}$. A similar structure like this diagram, shows $D_9^{\overline{ph}}$. Note that the prefactors for the contributions of a diagram are different from the particle-hole channel ones, where they simply were 1. Overall, we can group our four diagrams in two groups with similar behaviour. One

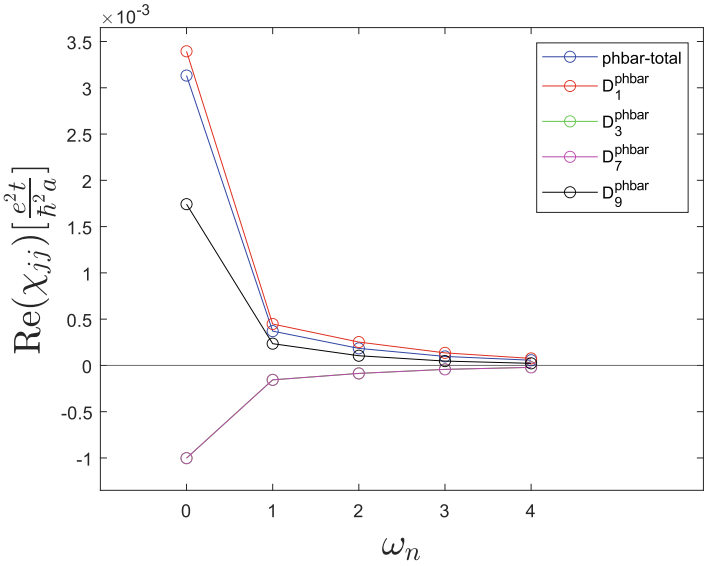


Figure 11: Graph of all contributions from the four diagrams ($D_i^{\overline{ph}}$) of the vertical particle-hole channel, where phbar-total is the sum of the contributions (see also equation (32)). The graph of $D_3^{\overline{ph}}$ is hidden under $D_7^{\overline{ph}}$.

group with a large positive first point and a steep fall afterward, another group with a smaller negative value for the first point and a less steep increase than the other group's decrease.

### 6.1.3. Particle-particle channel

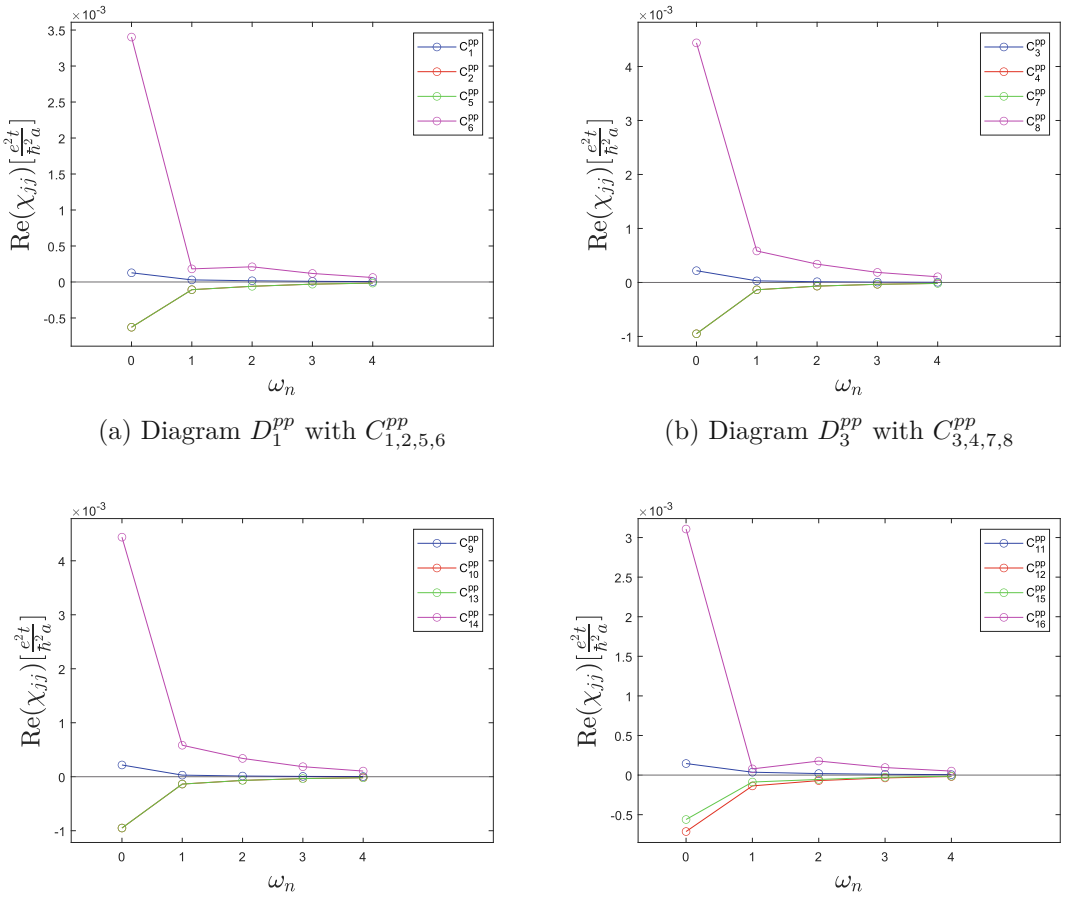


(a) Diagram $D_1^{pp}$ with $C_{1,2,5,6}^{pp}$

(b) Diagram $D_3^{pp}$ with $C_{3,4,7,8}^{pp}$

(c) Diagram $D_9^{pp}$ with $C_{9,10,13,14}^{pp}$

(d) Diagram $D_{11}^{pp}$ with $C_{11,12,15,16}^{pp}$

Figure 12: Particle-particle channel C contributions to the current-current correlation function, organised in their diagrams. See equation (31).

For the particle-particle channel, the behaviours differ from the vertical particle-hole and particle-hole channel. Firstly the grouping is different, instead of four diagrams with 4,2,2,1 spin combinations we get four diagrams with four spin combinations each. The next points is that the contributions to all diagrams look similar. Also for every diagram one contribution is not visible: It is the red contribution which is under the green one for all figures. It should be pointed out that the contributions are however not exactly equal. For every diagram in the lowest multi-boson order, the magnetic-magnetic spin combinations are very dominant in comparison to the other ones. The general magnitude of the particle-particle channel is comparable with the vertical particle-hole channel. The general tendency is as before, large first point and a decay towards zero, where the decay after the second point is quite linear for every graph, without bumps

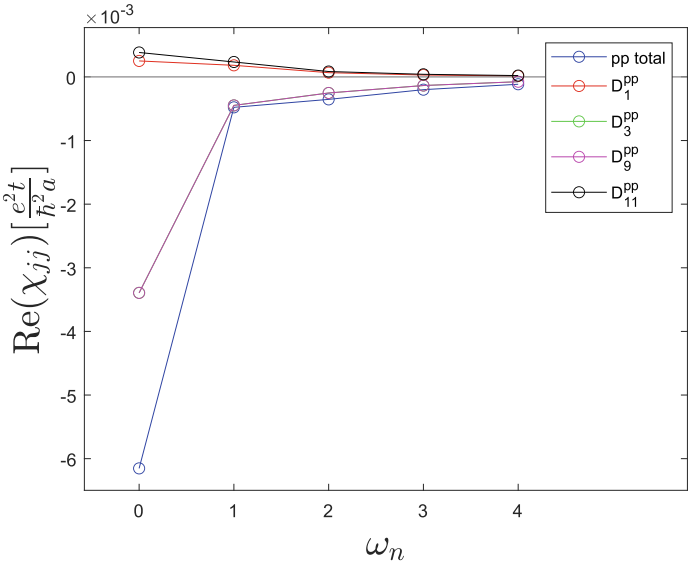


Figure 13: Graph of all contributions from the four diagrams ($D_i^{pp}$) of the particle-particle channel, where pp-total is the sum of the diagrams (see also equation (32)). The graph of $D_3^{pp}$ is hidden under the one from $D_9^{pp}$.

or other features, except for $C_{16}^{pp}$ and $C_6^{pp}$.

The total result for the particle-particle channel consist of two groups of similar contributions. That is, contributions itself are alike, but the prefactors for the total diagrams are different. They are the same for $D_1^{pp}, D_{11}^{pp}$ and $D_3^{pp}, D_9^{pp}$ which explains the two distinct groups. While $D_3^{pp}$ and $D_9^{pp}$ are almost identical and dominating, $D_1^{pp}, D_{11}^{pp}$ are smaller as well as more different to each other. For this different behaviour, we have not arrived at a proper understanding. This difference can also be observed for higher interaction values. It could simply be so that one of the diagrams is slightly larger, or it could be a finite size effect, but at this point we do not know it for sure. A finite size effect could have bigger influence than for other diagrams, since it has a complex argument structure. Every running grid variable has a fixed index range, but when combining them, the effective index range changes as well as the count of certain points. This is even more important for the frequency space since there is no periodic boundary condition like in the momentum space. This is the reason the summation of values changes, specific combinations get summoned up multiple times, and one gets also combinations (which are more or less dependent on the specific argument structure) which are out of the frequency box and therefore asymptotic values are used[14].

[14] E.g. we have two fermionic Matsubara frequencies $\nu_i, \nu_j \in [-15, 15]$ and $i, j \in [-8, 7]$. Now we add them, keeping the original value range the same. We get $\nu_i + \nu_j = \omega_k \in$[-30,30] and $k \in [-15, 15]$. So the effective index range and the value range of the frequency are increased. Also, we get multiple times the same value when running the indices i,j, e.g. $k = 8 = i + j + 1 = 3 + 4 + 1 = 4 + 3 + 1$. we

As for the total contribution of the particle-particle channel, it has a relatively large negative value for the first point, a big increase to the second point and a moderate linear decay towards zero (see figure 13).



get two times 8, one where i is 3 and j is 4 one where it changes. This indicates the influence of the argument combination on the calculation of the multi-boson contributions, and that for finite sizes these effects get more relevant, also depending on the specific argument structure.

### 6.1.4. Comparison of the full first and second order contributions

We have noticed several times that some graphs and contributions are looking quite similar, the reason is that there are mathematical relations connecting them. These relations, their influence, and derivations are discussed in appendix A, for an overview see the table 1 in appendix A. This is the mathematical background which supports the numerical evidence of certain similarities between some contributions.

Now we look at the single-boson contributions with nonzero value, figure 14, and the lowest multi-boson order[15] divided into the particle channel, figure 15. Furthermore, we have a look at a comparison between the bubble part and these orders, figure 16. The terms for the first order are looking like (31) except that the B terms are substituted by $-\frac{1}{2}\Delta^{\mathrm{d},\overline{ph}}_{k,k+q,k'-k}, -\frac{3}{2}\Delta^{\mathrm{m},\overline{ph}}_{k,k+q,k'-k}, \frac{1}{2}\Delta^{\mathrm{s},pp}_{k,k',k+k'+q}$. The particle-hole term is omitted because its contribution is zero for symmetry reasons. Calculating this, it is thus unnecessary. In figure 14 the data of this work is compared to the data from [3], to test if both codes produce the same values when calculating the same quantities. As we see, the data is in good agreement (the small numerical difference can be assigned to slightly different treatment of the asymptotic values in [3]). The contributions for each channel of the

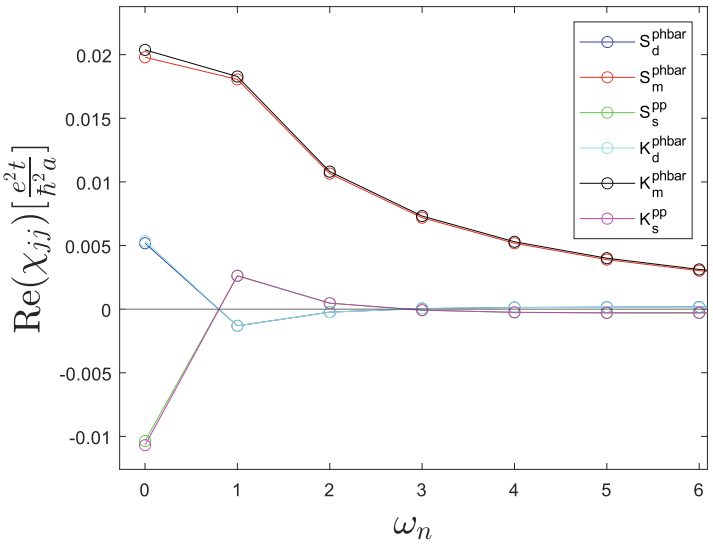


Figure 14: Comparison between the different single-boson (first order of $\chi_{jj}$) contributions. The $S$ terms are the contributions calculated in this work, while the K terms are from [3].

lowest multi-boson order are discussed already, now we compare them. As we can see in figure 15 the particle-hole channel is smaller than the others, which are in a similar

[15] The lowest multi-boson order is also called first multi-boson order, which is often used as label in the plots

regime. It is clearly seen that the vertical-particle hole channel and the particle-particle channel do not cancel each other fully. The latter one is a bit larger, in absolute terms. They all go fast towards zero. At last, it can be said that the total of the lowest multi-boson order has a smaller negative first point, goes faster to zero, does not feature such a large drop (absolute) from the first to the second point and also does not change its sign regarding the slope. In figure 16 we see that for the $U = 2$ case the vertex corrections

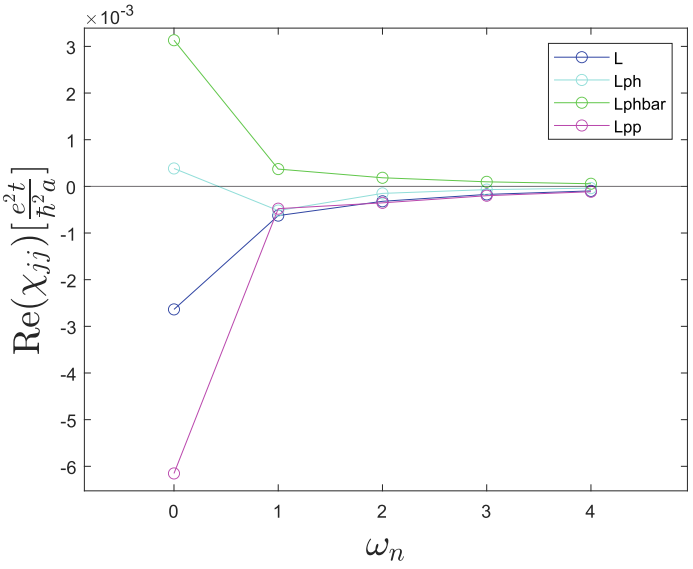


Figure 15: Comparison between the contributions of the different particle channels of the lowest multi-boson order $L$ to the current-current correlation function.

are both very small compared to the bubble part. It is not a surprise that the lowest multi-boson order is smaller than the single-boson order, in this weak coupling regime.

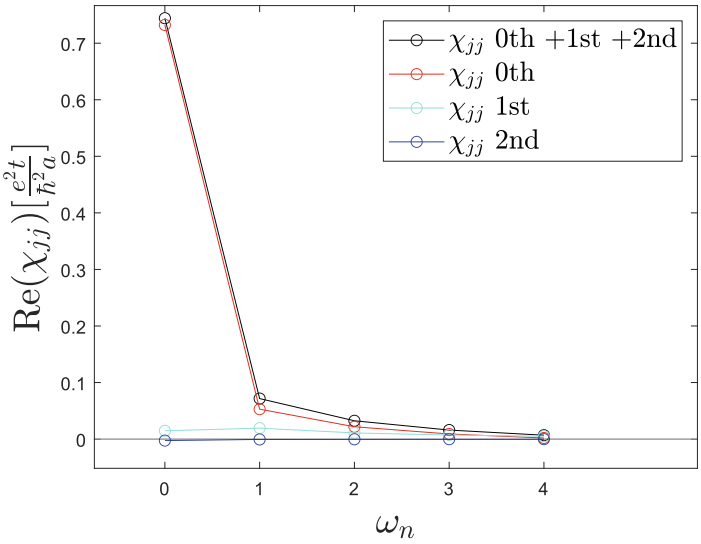


Figure 16: Comparison between the first three orders. The bubble part, 0th order, the single-boson part, first order, the lowest multi-boson part, the second order, for the current-current correlation function.

### 6.1.5. Comparison between the second-order and the full multi-boson contributions

To answer the question of how much the lowest multi-boson order contributes to the total higher order vertex corrections, we now compare the data of this work with the data of [3]. In [3] this total higher order (that means all except zeroth and first order) was calculated in a self-consistent loop scheme within the MBE-parquet approach [8]. In figure 17 we can see that the particle-hole channel is in good agreement. The vertical particle-hole channel is a bit smaller for the first point and less steep in the decrease, as the second point of the lowest multi-boson contributions is higher than the second point of the complete multi-boson order. When it comes to the particle-particle channel, the slope is quite equal to a certain degree. Overall, the pp contribution for the lowest multi-boson order is larger in absolute values, and there is a feature missing in it. Namely, the slope of the full multi-boson order is negative from point two to three (for the given temperature of $T = 0.2\mathrm{K}$) and changes then the sign back, while for the lowest multi-boson order it is always positive. In comparison to the vertical particle-hole channel, the particle-particle channel fits closer together. However, both of them are certainly not a very good approximation for the full multi-boson order, only the particle-hole channel is. The question that remains is how those contributions of the current-current correlation function translate to the optical conductivity. That can be answered only by analytically continuing the data to the real axis, which is a formidable task and beyond the scope of the current thesis.

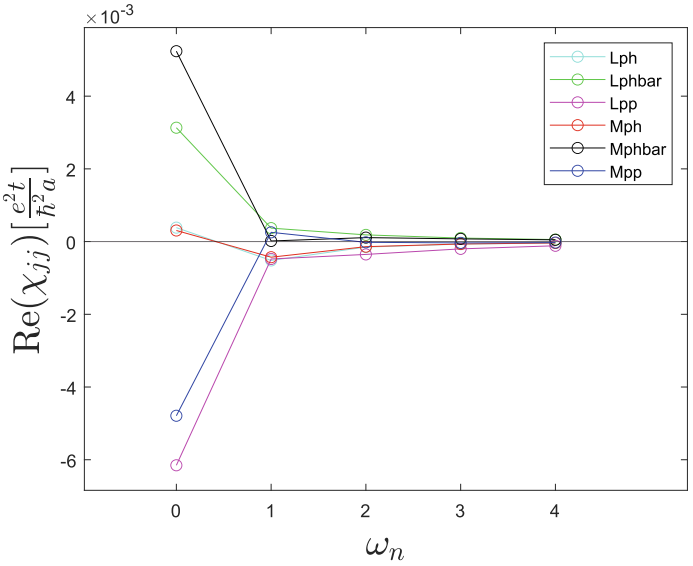


Figure 17: Comparison between the lowest multi-boson order $L$ and the complete multi-boson contribution $M$ from the full vertex function.

## 6.2. Higher U

Calculations with other data sets were also performed. Only $U$ and $\mu$ changed: $U = 3$, $\mu = 1.5$ and $U = 4$, $\mu = 2$. The same set of plots as for $U = 2$ is provided in appendix D.1 for $U = 3$ and in appendix D.2 for $U = 4$. Here we just present the comparison plots of the different particle channels and the overall contributions in different orders. The key takeaway messages are that the frequency dependencies of the respective contributions are similar to the $U = 2$ case. However, more steep and therefore some features become sharper. We get overall larger absolute values (also sign changes for some contributions which were near zero), what is not a surprise, but the first points are getting more pronounced in relation to the remaining points, i.e., the contributions become sharper at the $\omega_n = 0$ point. This is not only a fact for the $C$ terms, but also for the total and the contributions from the different particle channels. Another point is that for some spin combinations the contributions grow more with the interaction $U$ than for others, making certain contributions dominate their diagram more than for smaller interactions. In general, these are all contributions without the density spin channel involved. Whenever there is a density channel involved, the contribution becomes smaller.
Also, the particle-particle channel grows more than the vertical particle-hole channel, the deviation between them is getting bigger with the increase of the interaction. The terms do not cancel, contrary to the case of bare $U$ (see the next subchapter). With these results, I suspect that for $U \to 0$ they will be equal.
For $U = 3$ calculations were also made with the parquet approximation for the input data. This did not make a qualitative difference, just the quantitative deviation which

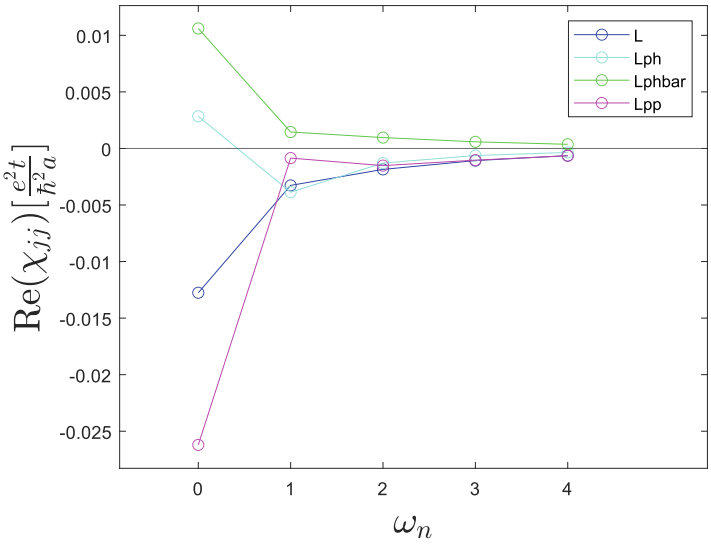


Figure 18: Comparison between the contributions of the different particle channels of the lowest multi-boson order $L$ for the $U = 3$ case.

is expected to occur between DΓA and the parquet approximation for this particular $U$ value.
At last, we look at the comparison in figure 22 between the lowest multi-boson orders for different $U$ strengths. For the most part the behaviour is as described before. Interesting is the development of clear features in the ph and the pp channel. For the ph channel we get a big drop, well below zero and a slower return to zero. A clearer minimum is therefore formed with higher $U$. For the pp channel it forms a clearer maximum at the second point, the line drops then to the third point, after which the values increase again. So we get in total a large negative value, a local maximum, followed by a minimum and then an almost linear course towards zero. For the $\overline{\text{ph}}$ channel, no feature builds up with higher $U$, just the slope for the lowest frequency points is getting bigger.

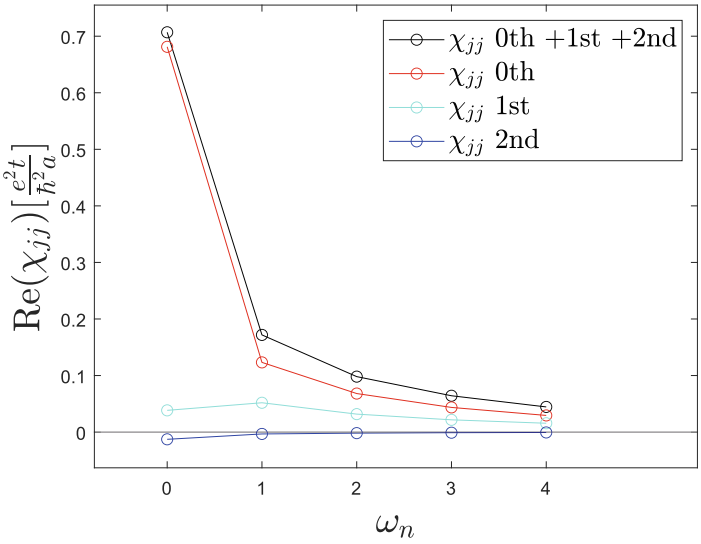


Figure 19: Comparison between the first three orders of the current-current correlation function for the $U = 3$ case.

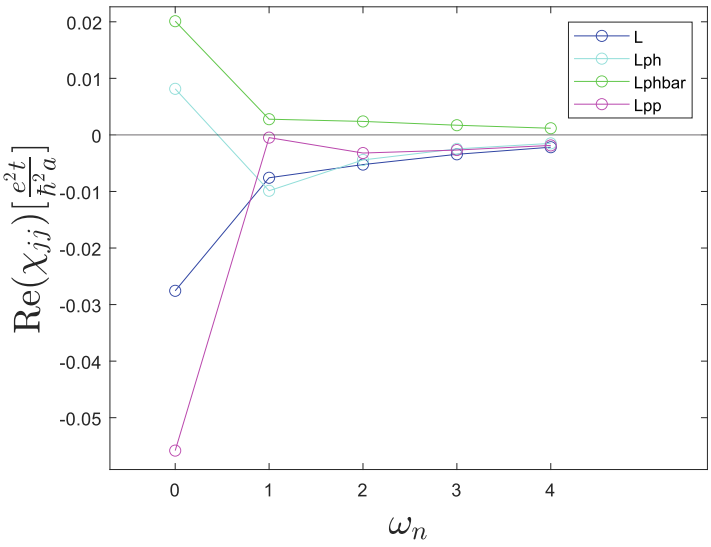


Figure 20: Comparison between the contributions of the different particle channels of the lowest multi-boson order $L$ for the $U = 4$ case.

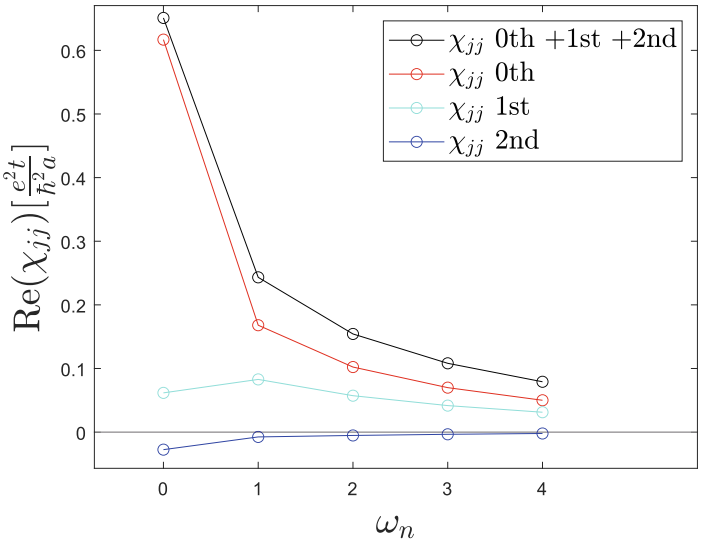


Figure 21: Comparison between the first three orders of the current-current correlation function for the $U = 4$ case.

## 6.3. Asymptotic approximation

Now we want to look on an approximation where the screened interaction and the Hedin vertices take constant values, which is their asymptotic behaviour. For this approximation we change the $\Delta$ terms back to their original form, so *for the asymptotic approximation $U$ is not subtracted from $\Delta$* ! With the approximation the $\Delta$ terms are reduced to $U$ if we then would subtract $U$ we get zero. So this approximation is in fact the bare interaction.
When we do this, in theory, the Feynman diagrams collapse which results in that every diagram within one particle channel has the same contribution, this means $D_i^\alpha = D_j^\alpha$ but not in general $C_i^\alpha = C_j^\alpha$. It is also expected that the particle-hole contribution is zero out of symmetry reasons. With $W$ and $\gamma = \text{const}$, just the outer and inner Green's functions are left. For the latter the symmetries of these functions ensure that the contribution vanishes. The inner Green's functions are different for each particle channel, therefore the other contributions are nonzero. However, the sum of the vertical particle-hole and the particle-particle channel should give zero for $q = 0$.
The data for the asymptotic approximation is calculated in the same way and for the same parameters as in 6.1, with $W$ and $\gamma$ substituted with their corresponding asymptotic values. Like expected, the particle-hole contribution is very small $< 10^{-17}$, which is below the machine precision and could for that be considered as numerically zero. One can also notice that in some cases for the higher frequency values, the values just fluctuate around zero. Because of the small values and the numerical fluctuation due to rounding errors a further analysis is unnecessary.

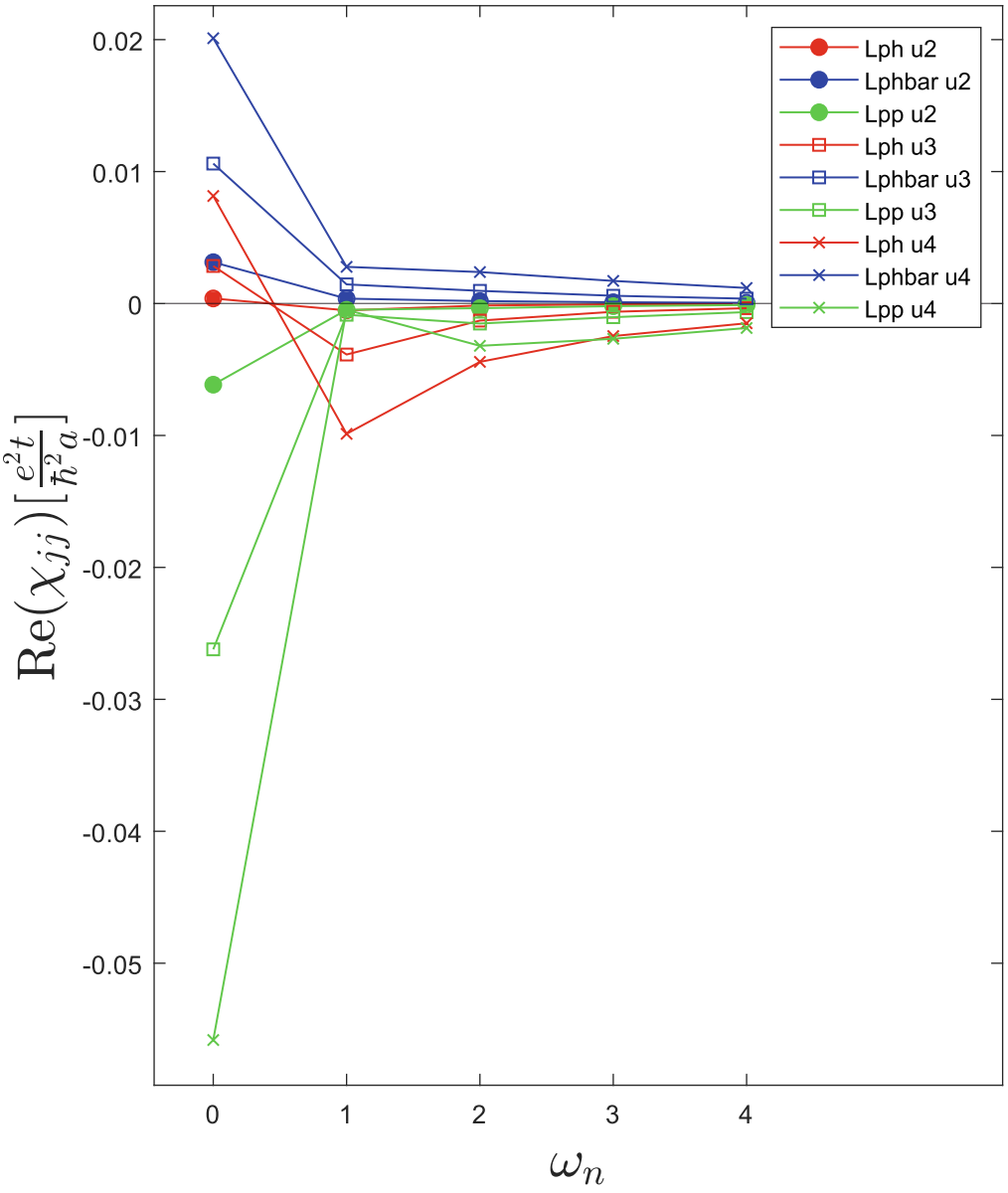


Figure 22: Comparison between the lowest order multi-boson contributions, divided in the different particle channels, for different values of $U$.

The general behaviour of the graphs in the asymptotic limit is sometimes similar to the original graphs, sometimes not. The important properties are the almost zero value

for the ph channel and that indeed $D_i^\alpha = D_j^\alpha$ is fulfilled for diagrams in all channels, although some values are very small. For the two other channels, it can be summarised that the frequency dependence of the total contributions in each channel is in decent agreement with the nonasymptotic ones. The values are, however, about one order of magnitude larger. The sum of the vertical particle-hole and the particle-particle channel is not exactly zero for the zeroth Matsubara frequency. Summed up and divided by either one of them, this relative error is $\approx -8.9 \cdot 10^{-8}$, which is in good agreement with the expectation regarding our achievable numerical precision and errors. For higher frequencies the value of the sum increases, the difference is getting bigger.
In the figure 23 we can see the total contributions of the diagrams in their channels and the comparison of all channels within the approximation to the nonasymptotic contributions is presented in figure 24. The difference in the order of magnitude is clearly visible. Out of these two figures, one can conclude that the asymptotic approximation mirrors badly the true lowest multi-boson order. If one tries to rescale the asymptotic values, the best scaling factor for pp and $\overline{\text{ph}}$ differs, even when using different scaling factors, the achievable match to the real data is not convincing. The results for larger $U$ are even worse. Additional plots for the asymptotic approximation can be found in appendix D.3.

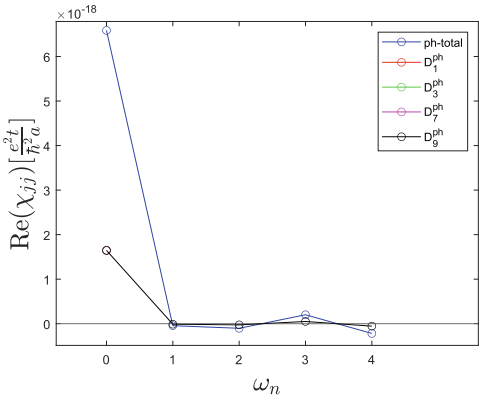


(a) All diagram contributions of the particle-hole channel

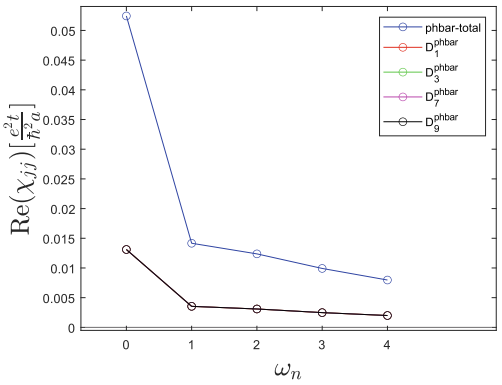


(b) All diagram contributions of the vertical particle-hole channel

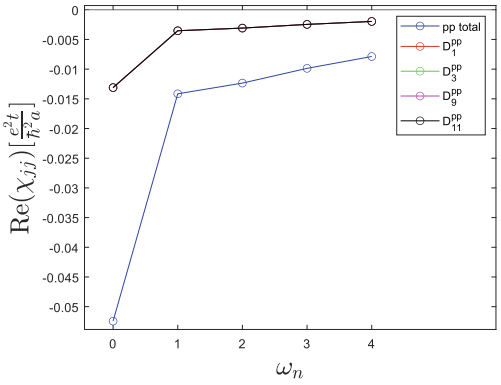


(c) All diagram contributions of the particle-particle channel

Figure 23: Graphs of the lowest multi-boson contributions within the asymptotic approximation. For the channel graphs, remember that all diagrams have the same contribution and therefore only one line is seen that hides the other lines.

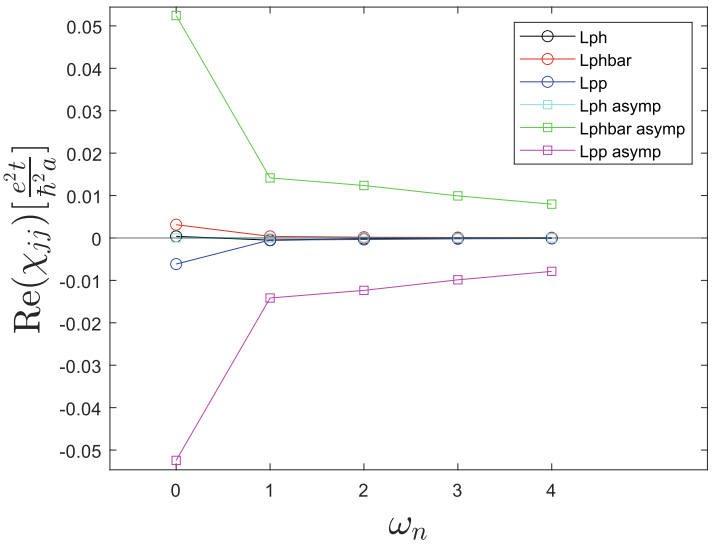


Figure 24: Comparison between the asymptotic approximation and without it, for the lowest multi-boson contributions.

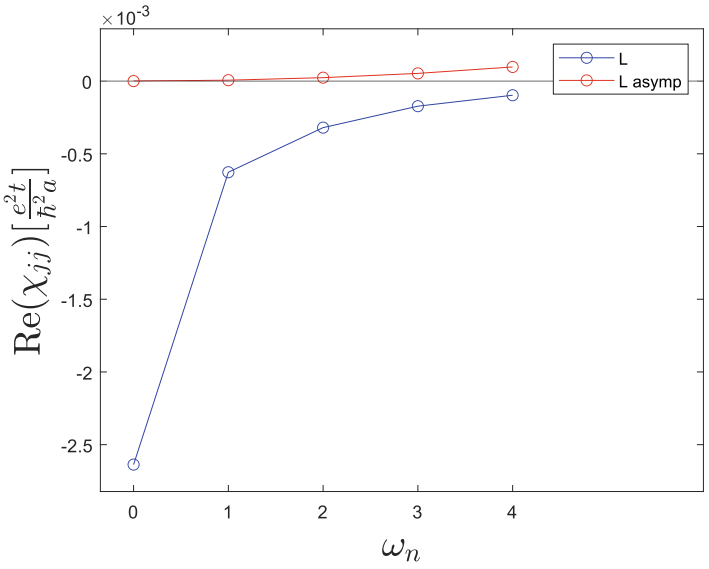


Figure 25: Comparison between the asymptotic approximation and without it, for the sum of the lowest multi-boson contributions.

# 7. Conclusion

In this thesis we have computed the lowest order multi-boson (MBE) contributions to the current-current correlation function. We have derived analytic formulas for all second order contributions (in the screened interaction), expressed in terms of the Green's function, screened interaction and the Hedin vertex $\gamma$. We have identified the derived formulas with the respective Feynman diagrams. The resulting equations have been applied to the case of the Hubbard model on a square lattice at half-filling and several values of the interaction with MBE parquet data from [3].

We have seen that the first (lowest) multi-boson order consists of twelve physical scattering processes in our MBE picture, and depicted these as Feynman diagrams. Each of the scattering processes have one or more possible spin combinations, which leads to a total of 34 contributions. We noticed similarities between contributions which can be explained on a theoretical basis, and we also noticed the dominance of terms without a density spin vertex part. The particle-particle contribution turned out to be the largest one out of the three and the vertical particle-hole contribution is of similar order of magnitude, but smaller. Those two contributions seem not to cancel exactly for a finite $U$. The ph channel is round about one order of magnitude smaller than the other channels and not to ignore, since the other channels are of similar size with different signs. In the derivation of the analytical terms we found out that not every spin combination contributes in the end to the current-current correlation function, anyway, the computational effort to calculate those expressions is serious. However, there is room to improve, the question is whether it is worth it in regard with full parquet calculations. For the asymptotic approximation, we could support theoretical claiming of a vanishing ph channel and with good probability an exact cancellation of the other two channels, for the first point. Besides this, the second order approximation has turned out to be insufficient to represent multi-boson contributions.
In the comparison with a full parquet calculation of the total multi-boson order, we discovered that only the particle hole channel was in reasonable agreement. The vertical particle-hole and particle-particle channel deviates for the significant points more than acceptable, but one can say that the full multi-boson contributions comes predominantly from the lowest order. In this regard, the vertical-particle hole channel is the worst out of the three, because the lowest order only contributes slightly more than 50 precent to the first point of the full multi-boson contribution, after that it would overestimate the full contribution which the ph channel does too. Excluding the zero frequency point, the lowest order is larger than the full order, except for the $n = 1$ point in the pp channel for $U = 3, 4$. The feature of changing slope sign, building small local extrema, can be seen for higher interaction values, where for the full order it can be recognised already for $U = 2$. The exception is the particle-hole channel, as mentioned before. These results are for the correlation function and not the optical conductivity, though. To obtain the optical conductivity, we have to perform an analytical continuation of our Matsubara data, which was no longer possible within the scope of this work. Then we could calculate

the conductivity and things may look different comparing the full multi-boson order to the lowest. This is a task for the future.

## References


[1] P. Pudleiner, "One-and two-particle vertex functions within monte carlo and parquet calculations of correlated electron systems", PhD thesis (Technische Universität Wien, 2019).

[2] F. Krien and A. Kauch, "The plain and simple parquet approximation: single- and multi-boson exchange in the two-dimensional Hubbard model", The European Physical Journal B **95**, 69 (2022).

[3] A. Kauch, "Single- and multi-boson contributions to optical conductivity in the 2d Hubbard model", (in preparation).

[4] R. D. Mattuck, *A guide to Feynman diagrams in the many-body problem*, Second (Dover Publications, Inc., New York, 1992).

[5] J. Hubbard, "Electron correlations in narrow energy bands iii. an improved solution", Proceedings of the Royal Society of London. Series A. Mathematical and Physical Sciences **281**, 401 (1964).

[6] G. Rohringer, "New routes towards a theoretical treatment of nonlocal electronic correlations", PhD thesis (Technische Universität Wien, 2013).

[7] L. Hedin, "New method for calculating the one-particle Green's function with application to the electron-gas problem", Physical Review **139**, A796 (1965).

[8] F. Krien, A. Kauch, and K. Held, "Tiling with triangles: parquet and GW$\gamma$ methods unified", Physical Review Research **3**, 013149 (2021).

[9] F. Krien, A. Valli, and M. Capone, "Single-boson exchange decomposition of the vertex function", Physical Review B **100**, 155149 (2019).

# A. Relations between multi-boson contributions

There are several relations between second-order multi-boson contributions one can derive under certain circumstances. By multi-boson contributions, their contribution to the current-current correlation function of the form (31) is meant. These relations are derived without the subtraction of $U$ from $\Delta$. To avoid misunderstandings, we label $B, C$ as $\tilde{B}$ and $\tilde{C}$ for this case. The relations originate from the Feynman diagrams, and the important quantity to look at is $\tilde{B}_i^\alpha$ since the other quantities in (31) stay the same for all contributions. The relations can be divided into two categories, one with relations between different Feynman diagrams and one within a Feynman diagram. The latter can be specified even further, since all relations are between density magnetic and magnetic density spin contributions. The relations themselves have in general the form of $\frac{\tilde{B}_i^\alpha}{\tilde{B}_j^\alpha} = \frac{W_k^\sigma}{W_{-k}^\sigma}$ and most of them are only valid for $q = 0$. The overview with all relations can be found at the end of this chapter in table (1). To verify the relations numerically, we would need the $B$ terms, but these are only calculated on the fly since they would require a large amount of memory space. Therefore, it is rather cumbersome to show it that way. Another point is that our observations of the diagram terms, which are the physically relevant quantities, are showing that the relations between the $B$ terms can in a certain way be translated into relations between the $C$ terms, which is not difficult to see (31). The question is how exactly the relations translate to the $C$ terms. Since the derivation is made with the $\Delta$s without subtracted $U$, the question is about the legitimacy of the following results. Several points are to be made: if the bare interaction is included, additional terms arise and the relations will have a different form. However, some of them will vanish in the sum of $C$ out of symmetry reasons, e.g. the result for $\Delta$ and $\Delta - U$ is equal in the particle hole channel. The next point is that the relations get summed up and some contributions cancel each other. Another point is that the numerical evidence of similarities between different $C_i^\alpha$ stays. At last the following derivation is not false, it is only not complete to some degree. As said, in some cases the effective relations given here are still holding true because additional terms caused by $\Delta \to \Delta - U$ disappear after the sum in $C$.
Now we look in detail on how the $\tilde{B}$ terms are connected to $\tilde{C}$:

$$\begin{aligned}
\frac{\tilde{C}_i^\alpha(q)}{\tilde{C}_j^\alpha(q)} &= \frac{\sum_{k,k',k''} y_\rho^{\boldsymbol{k}\frac{\boldsymbol{q}}{2}} y_\rho^{\boldsymbol{k'}\frac{\boldsymbol{q}}{2}} G_k G_{k+q} \tilde{B}_i^\alpha G_{k'+q} G_{k'}}{\sum_{k,k',k''} y_\rho^{\boldsymbol{k}\frac{\boldsymbol{q}}{2}} y_\rho^{\boldsymbol{k'}\frac{\boldsymbol{q}}{2}} G_k G_{k+q} \tilde{B}_j^\alpha G_{k'+q} G_{k'}} \\
&\underset{q\to 0}{=} \frac{\sum_{k,k',k''} y_\rho^{\boldsymbol{k}\frac{\boldsymbol{q=0}}{2}} y_\rho^{\boldsymbol{k'}\frac{\boldsymbol{q=0}}{2}} G_k G_k G_{k'} G_{k'} \tilde{B}_j^\alpha W_i^\sigma(p)/W_i^\sigma(-p)}{\sum_{k,k',k''} y_\rho^{\boldsymbol{k}\frac{\boldsymbol{q=0}}{2}} y_\rho^{\boldsymbol{k'}\frac{\boldsymbol{q=0}}{2}} G_k G_k G_{k'} G_{k'} \tilde{B}_j^\alpha} \\
\frac{\tilde{C}_i^\alpha(0)}{\tilde{C}_j^\alpha(0)} &\approx \frac{\sum_{k,k',k''} y_\rho^{\boldsymbol{k}\frac{\boldsymbol{q=0}}{2}} y_\rho^{\boldsymbol{k'}\frac{\boldsymbol{q=0}}{2}} G_k G_k G_{k'} G_{k'} \tilde{B}_j^\alpha}{\sum_{k,k',k''} y_\rho^{\boldsymbol{k}\frac{\boldsymbol{q=0}}{2}} y_\rho^{\boldsymbol{k'}\frac{\boldsymbol{q=0}}{2}} G_k G_k G_{k'} G_{k'} \tilde{B}_j^\alpha} \\
&= 1.
\end{aligned}$$

This derivation can be made in this manner for all relations. The argument $p$ stands for certain momenta combination. The important point is that the following applies to a square lattice:

$$W^{\sigma}_{-q} = W^{\sigma}_{-\boldsymbol{q},-\omega} = W^{\sigma}_{\boldsymbol{q},-\omega}.$$

With the general identity (19e) one can write this to:

$$\frac{W^{\sigma}_{q}}{W^{\sigma}_{-q}} = \frac{W^{\sigma}_{\boldsymbol{q},\omega}}{W^{\sigma}_{\boldsymbol{q},-\omega}} = \frac{W^{\sigma}_{\boldsymbol{q},\omega}}{W^{\sigma^*}_{\boldsymbol{q},\omega}} \approx 1.$$

Where we assume that the screened interaction has only a small imaginary part or is completely real, for the latter would yield exact 1. The deviation[16] from 1 (real part) is $2 \cdot \Im(W^{\sigma}_{q})^2$. If the imaginary part is small like $< 10^{-10}$ the deviation is $< 10^{-20}$ and negligible even if the numbre of summands in the total sum is high. For our dimensions, the upper sum would consist of $1.048576 \cdot 10^6$ summands. To make a significant impact on the result there have to be way more summands or the contribution from the other quantities have to be way larger. However it can be said that for a square lattice this approximation is always good for physical cases, the sums, the other quantities and the imaginary part of the screened interaction will be never that large to make a significant impact. There may be exceptions.
Since for our calculation the case of a square lattice applies we can validate our relations by looking at the differences of the $C$ terms[17], because this have to yield zero. That makes also sense because the similarity of contributions is that what is observed in the graphs for our physical multi-boson diagrams.
It has to be stressed that the derivation of the identities is independent from the lattice symmetry respectively the form of the light vertex and the dispersion relation as well as the Green's function etc., if there is a condition it is $q = 0$. On the other hand to evaluate how good these relations are fulfilled for our calculation and data we made an additional derivation fitting our explicit case, which was done above. So we can now effectively evaluate those relations with the differences of the $C$ terms which are also those terms we see in the plots and describing the Feynman diagram processes. To summarise it at this point how good the relations are fulfilled regarding the numerical data, they are in good agreement. The worst values for the relative differences are in the single digit percentage range, where the best value is an exact zero within the numerical precision. Surprisingly the relations hold up quite well for $\omega \neq 0$. Explanations and details can be found in the following chapter together with the derivations of the relations.

## A.1. Relations between contributions from different diagrams

In the analysis of the results for the different particle channels it is observed that some multi-boson contributions, $C$ terms, are almost equal. In fact for the optical conductivity, where $\boldsymbol{q} = 0$ applies, the almost equality of these terms can be shown when additionally

[16] $\frac{z}{z^*} = \frac{a^2-b^2-2ab\mathbf{i}}{a^2+b^2}$

[17] If we talk in these chapters about differences, or specific values have in mind that often the relative difference is meant

$\omega$ is set to zero (the case $\omega \neq 0$ and its consequences will be discussed at the end of the chapter). "Almost" means, that out of the lengthy terms just one quantity is slightly different, which results in a small difference. The important quantities to examine are the $\tilde{B}$ terms, since they contain the channel and diagram dependence. As shown above, for our explicit case, all relations would yield one, and they can be translated on to the $\tilde{C}$ respectively $C$ terms, which relative differences we compare to determine how good those relations are mirrored in the numerical data. However, the derivations are general and the only assumptions or approximations are marked as those, usually $q = 0$.

### $\tilde{B}^{ph}_{3,6}$ and $\tilde{B}^{ph}_{7,8}$

The almost equality is between 3 and 7 as well as 6 and 8. It follows the derivation for the first case:

$$\begin{aligned}
\tilde{B}^{ph}_{7} &= -\frac{1}{4}\Delta^{\mathrm{s}}_{k,k'',k+k''+q}\Delta^{\mathrm{d}}_{k'',k''+q,k'-k''} \rightarrow -\frac{1}{4}\Delta^{\mathrm{d}}_{k'',k'',k'-k''}\Delta^{\mathrm{s}}_{k,k'',k+k''} \\
&= -\frac{1}{4}\gamma^{\mathrm{d}}_{k'',k'-k''}W^{\mathrm{d}}_{k'-k''}\gamma^{\mathrm{d}}_{k'',k'-k''}\gamma^{\mathrm{s}}_{k,k+k''}W^{\mathrm{s}}_{k+k''}\gamma^{\mathrm{s}}_{k'',k+k''} \\
&= -\frac{1}{4}\gamma^{\mathrm{d}}_{k',k''-k'}W^{\mathrm{d}}_{k'-k''}\gamma^{\mathrm{d}}_{k',k''-k'}\gamma^{\mathrm{s}}_{k'',k+k''}W^{\mathrm{s}}_{k+k''}\gamma^{\mathrm{s}}_{k,k+k''} \\
&= -\frac{1}{4}\gamma^{\mathrm{d}}_{k,k''-k}W^{\mathrm{d}}_{k-k''}\gamma^{\mathrm{d}}_{k,k''-k}\gamma^{\mathrm{s}}_{k'',k'+k''}W^{\mathrm{s}}_{k\prime+k''}\gamma^{\mathrm{s}}_{k\prime,k'+k''}, \\
\tilde{B}^{ph}_{3} &= -\frac{1}{4}\gamma^{\mathrm{d}}_{k,k''-k}W^{\mathrm{d}}_{k''-k}\gamma^{\mathrm{d}}_{k,k''-k}\gamma^{\mathrm{s}}_{k'',k'+k''}W^{\mathrm{s}}_{k\prime+k''}\gamma^{\mathrm{s}}_{k\prime,k'+k''}, \\
\tilde{B}^{ph}_{3}/\tilde{B}^{ph}_{7} &= W^{\mathrm{d}}_{k''-k}/W^{\mathrm{d}}_{k-k''}.
\end{aligned}$$

For the derivation properties of the hedin vertices (19a) are used and a variable transformation as last step for 7 ($k \rightarrow k', k' \rightarrow k$). Contribution 3 is unchanged except $q = 0$. As one can see, only one term of the screened interaction is different, where the argument changes sign. For $\tilde{B}^{ph}_{8}$ and $\tilde{B}^{ph}_{6}$ the derivation is analogous, since the argument structure is equal, only the spin indices and the prefactor are changing, but this makes no difference for the calculation.

### $\tilde{B}^{\overline{ph}}_{3,6}$ and $\tilde{B}^{\overline{ph}}_{7,8}$

Here also $\tilde{B}^{ph}_{8}$ and $\tilde{B}^{ph}_{6}$ are similar as well as $\tilde{B}^{ph}_{3}$ and $\tilde{B}^{ph}_{7}$. For the latter we derive ($q = 0$):

$$
\begin{aligned}
\tilde{B}_3^{\overline{ph}} &= -\frac{1}{4}\Delta^{\mathrm{d}}_{k,k',k''-k}\Delta^{\mathrm{s}}_{k'',k,k''+k'} \\
&= -\frac{1}{4}\gamma^{\mathrm{d}}_{k,k''-k}W^{\mathrm{d}}_{k''-k}\gamma^{\mathrm{d}}_{k',k''-k}\gamma^{\mathrm{s}}_{k'',k''+k'}W^{\mathrm{s}}_{k''+k'}\gamma^{\mathrm{s}}_{k,k''+k'} \\
&= -\frac{1}{4}\gamma^{\mathrm{d}}_{k'',k-k''}W^{\mathrm{d}}_{k''-k}\gamma^{\mathrm{d}}_{k'+k''-k,k-k''}\gamma^{\mathrm{s}}_{k,k''+k'}W^{\mathrm{s}}_{k''+k'}\gamma^{\mathrm{s}}_{k'',k''+k'}, \\
\tilde{B}_7^{\overline{ph}} &= -\frac{1}{4}\Delta^{\mathrm{s}}_{k,k'',k''+k'}\Delta^{\mathrm{d}}_{k'',k''+k'-k,k-k''} \\
&= -\frac{1}{4}\gamma^{\mathrm{d}}_{k'',k-k''}W^{\mathrm{d}}_{k-k''}\gamma^{\mathrm{d}}_{k''+k'-k,k-k''}\gamma^{\mathrm{s}}_{k,k''+k'}W^{\mathrm{s}}_{k''+k'}\gamma^{\mathrm{s}}_{k'',k''+k'}, \\
\tilde{B}_3^{\overline{ph}}/\tilde{B}_7^{\overline{ph}} &= W^{\mathrm{d}}_{k''-k}/W^{\mathrm{d}}_{k-k''}.
\end{aligned}
$$

Again, the derivation for $\tilde{B}_6^{\overline{ph}}$ and $\tilde{B}_8^{\overline{ph}}$ is analogue. Like in the particle-hole case, the expressions differ by one screened interaction term in the density channel with just reversed signs.

### $\tilde{B}^{pp}_{1,2,5,6}$ and $\tilde{B}^{pp}_{11,12,15,16}$, $\tilde{B}^{pp}_{3,4,7,8}$ and $\tilde{B}^{pp}_{9,10,13,14}$

For the particle-particle case we have more contributions, also more contributions with this certain behaviour we investigate. Like before we set $q = 0$. For $\tilde{B}^{pp}_{1,2,5,6}$ and $\tilde{B}^{pp}_{11,12,15,16}$ we pick the contributions 1 and 11 for the derivation:

$$
\begin{aligned}
\tilde{B}_{11}^{pp} &= \frac{1}{4}\gamma^{\mathrm{d}}_{k,k''-k}W^{\mathrm{d}}_{k''-k}\gamma^{\mathrm{d}}_{k+k'-k'',k''-k}\gamma^{\mathrm{d}}_{k'',k'-k''}W^{\mathrm{d}}_{k'-k''}\gamma^{\mathrm{d}}_{k,k'-k''} \\
&= \frac{1}{4}\gamma^{\mathrm{d}}_{k'',-k''+k}W^{\mathrm{d}}_{k''-k}\gamma^{\mathrm{d}}_{k\prime,-k''+k}\gamma^{\mathrm{d}}_{k'',k'-k''}W^{\mathrm{d}}_{k'-k''}\gamma^{\mathrm{d}}_{k,k'-k''} \\
&= \frac{1}{4}\gamma^{\mathrm{d}}_{k'',k'-k''}W^{\mathrm{d}}_{k''-k'}\gamma^{\mathrm{d}}_{k,k'-k''}\Delta^{\mathrm{d}}_{k'',k',k-k''}, \\
\tilde{B}_{1}^{pp} &= \frac{1}{4}\gamma^{\mathrm{d}}_{k'',k'-k''}W^{\mathrm{d}}_{k'-k''}\gamma^{\mathrm{d}}_{k,k'-k''}\Delta^{\mathrm{d}}_{k'',k',k-k''}, \\
\tilde{B}_1^{pp}/\tilde{B}_{11}^{pp} &= W^{\mathrm{d}}_{k'-k''}/W^{\mathrm{d}}_{k''-k'}.
\end{aligned}
$$

A variable transformation was used ($k \to k', k' \to k$). For the other pairs, 2 and 12, 5 and 15, 6 and 16 the derivation is similar, just the prefactor and the spin indices are changing.
Next follows the derivation for the other diagram pair on the basis of $\tilde{B}_3^{pp}$ and $\tilde{B}_9^{pp}$:

$$
\begin{aligned}
\tilde{B}_9^{pp} &= \gamma^{\mathrm{d}}_{k,k''-k}W^{\mathrm{d}}_{k''-k}\gamma^{\mathrm{d}}_{k+k'-k'',k''-k}\Delta^{\mathrm{d}}_{k'',k',k-k''} \\
&= \gamma^{\mathrm{d}}_{k'',k-k'}W^{\mathrm{d}}_{k''-k}\gamma^{\mathrm{d}}_{k',k-k''}\Delta^{\mathrm{d}}_{k'',k',k-k''} \\
&= \gamma^{\mathrm{d}}_{k'',k'-k''}W^{\mathrm{d}}_{k''-k'}\gamma^{\mathrm{d}}_{k,k'-k''}\Delta^{\mathrm{d}}_{k'',k,k'-k''}, \\
\tilde{B}_3^{pp} &= \gamma^{\mathrm{d}}_{k'',k'-k''}W^{\mathrm{d}}_{k'-k''}\gamma^{\mathrm{d}}_{k,k'-k''}\Delta^{\mathrm{d}}_{k'',k,k'-k''}, \\
\tilde{B}_3^{pp}/\tilde{B}_9^{pp} &= W^{\mathrm{d}}_{k'-k''}/W^{\mathrm{d}}_{k''-k'}.
\end{aligned}
$$

We get a similar result as before. Another noticeable fact is that the diagram terms $\tilde{B}^{pp}_{1,2,5,6}$, $\tilde{B}^{pp}_{9,10,13,14}$, $\tilde{B}^{pp}_{11,12,15,16}$ and $\tilde{B}^{pp}_{3,4,7,8}$ share one Delta term with each other (in our $q = 0$ case). For example, the first Delta of $\tilde{B}^{pp}_{1}$ is the same as the first one in $\tilde{B}^{pp}_{3}$ and the second in $\tilde{B}^{pp}_{9}$ and $\tilde{B}^{pp}_{11}$. Also the argument structure is similar. These points explain that not only graphs of $C^{pp}_{1,2,5,6}$ $C^{pp}_{9,10,13,14}$ look similar but that all graphs for pp diagrams look similar, even though there are no relations linking contributions from $\tilde{B}^{pp}_{1,2,5,6}$ to $\tilde{B}^{pp}_{3,4,7,8}$ etc. on the same level as written in this chapter. The case of $\omega \neq 0$ and why its influence is only minor is discussed below.

As one can see, all these relations have the same pattern. They are between different Feynman diagrams and use $q = 0$. The result is that the difference is in a screened interaction in the density spin channel, where the argument has an opposite sign. With the summation over the momentum and frequency space as well as the fact that the density screened interaction has the smallest value range out of the screened interactions, the deviations between the contributions are small. Remember, they have the form of (31) and only differ in one screened interaction.
For the calculation in the optical conductivity regime $\boldsymbol{q} = 0$ applies but not $\omega = 0$, so these relations are only valid for the zero-frequency points. The question is now how the relation or a difference between those contributions will behave when $\omega \neq 0$. When looking at the data the answer is, they behave differently. The particle-hole relation $3, 7$ is fluctuating strong around $10^{-4}$, where $6, 8$ is getting smaller with frequency $10^{-5} \to 10^{-6}$. For the vertical particle-hole channel $3, 7$ becomes smaller by half an order of magnitude starting from $10^{-5}$, where $6, 8$ becomes larger by two and a half orders of magnitude starting from $10^{-5}$. For the particle-particle channel, $1, 11$ and $5, 15$ became half an order of magnitude smaller starting with $10^{-2}$. The relation for $2, 12$ and $6, 16$ shows no trend in the relative difference, they stay in the $10^{-2}$ regime. It seems counter-intuitive that the difference in some cases is getting smaller, but more things have to be considered. The particle-hole channel is smaller than the others. The data set is for $U = 2t = 2$. The relations still hold for the k-space, only one dimension (frequency) is violated. The sums over the momentum and frequency space will even things out, summands will cancel each other out in parts. The contributions are in general not very big, and they go with higher $\omega$ against zero. Although the deviation gains more importance with higher $\omega$, the values are also getting smaller, therefore these effects are contrary and cancel each other at some point. All these arguments make the analysis of the behaviour difficult and an explanation at this point without further analysis not possible. Nevertheless, we can say the contributions keep their similarity to a degree also at higher frequencies.

## A.2. Relations between density magnetic and magnetic density contributions within one diagram

Within certain diagrams there are $\tilde{B}$ contributions of the form $x\Delta^{\mathrm{d}}_{\xi}\Delta^{\mathrm{m}}_{\zeta}$ and $x\Delta^{\mathrm{m}}_{\xi}\Delta^{\mathrm{d}}_{\zeta}$. As one can see only the spin indices are swapped, the prefactor and the arguments are the same. In the following the relations are derived

### $\tilde{B}_2^{ph}$ and $\tilde{B}_4^{ph}$

$$
\begin{aligned}
\tilde{B}_4^{ph} &= \frac{3}{4}\Delta^{\mathrm{m}}_{k,k+q,k''-k}\Delta^{\mathrm{d}}_{k'',k''+q,k'-k''},\\
\tilde{B}_2^{ph} &= \frac{3}{4}\Delta^{\mathrm{d}}_{k,k+q,k''-k}\Delta^{\mathrm{m}}_{k'',k''+q,k'-k''}\\
&= \frac{3}{4}\gamma^{\mathrm{d}}_{k,k''-k}W^{\mathrm{d}}_{k''-k}\gamma^{\mathrm{d}}_{k+q,k''-k}\gamma^{\mathrm{m}}_{k'',k'-k''}W^{\mathrm{m}}_{k'-k''}\gamma^{\mathrm{m}}_{k''+q,k'-k''}\\
&= \frac{3}{4}\gamma^{\mathrm{d}}_{k'',k-k''}W^{\mathrm{d}}_{k''-k}\gamma^{\mathrm{d}}_{k''+q,k-k''}\gamma^{\mathrm{m}}_{k',k''-k'}W^{\mathrm{m}}_{k'-k''}\gamma^{\mathrm{m}}_{k'+q,k''-k'}\\
&= \frac{3}{4}\gamma^{\mathrm{d}}_{k'',k'-k''}W^{\mathrm{d}}_{k''-k'}\gamma^{\mathrm{d}}_{k''+q,k'-k''}\gamma^{\mathrm{m}}_{k,k''-k}W^{\mathrm{m}}_{k-k''}\gamma^{\mathrm{m}}_{k+q,k''-k},\\
\frac{\tilde{B}_2^{ph}}{\tilde{B}_4^{ph}} &= \frac{W^{\mathrm{d}}_{k''-k'}W^{\mathrm{m}}_{k-k''}}{W^{\mathrm{d}}_{k'-k''}W^{\mathrm{m}}_{k''-k}}.
\end{aligned}
$$

A variable transformation was used ($k \leftrightarrow k'$) and (19a). It is to stress out that this result is valid $\forall q$, no restrictions needed! Based on the numerical data the difference between those two quantities is smallest for the first point ($\omega = 0$), next point is larger, but then they get smaller with the frequency, This is to be expected since the relation holds true for all $\omega$ and they go to zero with higher frequencies.

### $\tilde{B}_2^{\overline{ph}}$ and $\tilde{B}_4^{\overline{ph}}$

$$
\begin{aligned}
\tilde{B}_2^{\overline{ph}} &= \frac{3}{4}\Delta^{\mathrm{d}}_{k,k',k''-k}\Delta^{\mathrm{m}}_{k'',k''+k'-k,k+q-k''}\\
&\to \gamma^{\mathrm{d}}_{k'',k-k''}\gamma^{\mathrm{d}}_{k'+k''-k,k-k''}W^{\mathrm{d}}_{k''-k}\gamma^{\mathrm{m}}_{k,k''-k}\gamma^{\mathrm{m}}_{k',k''-k}W^{\mathrm{m}}_{k-k''},\\
\frac{\tilde{B}_2^{\overline{ph}}}{\tilde{B}_4^{\overline{ph}}} &= \frac{W^{\mathrm{d}}_{k''-k}W^{\mathrm{m}}_{k-k''}}{W^{\mathrm{d}}_{k-k''}W^{\mathrm{m}}_{k''}-k}.
\end{aligned}
$$

In the derivation we set $q = 0$ and used as usual (19a). According to the data, this relative difference gets bigger with frequency, where at the last point ($n_w = 4$) the difference is about $1.7 \cdot 10^{-3}$.

$\tilde{B}_2^{pp}$ **and** $\tilde{B}_5^{pp}$

$$\begin{aligned}
\tilde{B}_5^{pp} &= -\frac{3}{4}\Delta^{\mathrm{m}}_{k,k'',k'+q-k''}\Delta^{\mathrm{d}}_{k'',k',k+q-k''},\\
\tilde{B}_2^{pp} &= -\frac{3}{4}\Delta^{\mathrm{d}}_{k,k'',k'+q-k''}\Delta^{\mathrm{m}}_{k'',k',k+q-k''}\\
&\quad k \leftrightarrow k'\\
&= -\frac{3}{4}\Delta^{\mathrm{d}}_{k',k'',k+q-k''}\Delta^{\mathrm{m}}_{k'',k,k'+q-k''}\\
&= -\frac{3}{4}\Delta^{\mathrm{d}}_{k'',k',k+q-k''}\Delta^{\mathrm{m}}_{k,k'',k'+q-k''},\\
\frac{\tilde{B}_2^{pp}}{\tilde{B}_5^{pp}} &= 1.
\end{aligned}$$

In the last step before the result, we interchanged the first two arguments of the $\Delta$ which we can easily do (see definition (17)). This relation holds true $\forall q$ and is unique in comparison to the other ones. The numerical data shows that the difference $\tilde{B}_2^{pp} - \tilde{B}_5^{pp}$ is indeed zero for every point, as the theory predicts, which is a nice consistency check.

$\tilde{B}_4^{pp}$ **and** $\tilde{B}_7^{pp}$

$$\begin{aligned}
\tilde{B}_4^{pp} &= -\frac{3}{4}\Delta^{\mathrm{d}}_{k,k'',k'+q-k''}\Delta^{\mathrm{m}}_{k'',k+q,k'-k''}\\
&\to -\frac{3}{4}\Delta^{\mathrm{d}}_{k'',k,k'-k''}\Delta^{\mathrm{m}}_{k,k'',k'-k''},\\
\tilde{B}_7^{pp} &= -\frac{3}{4}\Delta^{\mathrm{m}}_{k,k'',k'-k''}\Delta^{\mathrm{d}}_{k'',k,k'-k''},\\
\frac{\tilde{B}_4^{pp}}{\tilde{B}_7^{pp}} &= 1.
\end{aligned}$$

For this relation $q = 0$ is needed, also we interchanged again the arguments in the $\Delta$ terms. In our data set is $\boldsymbol{q} = 0$, so for the zero frequency point we should also get an absolute zero regarding the difference, this is in fact the case. For $\omega \neq 0$ we have small relative differences $\approx -1.4 \cdot 10^{-4}$ which increases slightly with frequency $\approx -6.7 \cdot 10^{-4}$.

$\tilde{B}_{10}^{pp}$ **and** $\tilde{B}_{13}^{pp}$

$$\begin{aligned}
\tilde{B}_{10}^{pp} &= -\frac{3}{4}\Delta^{\mathrm{d}}_{k,k+k'+q-k'',k''-k}\Delta^{\mathrm{m}}_{k'',k',k+q-k''}\\
&\to \gamma^{\mathrm{d}}_{k,k''-k}W^{\mathrm{d}}_{k''-k}\gamma^{\mathrm{d}}_{k+k'-k'',k''-k}\gamma^{\mathrm{m}}_{k'',k-k''}W^{\mathrm{m}}_{k-k''}\gamma^{\mathrm{m}}_{k',k-k''}\\
&= \gamma^{\mathrm{d}}_{k'',k-k''}W^{\mathrm{d}}_{k''-k}\gamma^{\mathrm{d}}_{k',k-k''}\gamma^{\mathrm{m}}_{k,k''-k}W^{\mathrm{m}}_{k-k''}\gamma^{\mathrm{m}}_{k'+k-k'',k''-k},\\
\frac{\tilde{B}_{10}^{pp}}{\tilde{B}_{13}^{pp}} &= \frac{W^{\mathrm{d}}_{k''-k}W^{\mathrm{m}}_{k-k''}}{W^{\mathrm{d}}_{k-k''}W^{\mathrm{m}}_{k''-k}}.
\end{aligned}$$

Again, this ratio applies only under $q = 0$. For the first point the difference is $-1.9 \cdot 10^{-6}$ and then drops to the $10^{-4}$ regime.

### $\tilde{B}_{12}^{pp}$ and $\tilde{B}_{15}^{pp}$

$$
\begin{aligned}
\tilde{B}_{15}^{pp} &= -\frac{3}{4}\Delta^{\mathrm{m}}_{k,k+k'+q-k'',k''-k}\Delta^{\mathrm{d}}_{k'',k+q,k'-k''} \\
&= \gamma^{\mathrm{d}}_{k',k''-k'}\gamma^{\mathrm{d}}_{k+q+k'-k'',k''-k'}W^{\mathrm{d}}_{k'-k''}\gamma^{\mathrm{m}}_{k'',k-k''}\gamma^{\mathrm{m}}_{k'+q,k-k''}W^{\mathrm{m}}_{k''-k} \\
k &\leftrightarrow k' \\
&= \gamma^{\mathrm{d}}_{k,k''-k}\gamma^{\mathrm{d}}_{k'+q+k-k'',k''-k}W^{\mathrm{d}}_{k-k''}\gamma^{\mathrm{m}}_{k'',k'-k''}\gamma^{\mathrm{m}}_{k+q,k'-k''}W^{\mathrm{m}}_{k''-k'}, \\
\tilde{B}_{15}^{pp} &= -\frac{3}{4}\Delta^{\mathrm{d}}_{k,k+k'+q-k'',k''-k}\Delta^{\mathrm{m}}_{k'',k+q,k'-k''}, \\
\frac{\tilde{B}_{12}^{pp}}{\tilde{B}_{15}^{pp}} &= \frac{W^{\mathrm{d}}_{k''-k}W^{\mathrm{m}}_{k'-k''}}{W^{\mathrm{d}}_{k-k''}W^{\mathrm{m}}_{k''-k'}}.
\end{aligned}
$$

This relation holds true $\forall q$. One could think that the difference is getting smaller with higher frequencies but in regard of the data set it fluctuates around $2.5 \cdot 10^{-2}$. For now there is no direct explanation for this behaviour. The limited frequency range in the data set paired with a slow convergence to zero for these contribution could be a factor. The value of the relative difference is not as good as others, but the feature of $\omega$ independence can be seen in the data.

| Relation | Is true for | Diagrams involved |
|---|---|---|
| $\frac{\tilde{B}^{ph}_{3}}{\tilde{B}^{ph}_{7}} = \frac{W^{\mathrm{d}}_{k''-k}}{W^{\mathrm{d}}_{k-k''}}$ | $q=0$ | $\tilde{B}^{ph}_{3,6}$ and $\tilde{B}^{ph}_{7,8}$ |
| $\frac{\tilde{B}^{ph}_{6}}{\tilde{B}^{ph}_{8}} = \frac{W^{\mathrm{m}}_{k''-k}}{W^{\mathrm{m}}_{k-k''}}$ | $q=0$ | $\tilde{B}^{ph}_{3,6}$ and $\tilde{B}^{ph}_{7,8}$ |
| $\frac{\tilde{B}^{\overline{ph}}_{3}}{\tilde{B}^{\overline{ph}}_{7}} = \frac{W^{\mathrm{d}}_{k''-k}}{W^{\mathrm{d}}_{k-k''}}$ | $q=0$ | $\tilde{B}^{\overline{ph}}_{3,6}$ and $\tilde{B}^{\overline{ph}}_{7,8}$ |
| $\frac{\tilde{B}^{\overline{ph}}_{6}}{\tilde{B}^{\overline{ph}}_{8}} = \frac{W^{\mathrm{m}}_{k''-k}}{W^{\mathrm{m}}_{k-k''}}$ | $q=0$ | $\tilde{B}^{\overline{ph}}_{3,6}$ and $\tilde{B}^{\overline{ph}}_{7,8}$ |
| $\frac{\tilde{B}^{pp}_{1}}{\tilde{B}^{pp}_{11}} = \frac{W^{\mathrm{d}}_{k'-k''}}{W^{\mathrm{d}}_{k''-k'}}$ | $q=0$ | $\tilde{B}^{pp}_{1,2,5,6}$ and $\tilde{B}^{pp}_{11,12,15,16}$ |
| $\frac{\tilde{B}^{pp}_{2}}{\tilde{B}^{pp}_{12}} = \frac{W^{\mathrm{d}}_{k'-k''}}{W^{\mathrm{d}}_{k''-k'}}$ | $q=0$ | $\tilde{B}^{pp}_{1,2,5,6}$ and $\tilde{B}^{pp}_{11,12,15,16}$ |
| $\frac{\tilde{B}^{pp}_{5}}{\tilde{B}^{pp}_{15}} = \frac{W^{\mathrm{m}}_{k'-k''}}{W^{\mathrm{m}}_{k''-k'}}$ | $q=0$ | $\tilde{B}^{pp}_{1,2,5,6}$ and $\tilde{B}^{pp}_{11,12,15,16}$ |
| $\frac{\tilde{B}^{pp}_{6}}{\tilde{B}^{pp}_{16}} = \frac{W^{\mathrm{m}}_{k'-k''}}{W^{\mathrm{m}}_{k''-k'}}$ | $q=0$ | $\tilde{B}^{pp}_{1,2,5,6}$ and $\tilde{B}^{pp}_{11,12,15,16}$ |
| $\frac{\tilde{B}^{pp}_{3}}{\tilde{B}^{pp}_{9}} = \frac{W^{\mathrm{d}}_{k'-k''}}{W^{\mathrm{d}}_{k''-k'}}$ | $q=0$ | $\tilde{B}^{pp}_{3,4,7,8}$ and $\tilde{B}^{pp}_{9,10,13,14}$ |
| $\frac{\tilde{B}^{pp}_{4}}{\tilde{B}^{pp}_{10}} = \frac{W^{\mathrm{d}}_{k'-k''}}{W^{\mathrm{d}}_{k''-k'}}$ | $q=0$ | $\tilde{B}^{pp}_{3,4,7,8}$ and $\tilde{B}^{pp}_{9,10,13,14}$ |
| $\frac{\tilde{B}^{pp}_{7}}{\tilde{B}^{pp}_{13}} = \frac{W^{\mathrm{m}}_{k'-k''}}{W^{\mathrm{m}}_{k''-k'}}$ | $q=0$ | $\tilde{B}^{pp}_{3,4,7,8}$ and $\tilde{B}^{pp}_{9,10,13,14}$ |
| $\frac{\tilde{B}^{pp}_{8}}{\tilde{B}^{pp}_{14}} = \frac{W^{\mathrm{m}}_{k'-k''}}{W^{\mathrm{m}}_{k''-k'}}$ | $q=0$ | $\tilde{B}^{pp}_{3,4,7,8}$ and $\tilde{B}^{pp}_{9,10,13,14}$ |
| $\frac{\tilde{B}^{pp}_{1}}{\tilde{B}^{pp}_{11}} - \frac{\tilde{B}^{pp}_{2}}{\tilde{B}^{pp}_{12}} = 0$ | $q=0$ | $\tilde{B}^{pp}_{1,2,5,6}$ and $\tilde{B}^{pp}_{11,12,15,16}$ |
| $\frac{\tilde{B}^{pp}_{5}}{\tilde{B}^{pp}_{15}} - \frac{\tilde{B}^{pp}_{6}}{\tilde{B}^{pp}_{16}} = 0$ | $q=0$ | $\tilde{B}^{pp}_{1,2,5,6}$ and $\tilde{B}^{pp}_{11,12,15,16}$ |
| $\frac{\tilde{B}^{pp}_{3}}{\tilde{B}^{pp}_{9}} - \frac{\tilde{B}^{pp}_{4}}{\tilde{B}^{pp}_{10}} = 0$ | $q=0$ | $\tilde{B}^{pp}_{3,4,7,8}$ and $\tilde{B}^{pp}_{9,10,13,14}$ |
| $\frac{\tilde{B}^{pp}_{7}}{\tilde{B}^{pp}_{13}} - \frac{\tilde{B}^{pp}_{8}}{\tilde{B}^{pp}_{14}} = 0$ | $q=0$ | $\tilde{B}^{pp}_{3,4,7,8}$ and $\tilde{B}^{pp}_{9,10,13,14}$ |
| $\frac{\tilde{B}^{ph}_{2}}{\tilde{B}^{ph}_{4}} = \frac{W^{\mathrm{d}}_{k''-k'}W^{\mathrm{m}}_{k-k''}}{W^{\mathrm{d}}_{k'-k''}W^{\mathrm{m}}_{k''-k}}$ | $\forall q$ | $\tilde{B}^{ph}_{1,2,4,5}$ |
| $\frac{\tilde{B}^{\overline{ph}}_{2}}{\tilde{B}^{\overline{ph}}_{4}} = \frac{W^{\mathrm{d}}_{k''-k}W^{\mathrm{m}}_{k-k''}}{W^{\mathrm{d}}_{k-k''}W^{\mathrm{m}}_{k''}-k}$ | $q=0$ | $\tilde{B}^{\overline{ph}}_{1,2,4,5}$ |
| $\frac{\tilde{B}^{pp}_{2}}{\tilde{B}^{pp}_{5}} = 1$ | $\forall q$ | $\tilde{B}^{pp}_{1,2,5,6}$ |
| $\frac{\tilde{B}^{pp}_{4}}{\tilde{B}^{pp}_{7}} = 1$ | $q=0$ | $\tilde{B}^{pp}_{3,4,7,8}$ |
| $\frac{\tilde{B}^{pp}_{10}}{\tilde{B}^{pp}_{13}} = \frac{W^{\mathrm{d}}_{k''-k}W^{\mathrm{m}}_{k-k''}}{W^{\mathrm{d}}_{k-k''}W^{\mathrm{m}}_{k''-k}}$ | $q=0$ | $\tilde{B}^{pp}_{9,10,13,14}$ |
| $\frac{\tilde{B}^{pp}_{12}}{\tilde{B}^{pp}_{15}} = \frac{W^{\mathrm{d}}_{k''-k}W^{\mathrm{m}}_{k'-k''}}{W^{\mathrm{d}}_{k-k''}W^{\mathrm{m}}_{k''-k'}}$ | $\forall q$ | $\tilde{B}^{pp}_{11,12,15,16}$ |

Table 1: Overview over all relations between multi-boson contributions

## B. Proof of realness of the bubble part of the current-current correlation function within optical conductivity

From the definition of the fermionic Matsubara frequency, an evenly spaced space leads to an asymmetric Matsubara index space. E.g. we have 8 frequencies in total and want to spread them evenly from negative to positive. The lowest and highest would be $\mp 7\frac{\pi}{\beta}$ but written in indices these frequencies are $\nu_{-4}$ and $\nu_3$. The indices would run from $-4$ to 3 including zero.
Now we look at the bubble part of the current-current correlation function. One can derive two relations within the regime of optical conductivity, one is general and one where the frequency is zero. The imaginary part vanishes at this point and the quantity is purely real, which is a good test for programs and numerical calculations.

$$
\begin{aligned}
\chi_0(q) &= -\frac{2}{N_k\beta}\int \boldsymbol{dk}\sum_{\nu}(y_\rho^{\boldsymbol{kq}/2})^2 G(k)G(k+q)\\
\boldsymbol{q}=0 \rightarrow &-\frac{2}{N_k\beta}\sum_{\boldsymbol{k}}\frac{\partial\epsilon_k}{\partial k_\rho}^2\sum_{\nu}G(\nu,\boldsymbol{k})G(\nu+\omega,\boldsymbol{k}),\\
\xi &= \sum_{\nu_{-m-1}}^{\nu_{-1}} G(\nu,\boldsymbol{k})G(\nu+\omega,\boldsymbol{k}) + \sum_{\nu_0}^{\nu_m} G(\nu,\boldsymbol{k})G(\nu+\omega,\boldsymbol{k})\\
&= \sum_{-\nu_0}^{-\nu_{m+1}} G(\nu,\boldsymbol{k})G(\nu+\omega,\boldsymbol{k}) - G(\nu_{-1},\boldsymbol{k})G(\nu_{-1}+\omega,\boldsymbol{k}) + \sum_{\nu_0}^{\nu_m} G(\nu,\boldsymbol{k})G(\nu+\omega,\boldsymbol{k})\\
&= \sum_{\nu_0}^{\nu_m} G(-\nu,\boldsymbol{k})G(-\nu+\omega,\boldsymbol{k}) + \sum_{\nu_0}^{\nu_m} G(\nu,\boldsymbol{k})G(\nu+\omega,\boldsymbol{k})\\
&= \sum_{\nu_0}^{\nu_m} G^*(\nu,\boldsymbol{k})G(-\nu+\omega,\boldsymbol{k}) + G(\nu,\boldsymbol{k})G(\nu+\omega,\boldsymbol{k})\\
\omega=0 \rightarrow &= \sum_{\nu_0}^{\nu_m} G^{*^2}(\nu,\boldsymbol{k}) + G^2(\nu,\boldsymbol{k})\\
&= \sum_{\nu_0}^{\nu_m} 2\Re(G(\nu,\boldsymbol{k}))^2 - 2\Im(G(\nu,\boldsymbol{k}))^2 = \sum_{\nu_0}^{\nu_m} 2\Re(G(\nu,\boldsymbol{k})^2).
\end{aligned}
\tag{34}
$$

The first part with the derivation of the dispersion relation is real, therefore we did not consider it further. We then wrote out the Matsubara sum over an evenly spread frequency space and separated the sums to a negative and positive one. To equalise the sums we change the argument order of the first sum, using (7), expand the sum and subtract therefore a term. The last step is confusing, note that $-\nu_0$ and $\nu_{-1}$ describes the same frequency. So the sum counts two times the same term, thus we subtract one. The reason we do this is to equalise the sums. For a better understanding one can write a number line with the indices and the corresponding frequencies, then the retracing

over the accounting of the terms is easier. Next we change for the first sum the sign of $\nu$, then we use (20b). The line before we set $\omega = 0$ is the general result. The last line than is the result for the zero frequency point were one can see that the term is purely real[18]. With the real prefactors, the whole bubble part of the current-current correlation function is purely real.



[18] $z = a + ib \in \mathbb{C}; (z^*)^2 = (z^2)^*; z + z^* = 2\Re(z); z^2 + z^{*^2} = 2\Re(z)^2 - 2\Im(z)^2 = 4\Re(z)^2 - 2|z|^2 = 2\Re(z^2)$

## C. Proof of realness of a first order term of the current-current correlation function within optical conductivity

There can be relations derived as in the chapter before. we can also just see it as a transformation on only positive Matsubara frequencies. The same tools as before are used, but additional also (19). At the end we can show that for the $q = 0$ point and no further assumptions than inversion symmetry (needed for (19d)) the single-boson contributions (first order of the current-current correlation function) are real. We start with a general expression that is the core of all first order contributions ($\propto G_{k'}G_{k'+q}\gamma W\gamma$). The light vertex terms are real, therefore not of interest, again $\boldsymbol{q} = 0$. Here not all minor steps are written out and explained in detail, as said in principle it is analogue to the derivation in B. We derive it on the example of the vertical particle-hole contributions. For this derivation $\Delta$ is not transformed to $\Delta - U$ since we are investigating single-boson terms and $U$ is anyway real.

$$
\begin{aligned}
\chi_I &= -\frac{2}{N_k^2\beta^2}\sum_{\boldsymbol{k},\boldsymbol{k'}}\sum_{\nu\nu'} G_k G_{k+q} G_{k'} G_{k'+q}\gamma^{\alpha}W^{\alpha}\gamma^{\alpha}y^{\boldsymbol{kq}/2}y^{\boldsymbol{k'q}/2},\\
\xi &= \sum_{i=0}^{m} G(\nu_i,k)G(\nu_i+\omega k+q)(\sum_{i'=0}^{m} G(-\nu_i',\boldsymbol{k'})G(-\nu_i'+\omega,\boldsymbol{k'})\gamma^{\mathrm{d/m}}_{-\nu_i,-\nu_i'-\nu_i}W^{\mathrm{d/m}}_{-\nu_i'-\nu_i}\gamma^{\mathrm{d/m}}_{-\nu_i+\omega,-\nu_i'-\nu_i}\\
&\quad+\sum_{i'=0}^{m} G(\nu_i',\boldsymbol{k'})G(\nu_i'+\omega,\boldsymbol{k'})\gamma^{\mathrm{d/m}}_{\nu_i,\nu_i'-\nu_i}W^{\mathrm{d/m}}_{\nu_i'-\nu_i}\gamma^{\mathrm{d/m}}_{\nu_i+\omega,\nu_i'-\nu_i})\\
&= \sum_{i=0}^{m}\sum_{i'=0}^{m} G(-\nu_i,\boldsymbol{k})(-\nu_i+\omega,\boldsymbol{k})G(-\nu_i',\boldsymbol{k'})G(-\nu_i'+\omega,\boldsymbol{k'})\gamma^{\mathrm{d/m}}_{-\nu_i,-\nu_i'+\nu_i}W^{\mathrm{d/m}}_{-\nu_i'+\nu_i}\gamma^{\mathrm{d/m}}_{-\nu_i+\omega,-\nu_i'+\nu_i}\\
&\quad+\sum_{i=0}^{m}\sum_{i'=0}^{m} G(\nu_i,\boldsymbol{k})(\nu_i+\omega,\boldsymbol{k})G(\nu_i',\boldsymbol{k'})G(\nu_i'+\omega,\boldsymbol{k'})\gamma^{\mathrm{d/m}}_{\nu_i,\nu_i'-\nu_i}W^{\mathrm{d/m}}_{\nu_i'-\nu_i}\gamma^{\mathrm{d/m}}_{\nu_i+\omega,\nu_i'-\nu_i}.
\end{aligned}
\tag{35}
$$

This derivation is for the density and magnetic spin configuration of the vertical particle-hole channel, the other channels have other arguments for $\gamma W\gamma$. This is the general result for the optical conductivity regime, notice the relative high symmetry in the terms. For the Hedin vertices and the screened interaction the momenta arguments are left out, they are not changed from the normal form as seen in (21).
Next we set $\omega = 0$, use (20)and (19e), and then we also write out the omitted momenta.

$\omega = 0$

$$
\begin{aligned}
\xi_{\boldsymbol{k},\boldsymbol{k'}} &= \sum_{i=0}^{m}\sum_{i'=0}^{m} G^*(\nu_i,\boldsymbol{k})G^*(\nu_i,\boldsymbol{k})G^*(\nu_i',\boldsymbol{k'})G^*(\nu_i',\boldsymbol{k'}) \\
&\quad W^{\mathrm{d/m}^*}_{\nu_i'-\nu_i}\gamma^{\mathrm{d/m}}(-\nu_i,\boldsymbol{k},-\nu_i'+\nu_i,\boldsymbol{k'}-\boldsymbol{k})\gamma^{\mathrm{d/m}}(-\nu_i+0,\boldsymbol{k}+0,-\nu_i'+\nu_i,\boldsymbol{k'}-\boldsymbol{k}) \\
&\quad + G(\nu_i,\boldsymbol{k})G(\nu_i+0,\boldsymbol{k})G(\nu_i',\boldsymbol{k'})G(\nu_i'+0,\boldsymbol{k'}) \\
&\quad W^{\mathrm{d/m}}_{\nu_i'-\nu_i}\gamma^{\mathrm{d/m}}(\nu_i,\boldsymbol{k},\nu_i+0,\boldsymbol{k'}-\boldsymbol{k})\gamma^{\mathrm{d/m}}(\nu_i+0,\boldsymbol{k}+0,\nu_i'-\nu_i,\boldsymbol{k'}-\boldsymbol{k}) \\
&= \sum_{i=0}^{m}\sum_{i'=0}^{m} G^{*^2}(\nu_i,\boldsymbol{k})G^{*^2}(\nu_i',\boldsymbol{k'})W^{\mathrm{d/m}^*}_{\nu_i'-\nu_i,\boldsymbol{k'}-\boldsymbol{k}}\gamma^{\mathrm{d/m}^{*^2}}(\nu_i,\boldsymbol{k},\nu_i'-\nu_i,\boldsymbol{k'}-\boldsymbol{k}) \\
&\quad + G^2(\nu_i,\boldsymbol{k})G^2(\nu_i',\boldsymbol{k'})W^{\mathrm{d/m}}_{\nu_i'-\nu_i,\boldsymbol{k'}-\boldsymbol{k}}\gamma^{\mathrm{d/m}^2}(\nu_i,\boldsymbol{k},\nu_i'-\nu_i,\boldsymbol{k'}-\boldsymbol{k}) \\
&= \sum_{i=0}^{m}\sum_{i'=0}^{m} 2\Re(G^2(\nu_i,\boldsymbol{k})G^2(\nu_i',\boldsymbol{k'})W^{\mathrm{d/m}}_{\nu_i'-\nu_i,\boldsymbol{k'}-\boldsymbol{k}}\gamma^{\mathrm{d/m}^2}(\nu_i,\boldsymbol{k},\nu_i'-\nu_i,\boldsymbol{k'}-\boldsymbol{k})).
\end{aligned}
\tag{36}
$$

For the second equal sign, we used (19d) to also get a complex conjugation on the $\gamma$. This shows that the whole term $\chi_I(0)$ is real. Therefore, the part of the optical conductivity which depends on the principal value of the imaginary part of the current-current correlation function is zero.

It is worth mentioning that there is another derivation which is quite tedious and uses $W_{\boldsymbol{q},w} = W_{-\boldsymbol{q},w}$ instead of the $\gamma$ identity above. The identity for the screened interaction applies only for cubic lattice and since this lattice possesses inversion symmetry the above derivation is more general, covers the cubic lattice case and is way shorter and easier.

# D. Additional plots and data

In this chapter we find the plot for each Feynman diagram from all particle channels and their totals for different values of the bare interaction and these plots within the asymptotic approximation. Remember that in general the diagram contribution $D_i^\alpha$ is not the sum of the associated $C$ terms (see (32)). For the comparison plots, interpretation, explanation and the detailed parameters see the chapters 5, 6.2 and 6.3.

## D.1. U=3

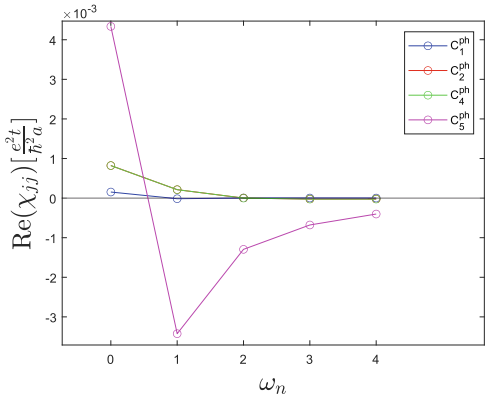


(a) Diagram $D_1^{ph}$ with $C_{1,2,4,5}^{ph}$

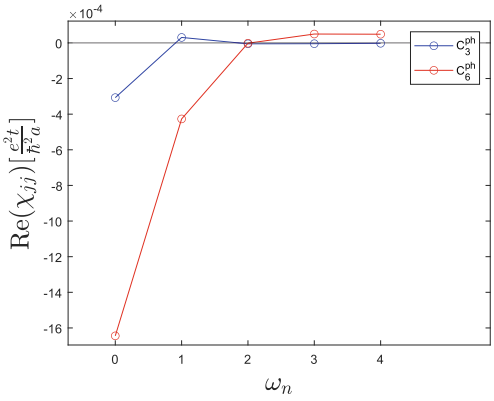


(b) Diagram $D_3^{ph}$ with $C_{3,6}^{ph}$

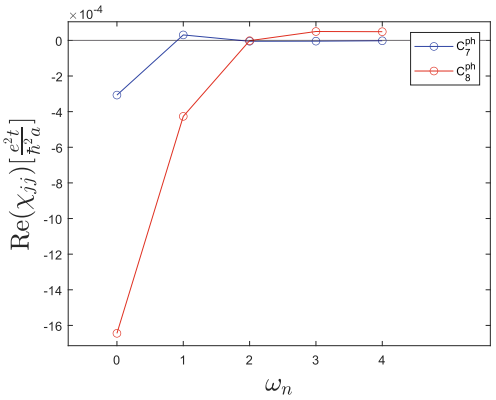


(c) Diagram $D_7^{ph}$ with $C_{7,8}^{ph}$

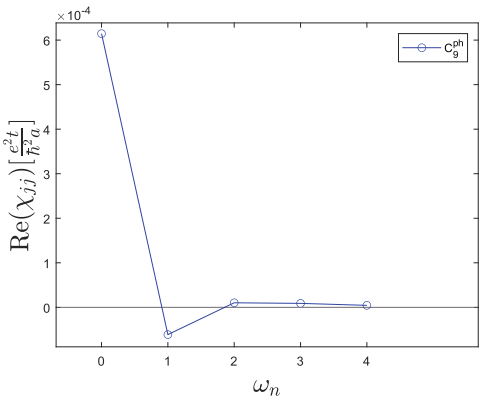


(d) Diagram $D_9^{ph}$ with $C_9^{ph}$

Figure 26: The particle-hole channel C contributions for their respective diagrams, $U = 3$.

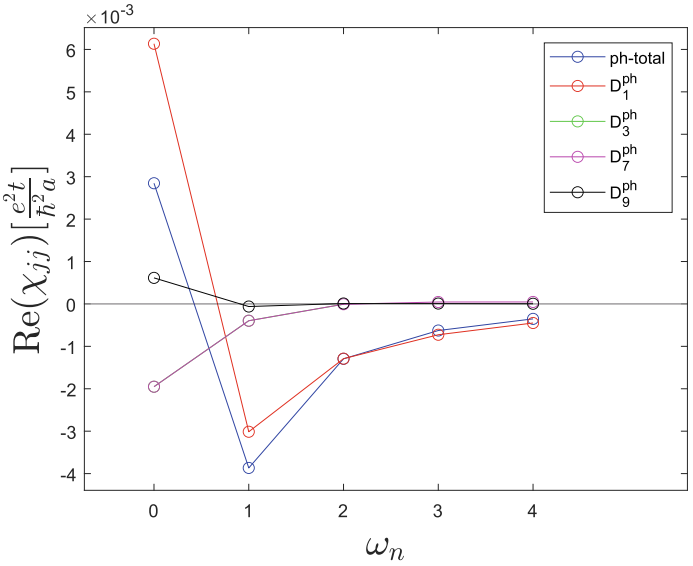


Figure 27: Graph of all contributions from the four diagrams ($D_i^{ph}$) of the particle-hole channel, where ph-total is the sum of the diagrams, $U = 3$.

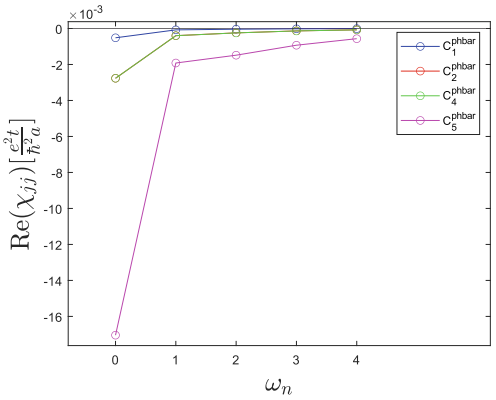


(a) Diagram $D_1^{\overline{ph}}$ with $C_{1,2,4,5}^{\overline{ph}}$

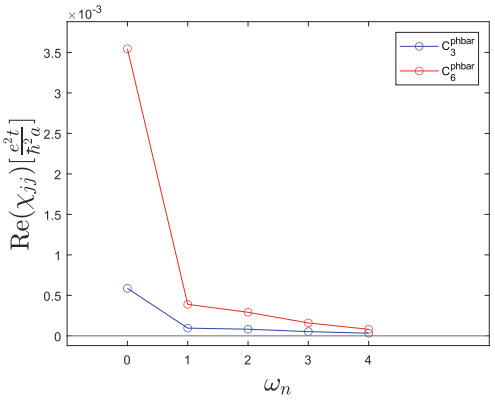


(b) Diagram $D_3^{\overline{ph}}$ with $C_{3,6}^{\overline{ph}}$

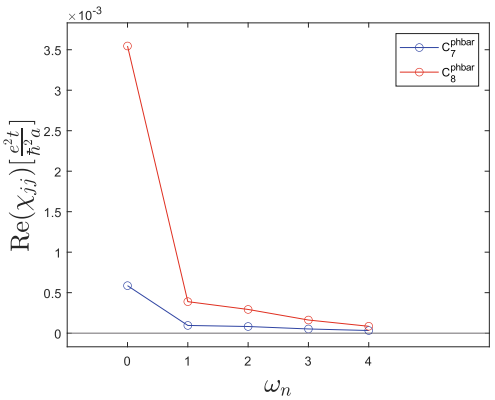


(c) Diagram $D_7^{\overline{ph}}$ with $C_{7,8}^{\overline{ph}}$

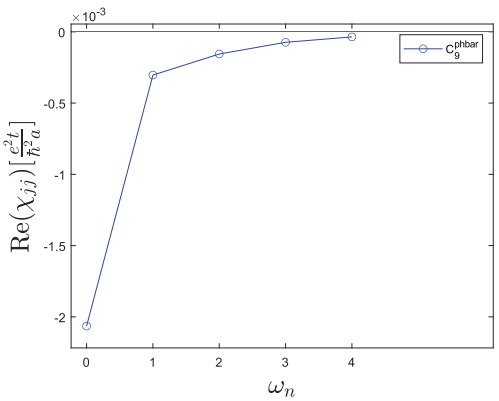


(d) Diagram $D_9^{\overline{ph}}$ with $C_9^{\overline{ph}}$

Figure 28: The vertical particle-hole channel C contributions for their respective diagrams, $U = 3$.

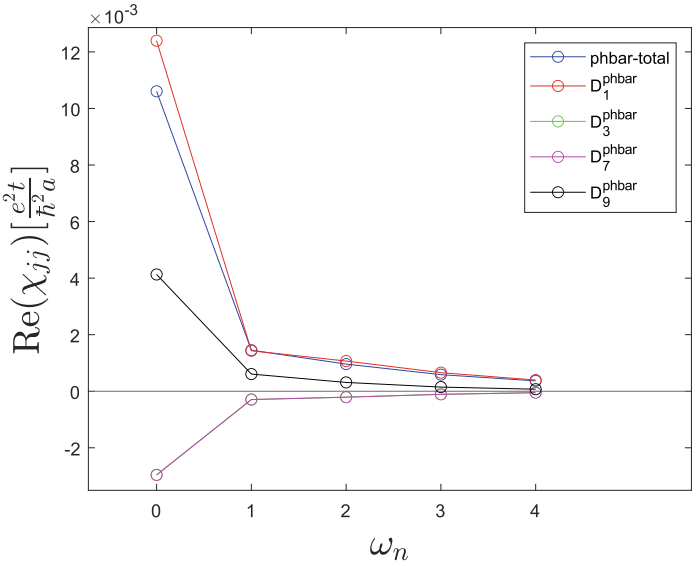


Figure 29: Graph of all contributions from the four diagrams ($D_i^{\overline{ph}}$) of the vertical particle-hole channel, where phbar-total is the sum of the diagrams, $U = 3$.

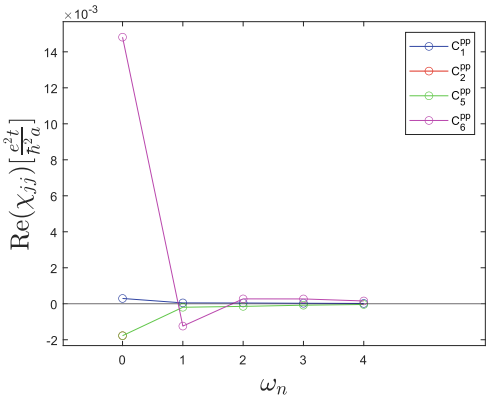


(a) Diagram $D_1^{pp}$ with $C_{1,2,5,6}^{pp}$

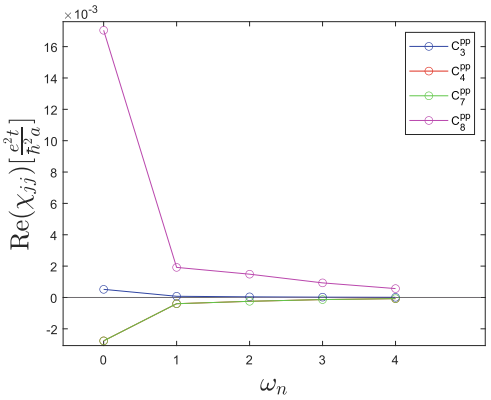


(b) Diagram $D_3^{pp}$ with $C_{3,4,7,8}^{pp}$

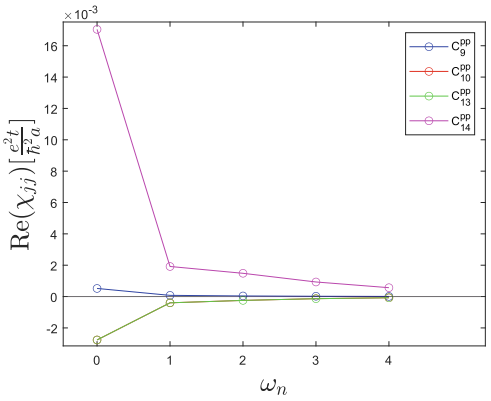


(c) Diagram $D_9^{pp}$ with $C_{9,10,13,14}^{pp}$

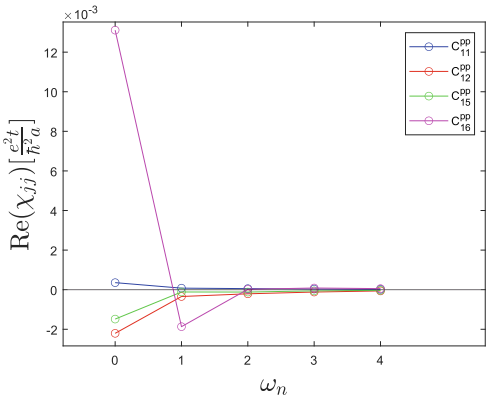


(d) Diagram $D_{11}^{pp}$ with $C_{11,12,15,16}^{pp}$

Figure 30: The particle-particle channel C contributions for their respective diagrams, $U = 3$.

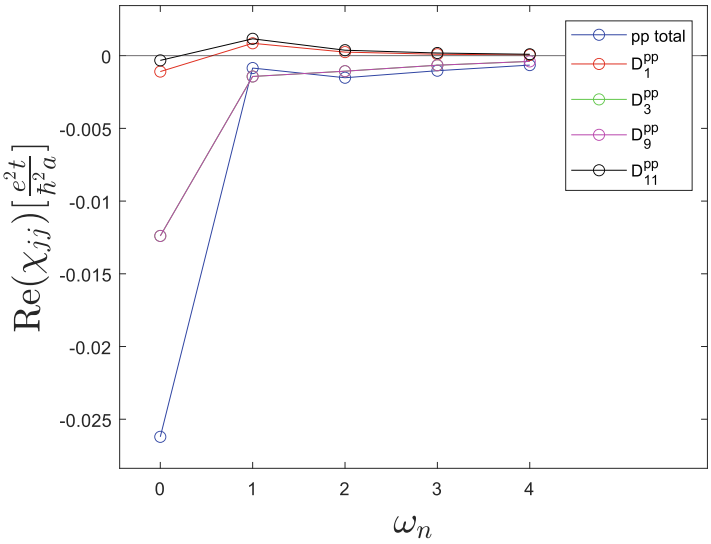


Figure 31: Graph of all contributions from the four diagrams ($D_i^{ph}$) of the particle-hole channel, where pp-total is the sum of the diagrams, $U = 3$.

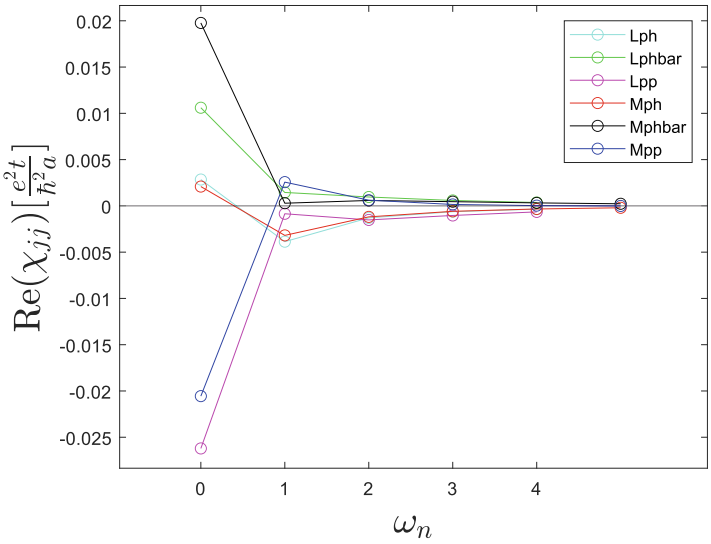


Figure 32: Comparison between different particle-channels of the lowest multi-boson order and the full multi-boson order for $U = 3$.

## D.2. U=4

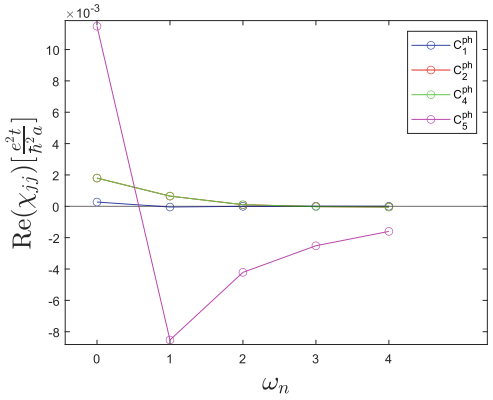


(a) Diagram $D_1^{ph}$ with $C_{1,2,4,5}^{ph}$

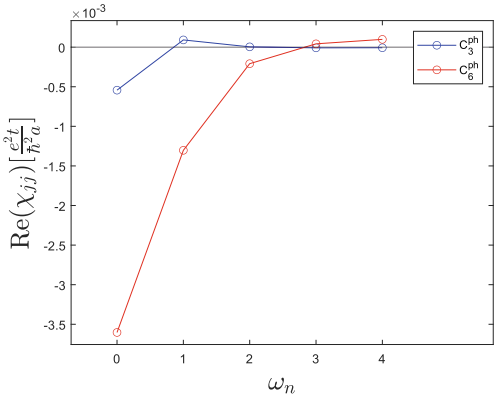


(b) Diagram $D_3^{ph}$ with $C_{3,6}^{ph}$

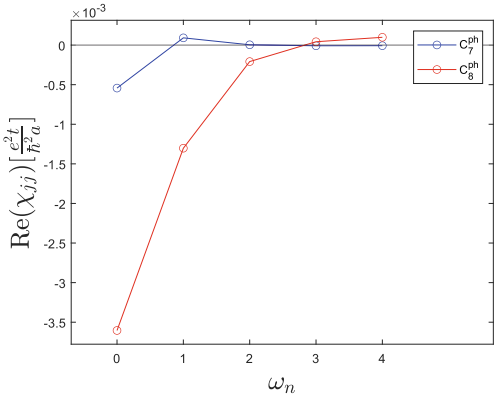


(c) Diagram $D_7^{ph}$ with $C_{7,8}^{ph}$

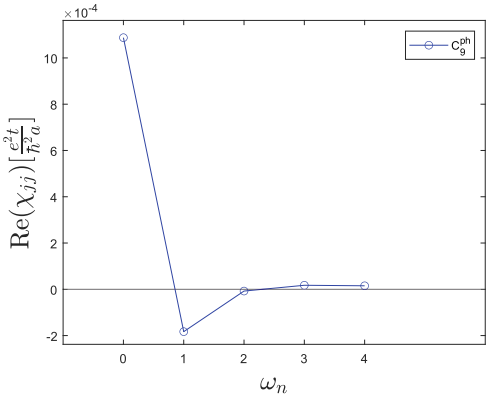


(d) Diagram $D_9^{ph}$ with $C_9^{ph}$

Figure 33: The particle-hole channel C contributions for their respective diagrams, $U = 4$.

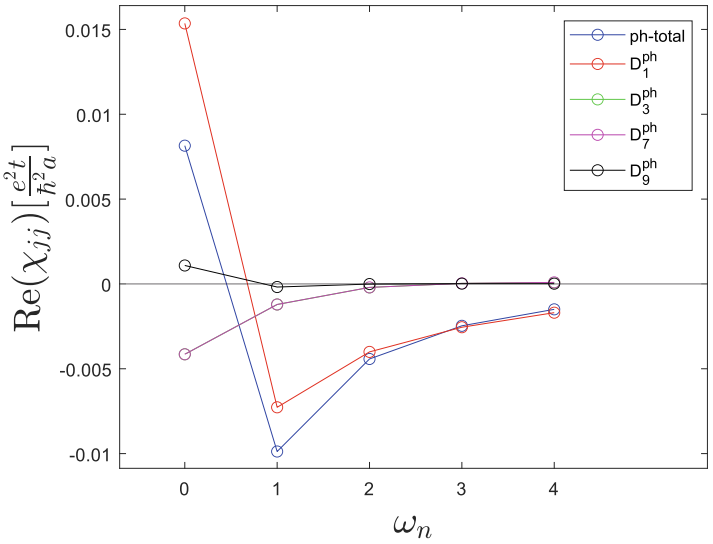


Figure 34: Graph of all contributions from the four diagrams ($D_i^{ph}$) of the particle-hole channel, where ph-total is the sum of the diagrams, $U = 4$.

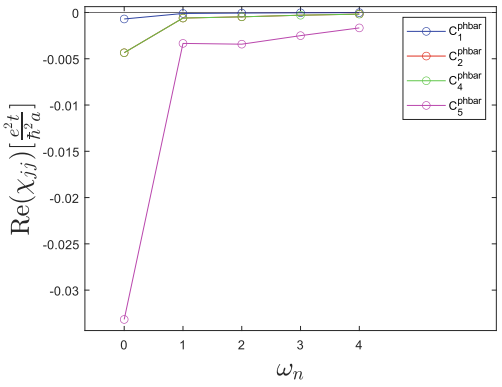


(a) Diagram $D_1^{\overline{ph}}$ with $C_{1,2,4,5}^{\overline{ph}}$

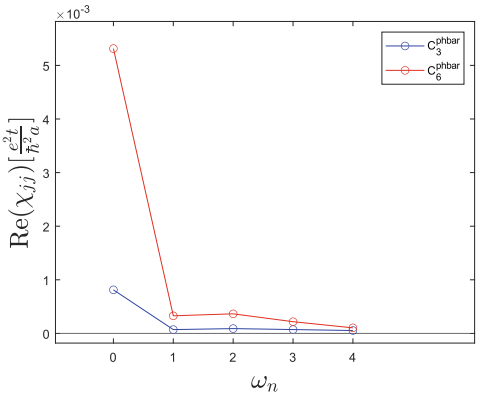


(b) Diagram $D_3^{\overline{ph}}$ with $C_{3,6}^{\overline{ph}}$

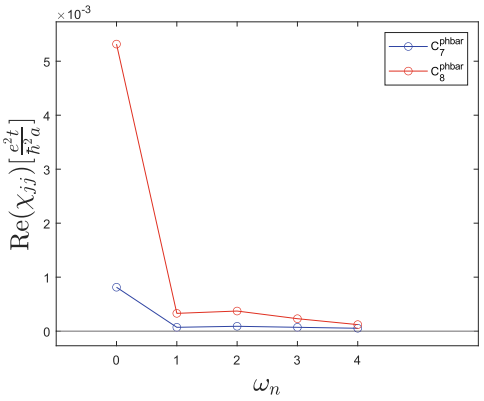


(c) Diagram $D_7^{\overline{ph}}$ with $C_{7,8}^{\overline{ph}}$

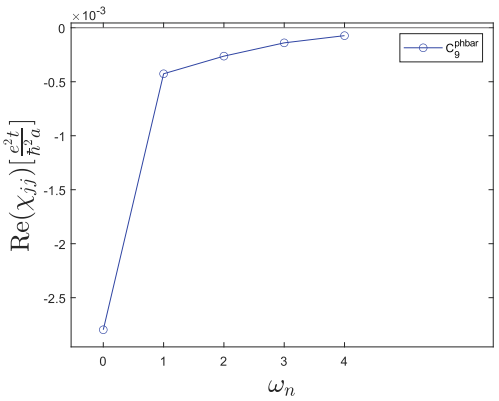


(d) Diagram $D_9^{\overline{ph}}$ with $C_9^{\overline{ph}}$

Figure 35: The vertical particle-hole channel C contributions for their respective diagrams, $U = 4$.

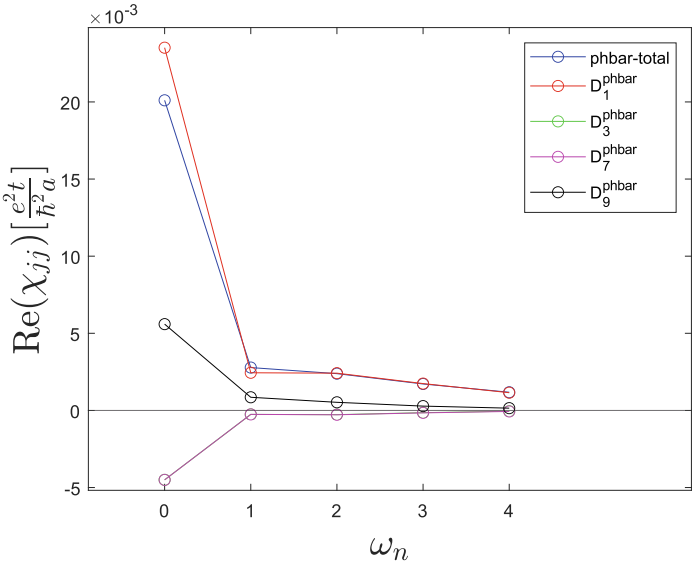


Figure 36: Graph of all contributions from the four diagrams ($D_i^{\overline{ph}}$) of the vertical particle-hole channel, where phbar-total is the sum of the diagrams, $U = 4$.

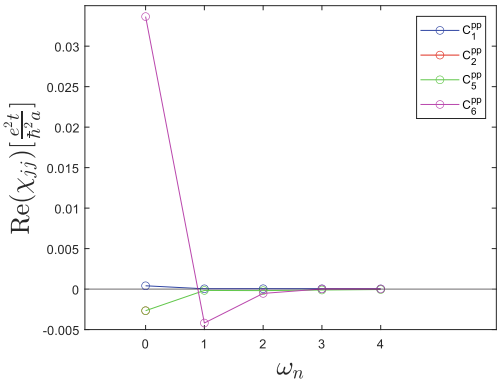


(a) Diagram $D_1^{pp}$ with $C^{pp}_{1,2,5,6}$

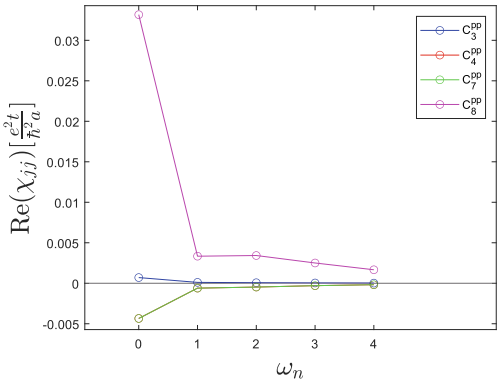


(b) Diagram $D_3^{pp}$ with $C^{pp}_{3,4,7,8}$

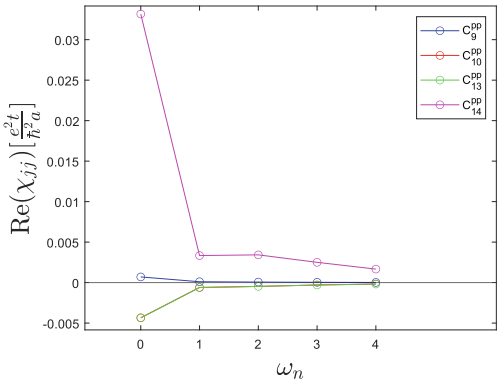


(c) Diagram $D_9^{pp}$ with $C^{pp}_{9,10,13,14}$

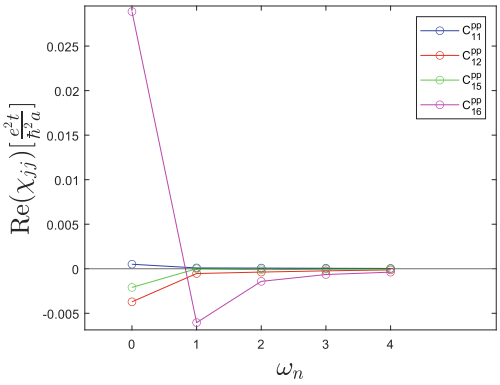


(d) Diagram $D_{11}^{pp}$ with $C^{pp}_{11,12,15,16}$

Figure 37: The particle-particle channel C contributions for their respective diagrams, $U = 4$.

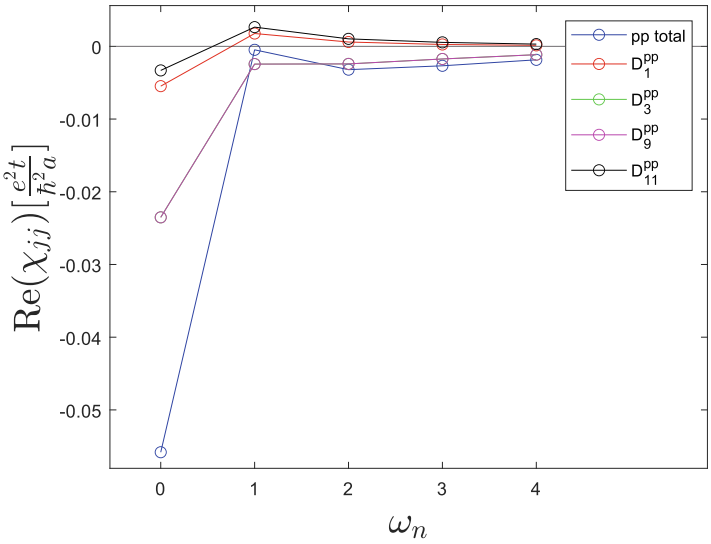


Figure 38: Graph of all contributions from the four diagrams ($D_i^{ph}$) of the particle-hole channel, where pp-total is the sum of the diagrams, $U = 4$.

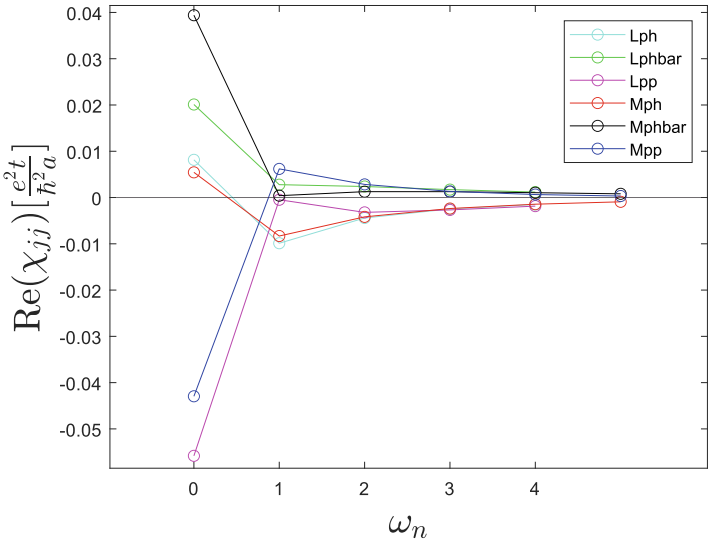


Figure 39: Comparison between different particle-channels of the lowest multi-boson order and the full multi-boson order for $U = 4$.

## D.3. Asymptotic Approximation

### D.3.1. U=2

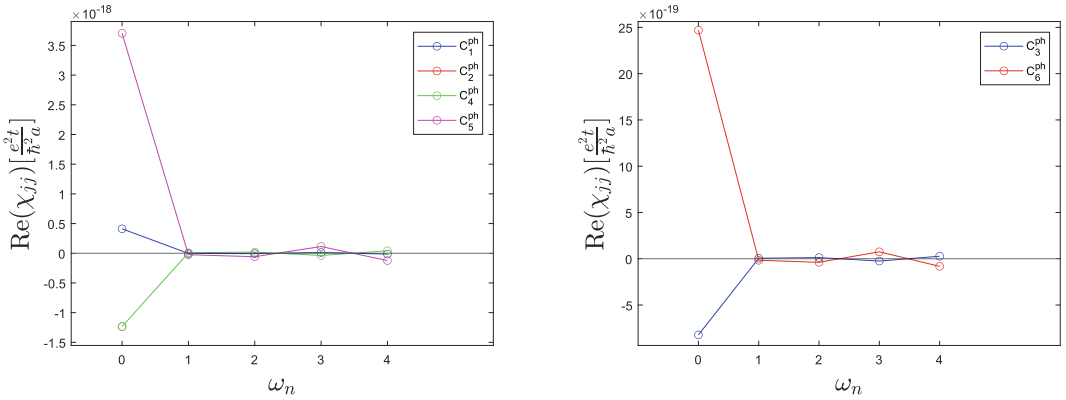


(a) Diagram $D_1^{ph}$ with $C_{1,2,4,5}^{ph}$

(b) Diagram $D_3^{ph}$ with $C_{3,6}^{ph}$

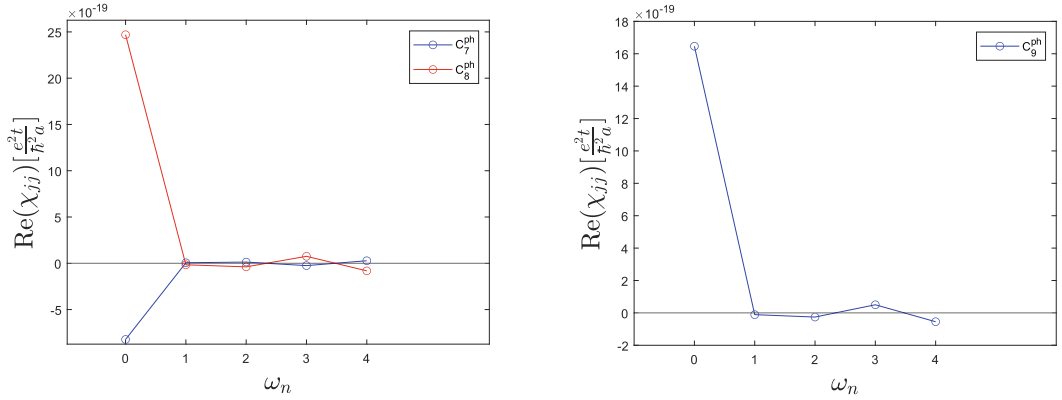


(c) Diagram $D_7^{ph}$ with $C_{7,8}^{ph}$

(d) Diagram $D_9^{ph}$ with $C_9^{ph}$

Figure 40: The particle-hole channel C contributions for their respective diagrams. Bare interaction $U = 2$ and the asymptotic approximation is used.

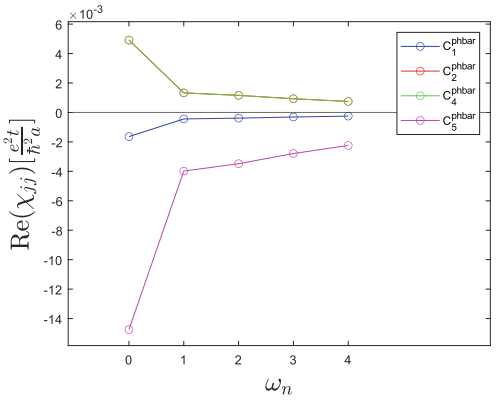


(a) Diagram $D_1^{\overline{ph}}$ with $C_{1,2,4,5}^{\overline{ph}}$

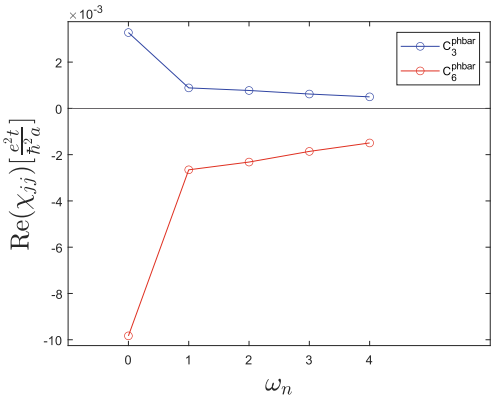


(b) Diagram $D_3^{\overline{ph}}$ with $C_{3,6}^{\overline{ph}}$

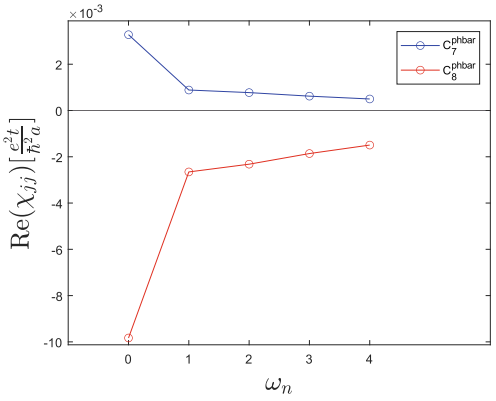


(c) Diagram $D_7^{\overline{ph}}$ with $C_{7,8}^{\overline{ph}}$

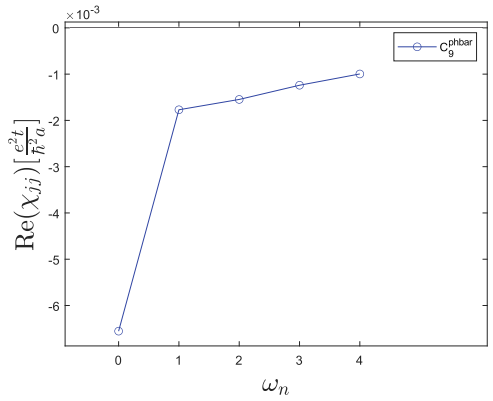


(d) Diagram $D_9^{\overline{ph}}$ with $C_9^{\overline{ph}}$

Figure 41: The vertical particle-hole channel C contributions for their respective diagrams. Bare interaction $U = 2$ and the asymptotic approximation is used.

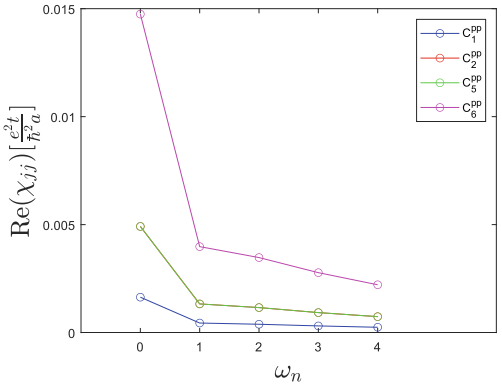


(a) Diagram $D_1^{pp}$ with $C^{pp}_{1,2,5,6}$

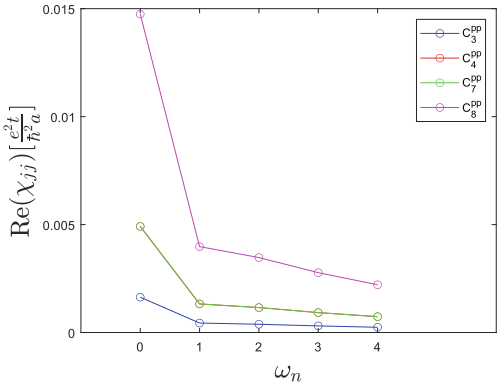


(b) Diagram $D_3^{pp}$ with $C^{pp}_{3,4,7,8}$

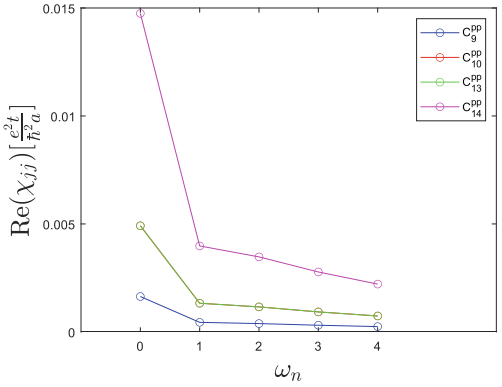


(c) Diagram $D_9^{pp}$ with $C^{pp}_{9,10,13,14}$

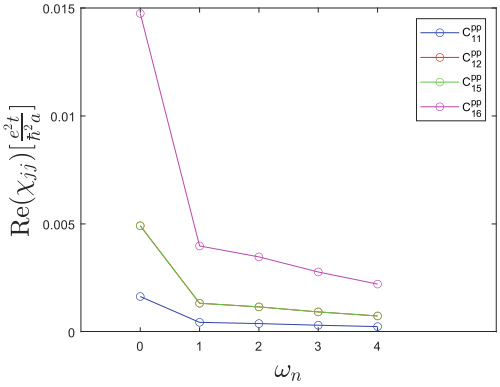


(d) Diagram $D_{11}^{pp}$ with $C^{pp}_{11,12,15,16}$

Figure 42: The particle-particle channel C contributions for their respective diagrams. Bare interaction $U = 2$ and the asymptotic approximation is used.

### D.3.2. U=3

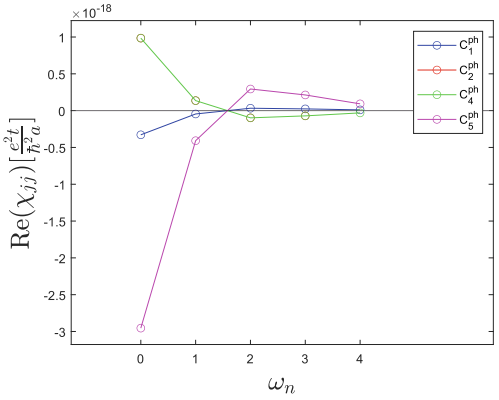


(a) Diagram $D_1^{ph}$ with $C_{1,2,4,5}^{ph}$

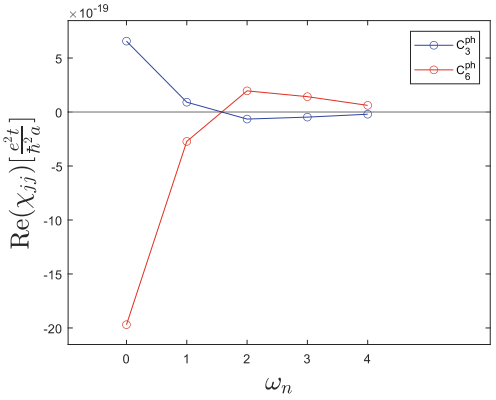


(b) Diagram $D_3^{ph}$ with $C_{3,6}^{ph}$

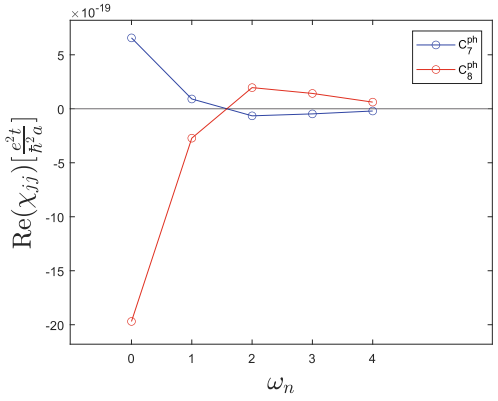


(c) Diagram $D_7^{ph}$ with $C_{7,8}^{ph}$

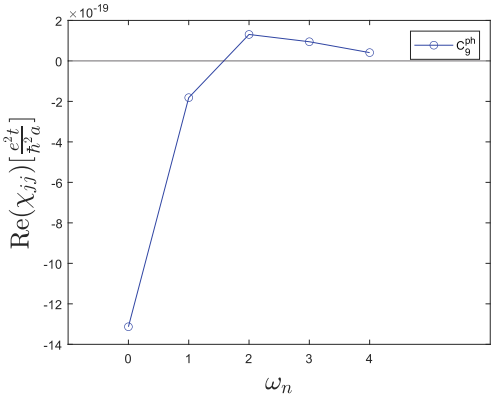


(d) Diagram $D_9^{ph}$ with $C_9^{ph}$

Figure 43: The particle-hole channel C contributions for their respective diagrams. Bare interaction $U = 3$ and the asymptotic approximation is used.

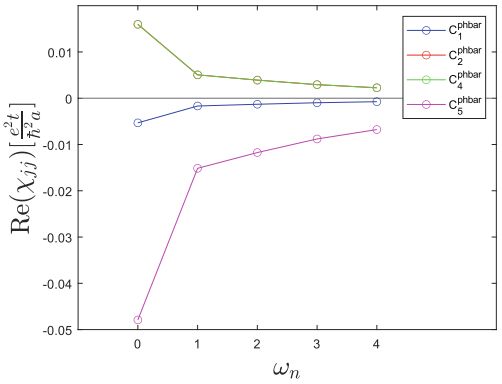


(a) Diagram $D_1^{\overline{ph}}$ with $C_{1,2,4,5}^{\overline{ph}}$

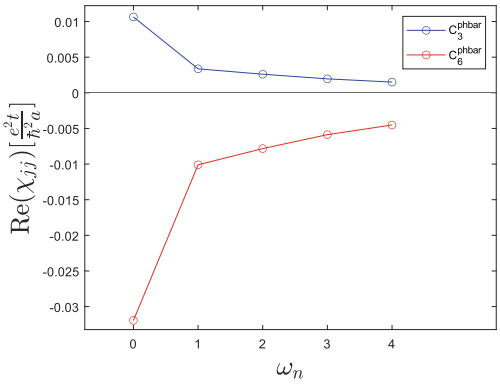


(b) Diagram $D_3^{\overline{ph}}$ with $C_{3,6}^{\overline{ph}}$

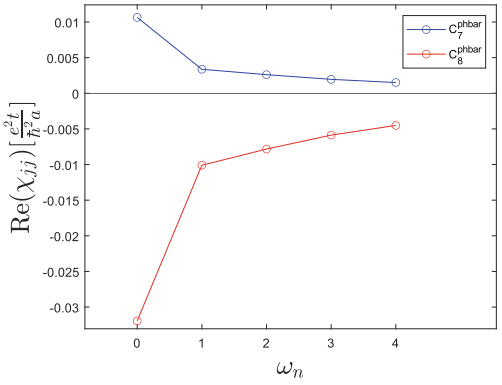


(c) Diagram $D_7^{\overline{ph}}$ with $C_{7,8}^{\overline{ph}}$

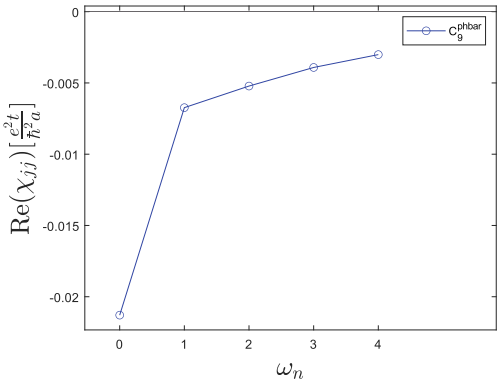


(d) Diagram $D_9^{\overline{ph}}$ with $C_9^{\overline{ph}}$

Figure 44: The vertical particle-hole channel C contributions for their respective diagrams. Bare interaction $U = 3$ and the asymptotic approximation is used.

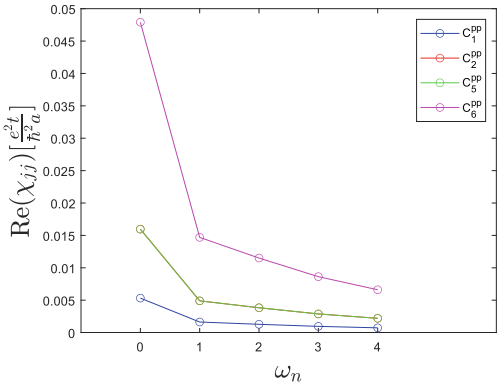


(a) Diagram $D_1^{pp}$ with $C^{pp}_{1,2,5,6}$

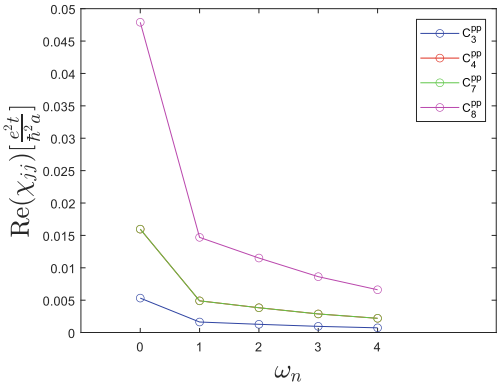


(b) Diagram $D_3^{pp}$ with $C^{pp}_{3,4,7,8}$

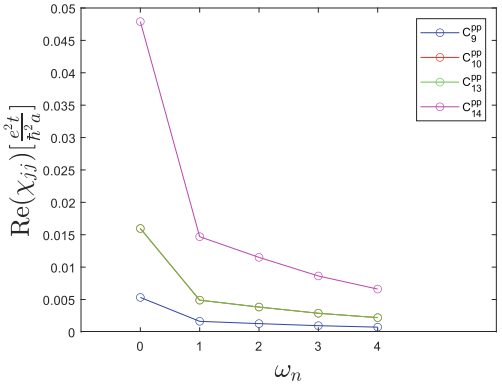


(c) Diagram $D_9^{pp}$ with $C^{pp}_{9,10,13,14}$

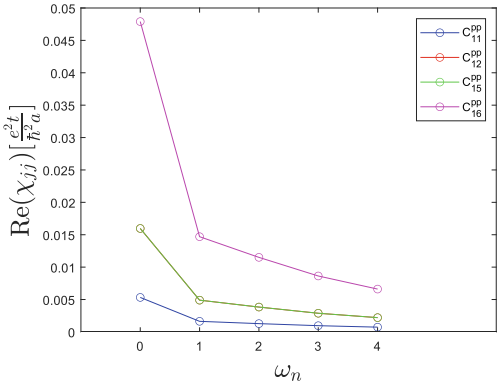


(d) Diagram $D_{11}^{pp}$ with $C^{pp}_{11,12,15,16}$

Figure 45: The particle-particle channel C contributions for their respective diagrams. Bare interaction $U = 3$ and the asymptotic approximation is used.

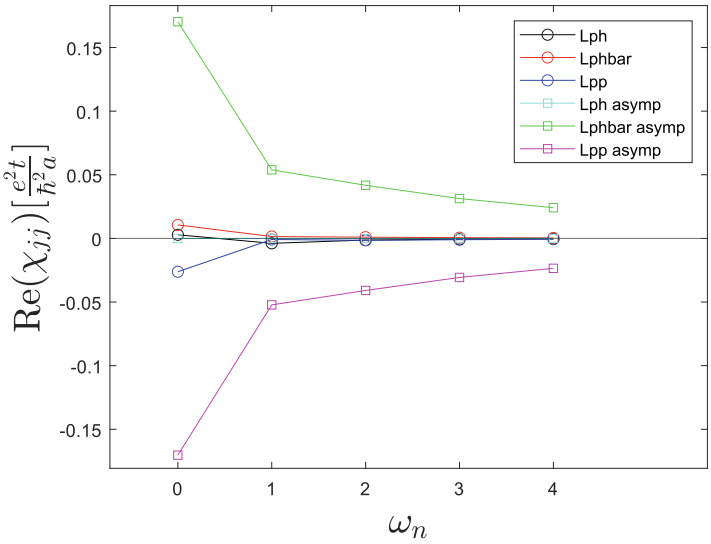


Figure 46: Graph of all different particle contributions with and without the asymptotic approximation, $U = 3$.

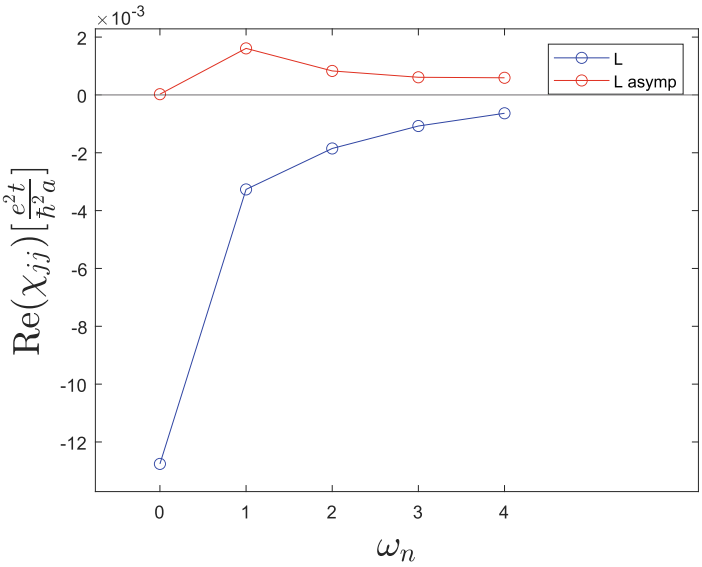


Figure 47: Graph of the total lowest multi-boson order, with and without the approximation, $U = 3$.

### D.3.3. U=4

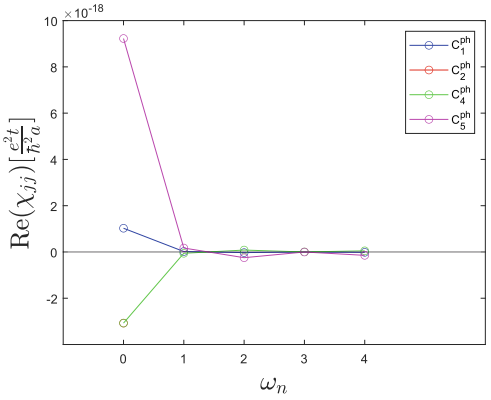


(a) Diagram $D_1^{ph}$ with $C_{1,2,4,5}^{ph}$

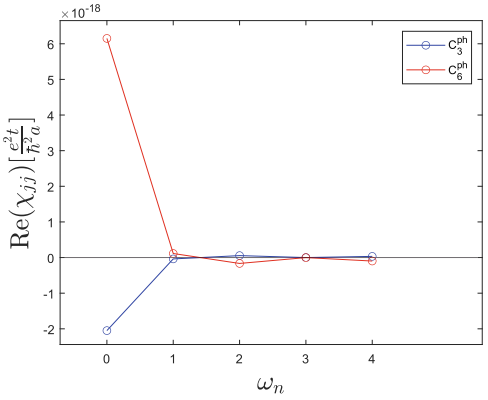


(b) Diagram $D_3^{ph}$ with $C_{3,6}^{ph}$

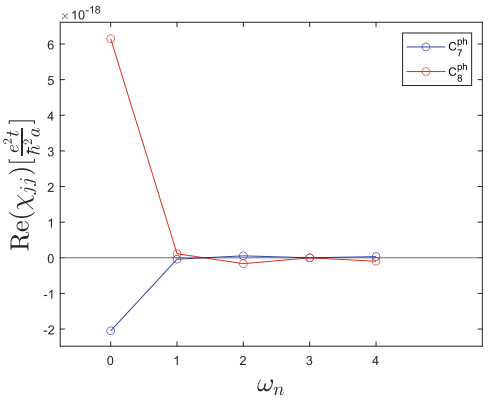


(c) Diagram $D_7^{ph}$ with $C_{7,8}^{ph}$

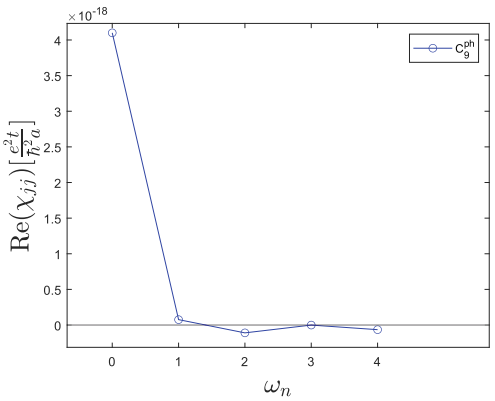


(d) Diagram $D_9^{ph}$ with $C_9^{ph}$

Figure 48: The particle-hole channel C contributions for their respective diagrams. Bare interaction $U = 4$ and the asymptotic approximation is used.

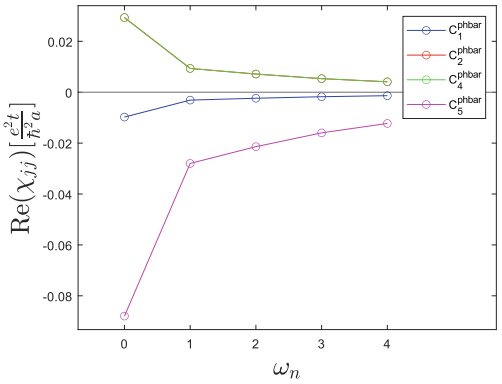


(a) Diagram $D_1^{\overline{ph}}$ with $C_{1,2,4,5}^{\overline{ph}}$

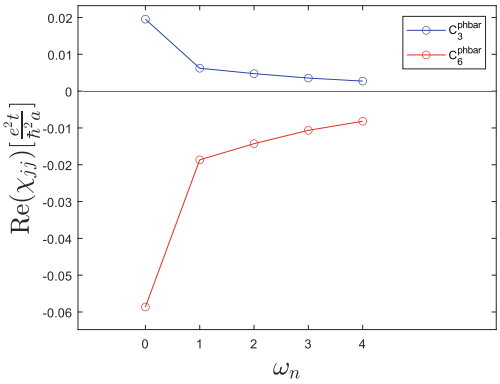


(b) Diagram $D_3^{\overline{ph}}$ with $C_{3,6}^{\overline{ph}}$

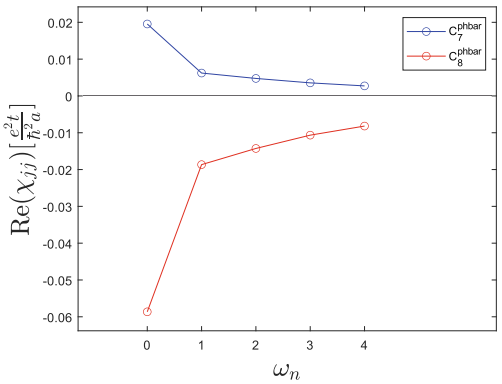


(c) Diagram $D_7^{\overline{ph}}$ with $C_{7,8}^{\overline{ph}}$

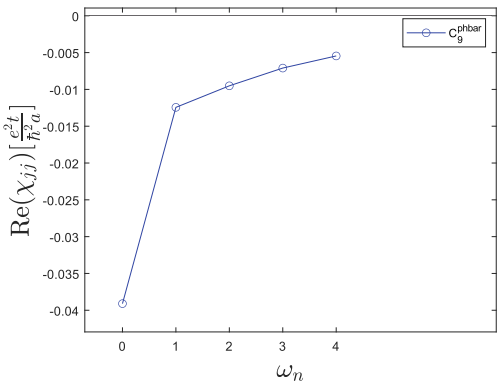


(d) Diagram $D_9^{\overline{ph}}$ with $C_9^{\overline{ph}}$

Figure 49: The vertical particle-hole channel C contributions for their respective diagrams. Bare interaction $U = 4$ and the asymptotic approximation is used.

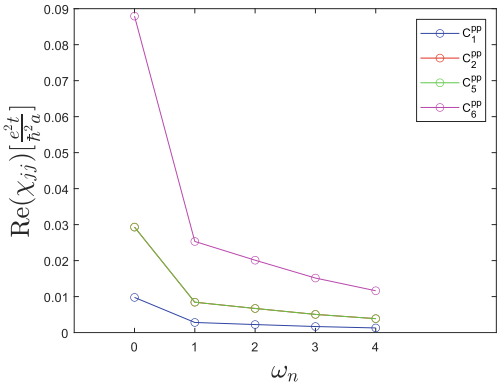


(a) Diagram $D_1^{pp}$ with $C^{pp}_{1,2,5,6}$

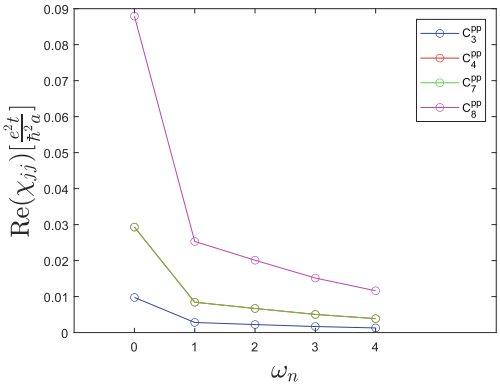


(b) Diagram $D_3^{pp}$ with $C^{pp}_{3,4,7,8}$

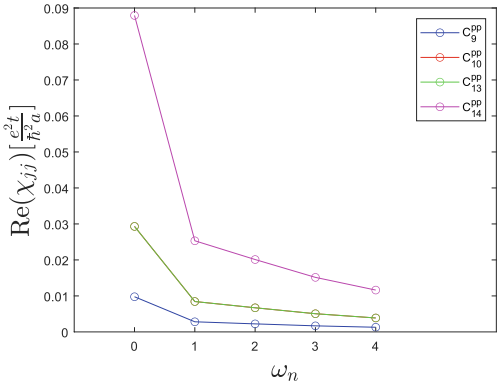


(c) Diagram $D_9^{pp}$ with $C^{pp}_{9,10,13,14}$

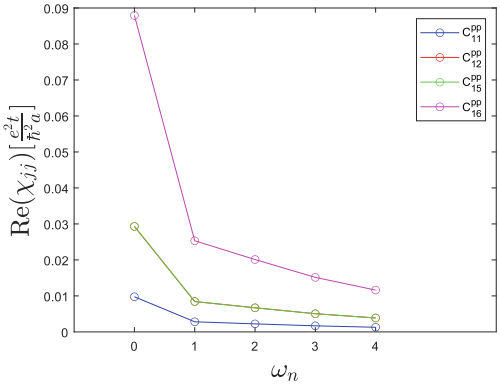


(d) Diagram $D_{11}^{pp}$ with $C^{pp}_{11,12,15,16}$

Figure 50: The particle-particle channel C contributions for their respective diagrams. Bare interaction $U = 4$ and the asymptotic approximation is used.

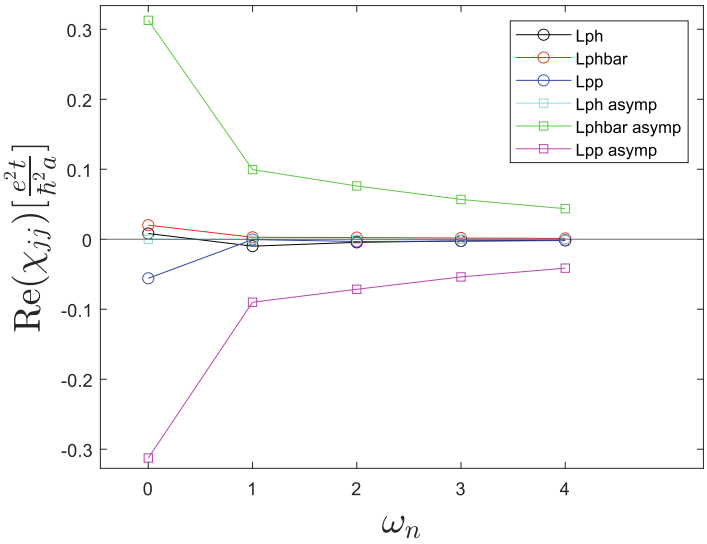


Figure 51: Graph of all different particle contributions with and without the asymptotic approximation, $U = 4$.

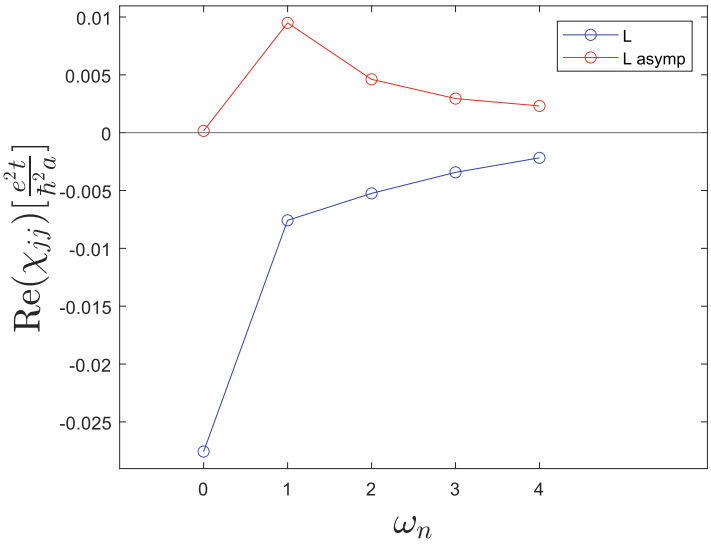


Figure 52: Graph of the total lowest multi-boson order, with and without the approximation, $U = 4$.

# Danksagung

Ich möchte mich an dieser Stelle bei meinem Betreuer Prof. Karsten Held bedanken, für die angenehme Arbeitsatmosphäre, die freundliche Aufnahme in die Arbeitsgruppe, sowie seine Betreuung für diese Diplomarbeit und eine Projektarbeit. Vor allem möchte ich mich auch bei meiner Co-Betreuerin Dr. Anna Kauch bedanken für die gute Zusammenarbeit, ihre herausragende Betreuung und viele lehrreiche Gespräche.

Mein größter Dank gilt meinen Eltern, Sigrun und Markus. Nur durch sie konnte ich hier in Wien mein Studium auf die Art und Weise führen, wie ich es tat. Ihre Liebe und Unterstützung waren mir stets sicher und stärkten mir immer den Rücken. Auch meiner restlichen Familie bin ich sehr dankbar für ihre Unterstützung in jedweder Hinsicht.

Des Weiteren möchte ich mich bei meinen Freunden in Wien und in Deutschland bedanken, die in meiner Studienzeit für mich da waren.

Ich möchte auch nochmal allen Personen danken, die mich durch die persönlich schwierigen Zeiten begleitet haben, die ich während meines Studiums erleben musste.

Ebenfalls explizit danken möchte ich Denise R. für ihre Unterstützung.

Zuletzt möchte ich mich auch bei meiner vorherigen Arbeitsgruppe von Prof.in Silke Bühler-Paschen bedanken, für die Kameradschaft, die tollen Gespräche und die wissenschaftlichen Erfahrungen, die ich dort sammeln konnte.